# Induced-Charge Electrokinetic Motion of a Heterogeneous Particle and Its Corresponding Applications

by

Yasaman Daghighi

A thesis
presented to the University of Waterloo
in fulfilment of the
thesis requirement for the degree of
Doctor of Philosophy
in
Mechanical Engineering

Waterloo, Ontario, Canada, 2013

## AUTHOR'S DECLARATION

I hereby declare that I am the sole author of this thesis. This is a true copy of the thesis, including any required final revisions, as accepted by my examiners.

I understand that my thesis may be made electronically available to the public.

## ABSTRACT

This thesis conducts numerical and experimental studies of the nonlinear electrokinetic motion of heterogeneous particles in microfluidic systems and their corresponding applications in laboratory-on-a-chip (LOC) systems. Induced-charge electrokinetic (ICEK) phenomena flow is generated by applying an external electric field to a conducting particle immersed in an aqueous solution. As a result of this field, micro-vortices form around the conducting particle. Using this phenomenon, many shortcomings of classical electrokinetics (e.g. poor mixing, leakage, back flow problem) can be improved.

This thesis proposes and investigates a complete 3-D numerical multi-physics method to calculate the induced zeta potential on the conducting surface of a heterogeneous object. To model the ICEK motion of a heterogeneous particle in a DC electric field, the moving grid technique is used to conduct the particle-fluid simulation. It was numerically shown that the vortices form near the conducting surface of a particle. Both transitional and rotational motions of heterogeneous particles are investigated.

A set of novel experiments are designed and conducted to investigate several aspecs of ICEK. It is demonstrated for the first time that four vortices form around a conducting sphere in contact with an aqueous solution while the DC electric field is applied. The motions of heterogeneous particles are experimentally studied. The speed of a heterogeneous particle is compared with the same size non-conducting particle under the same experimental conditions and it is shown that the heterogeneous particle moves significantly faster than the non-conducting particle. It is also shown that the micro-vortices on the conducting section of the heterogeneous particle act like an engine and push the particle to move faster. These experiments verify the results of our simulation studies.

We introduce three applications for induced-charge electrokinetic phenomena in ths thesis: ICEK micro-valve, ICEK micro-mixer, and ICEK micro-motor, which can be used in microfluidics and lab-on-a-chip devises.

This ICEK micro-valve significantly improves many shortcomings of other micro-valves reported in the literature (such as leakage, considerable dead volume and complicated fabrication processes). Our ICEK micro-mixers take the advantages of induced micro-vortices and boost the mixing process in a micro-channel. As a result well mixed homogeneous (100%) mixture could be obtained at the downstream of the mixer. Our proposed no-contact ICEK micro-motor rotates as long as the DC electric field is being applied.

This thesis develops a new understanding of several ICEK phenomena and applications related to heterogeneous particles. The 3D numerical model developed in this thesis along with the experimental studies are capable of describing the ICEK motion of a heterogeneous particle and is a considerable step to calculate the ICEK phenomena for real-world applications. This thesis, for the first time, experimentally visualized and verified the induced micro-vortices around conducting particles under applied DC electric field. The proposed ICEK micro-mixers, valve and motor can be used in various LOC devices and applications.

## ACKNOWLEDGMENTS

I am grateful to all of those who made this study possible. I would like to express my appreciation for the positive support and consultation received from my supervisors, Professor Dongqing Li. It was a great pleasure to work under supervision of Prof. D. Li whose guidance and help was greatly appreciated during my graduate studies. I would like to express my sincere gratitude to my parents for their support and encouragement during my academic life. I would like to thank my husband for all of his supports and help that I shall forever be indebted. This work would not have been possible without the support from my supervisor and my family.

## TABLE OF CONTENTS

**Page**

## LIST OF FIGURES

**Figure** **Page**

## LIST OF TABLES

**Table** **Page**

## LIST OF ABBREVIATIONS

| | |
|---|---|
| EK | Electrokinetics |
| EP | Electrophoretic |
| EO | Electro-osmotic |
| EOF | Electro-osmotic Flow |
| ICEK | Induced-charge electrokinetics |
| ICEP | Induced-charge electrophoretic |
| ICEO | Induced-charge electro-osmotic |
| DC-ICEK | DC induced-charge electrokinetics |
| DEP | Dielectrophoresis |
| EDL | Electric double layer |
| LOC | lab-on-a-chip |
| THP | Triangular Heterogeneous Particle |
| CHP | Circular Heterogeneous Particle |
| AC-EOF | AC electro-osmotic flow |
| N/C | Non-conducting |
| C | Conducting |
| JP | Janus Particle |

## NOMENCLATURE

| | |
|---|---|
| $\vec{U}$ | Fluid velocity |
| $\vec{U}_{slip\_w}$ | Electro-osmotic slip velocity on the microchannel wall |
| $\vec{U}_{slip\_NC}$ | Electro-osmotic slip velocity on the non-conducting surface of the heterogeneous particle |
| $\vec{U}_{slip\_C}$ | Electro-osmotic slip velocity on the conducting surface of the heterogeneous particle |
| $\vec{U}_{ep}$ | Electrophoretic velocity |
| $\vec{U}_{eo}$ | Electro-osmotic velocity |
| $\vec{U}_i$ | Electrophoretic velocity of a fully conducting particle |
| $\vec{G}$ | Total body force |
| g | Acceleration due to gravity. |
| e | Fundamental charge of the electrons, $1.602\times10^{-19}C$ |
| z | Value of ionic valence |
| $\nabla P$ | Pressure gradient |
| S | Conducting Surface |
| $\varepsilon$ | Dielectric constant in the medium |
| $\varepsilon_0$ | Dielectric constant in the vacuum |
| $\varepsilon_w$ | dielectric constant, $\varepsilon_w = \varepsilon_0 \times \varepsilon$ |
| $\phi_e$ | Applied electrical potential |
| $\phi_c$ | Constant electrical potential |
| $\vec{E}_{applied}$ | External applied electric field |
| $\vec{E}_{induced}$ | local induced electric field |
| $\lambda_D$ | Debye screening length |
| $\kappa$ | Debye–Hückel parameter |
| $\kappa^{-1}$ | Electric double layer thickness |
| $K_B$ | Boltzmann constant $1.38\times10^{-23}J/K$ |
| μ | Viscosity of the fluid |
| $\mu_{eo}$ | Electro-osmotic mobility |
| $\mu_{ep}$ | Electrophoretic mobility |
| | |

| | |
|---|---|
| $f_{CM}$ | Clausius-Mossotti (CM) factor |
| $\vec{F}_{total}$ | The resultant force acting on the heterogeneous particle |
| $\vec{F}_{h\_out}$ | The hydrodynamic force acting on the particle by the fluid flow in the region outside the EDL |
| $\vec{F}_{h\_in}$ | The hydrodynamic force acting on the particle by the fluid flow in the region inside the |
| $\vec{F}_h$ | The hydrodynamic force |
| $\vec{F}_E$ | The electrostatic force |
| $\zeta$ | zeta potential |
| $\zeta_0$ | initial zeta potential |
| $\zeta_w$ | Zeta potential on the channel wall |
| $\zeta_{P-NC}$ | Zeta potential on the non-conducing section of a heterogeneous particle |
| $\zeta_{induced}$ | Induced zeta potential on the conducing surface |
| ρ | Density of the fluid |
| $\rho_p$ | Heterogeneous particle density |
| $\rho_e$ | Free charge density |
| $n_0$ | Ionic number concentration in the bulk solution |
| $\vec{n}$ | normal vector |
| $\bar{\bar{I}}$ | Identity tensor |
| $\sigma_p$ | Stress tensor |
| $T_{net}$ | Total torque acting on the particle |
| $T_e$ | Maxwell stress tensor |
| T | Absolute Temperature in Kelvin |
| t | Time |
| $m_P$ | Mass of inertia of the particle |
| $J_P$ | Moment of inertia of the particle |
| $C_i$ | Concentration of fluid stream (i) |
| $D$ | Diffusion coefficient |
| Q | Net surface charge |
| | |

**CHAPTER I : Introduction**

## A Background on Electrokinetics and Related Applications

Electrokinetics is the interaction between the applied electric field and the electric double layer (EDL) formed on the surface of any solid object, e.g. a Janus particle that is in contact with an aqueous solution. Electrokinetics is one of the oldest areas of study in surface and colloid sciences. However, the advances in technology -have opened new aspects for electrokinetics to get involve in microfluidics and lab-on-a-chip (LOC) applications, such as: pumping [1], mixing [2, 3], molecule or protein separation [4, 5], DNA or cell concentration [6, 7], etc.

In 1809, Reuss [8] controlled the level of water in a U-shape tube by applying voltage to the branches of the tube. He also repeated his experiment by replacing water with a mixture of sand and clay and noticed that once the electric field is applied the clay particles move through the sand layers. Using an electric field to control the motion of fluids and particles was later called "electro-osmotic flow" (EOF) and "electrophoresis" (EP) respectively which are two main branches of the electrokinetics. Since electro-osmosis in compression with electrophoresis was easier to carry out, many quantitative experiments had been done to characterize the electro-osmotic flow [9-12]. These experiments illustrated that the electro-osmosis could be observed using many different systems; but they were unable to discover the mechanism that caused electro-osmotic flow. Wiedemann [9] in 1852 showed that the mass of the transported water is independent of the cross sectional area of the tube and the applied voltage as long as the electric

current is kept constant. Seven years later, in 1859, Quincke [10] measured the electric potential difference which was applied to the ends of a tube filled with water. Repeating his experiment using different types of materials, Quincke [10] noticed that the magnitude of the electric potential difference dependents on the testing materials. He also postulated that there is a charged space outside of the charge surface of the material. Electric double layer (EDL) was then discovered based on Quincke's postulates. However a quantitative theoretical description of the electrokinetic (EK) phenomena was derived about twenty years later in 1879 by Helmholtz [11] based on the Quincke's EDL idea.

By 1880, many different aspects of electrokinetics were discovered, their basic characteristics were understood, and most of their limitations were investigated. The classical studies assumed the electrokinetic phenomena (i.e. electro-osmosis and electrophoresis) have a linear relationship with the applied electric field. Those classical studies consider a fixed static surface charge for the surfaces and particles involved in electrokinetic experiments. Such assumptions significantly limited the applications of classical electrokinetics (e.g. the particles with fixed constant zeta potential cannot be separated by their size or shape). In practice, the surface or the particle might not have a constant fixed electric charge or does not respond linearly to the applied electric field. Solutions for such drawbacks are introducing a new branch of electrokinetics called "Induced-charge Electrokinetics" (ICEK).

Levich [13] is known as a pioneer of "Induced-charge electrokinetics" who, for the first time used a fully conducting sphere in an electrokinetic system and calculated the perturbed slip profile around it. It is theoretically predicted that vortices induced around a conducting surface in contact with electrolyte once the electric field is applied. These vortices are the key components in induced-charge electrokinetic studies. Others, then, studied the behavior of the flow around a

fully conducting surface [14-19]. After one decade, Simonov and Dukhin [18] theoretically analyzed the structure of the induced-double layer. But, Gamayunov *et al.* [17] was the first person to experimentally observe the quadrupolar induced-charge electro-osmotic flow (ICEO) around a fully conducting sphere (known as induced vortices) which was caused by low frequency AC electric field (AC-EOF). In addition to these induced vortices they also reported the hydrodynamic interaction between two fully conducting particles for the first time. Following that, the motion of irregular-shaped quartz particles was investigated by Murtsovkin and Mantrov [20, 21] and Gamayunov *et al.* [17]. They observed a second order relationship between applied electric field and motion of irregular-shaped quartz particles which was not theoretically proven for a long time after. Ramos *et al.* [22] used active micro-electrodes and observed the AC-EOF over their fully conducting surfaces. One year later Ajdari [23] proposed a low voltage AC micro-pump method based on Ramos's idea [22]. Between 2000 to 2004, Green *et al.* [24, 25], Gonzalez *et al.* [26], Brown *et al.*[27] and Studer *et al.* [28] experimentally used non-linear AC electrokinetics. They developed different applications for AC-ICEK in microfluidics. In 2005, induced-charge electro-osmotic flow (ICEO) around a fully conducting metal wire in a micro-chamber was reported by Lenitan et al. [29]. They also used AC electric field for their experiments and showed vortices induced around the fully conducting wire. Yariv [30] derived a general model to calculate the velocity of a non-spherical fully conducting particle under applied electric field. The hydrodynamic interactions of rod particles which have induced-charge electrophoretic (ICEP) motion were statistically analyzed by Saintillan *et al.* [31, 32]. Rose *et al.* [33] studied the dynamics of the transient alignment of rod-like asymmetric fully conducting particles. In the next few years, Wu and Li [34, 35] numerically modeled motion of fully conducting particles in microchannels and their interactions with each other. They also proposed

a DC induced-charge electrokinetic (DC-ICEK) micro-mixer based on numerical and experimental works [36, 37]. Kim *et al.* [38] illustrated the ICEO around three active electrodes using AC electric field and employed the induced vortices for pumping the fluid.

The majority of the studies mentioned earlier, investigated the induced-charge electrokinetics for a fully conducting surface or particle. Many materials in nature are not 100% homogeneous (i.e. fully conducting or totally non-conducting). This has to be taken into account to have an accurate model of the physical system. It is important to understand how a heterogeneous particle reacts when it is in contact with an aqueous electrolyte solution and an electric field is applied. Characterizing the behavior of a heterogeneous particle in an electrokinetic system is very important yet only a few ICEK studies have considered it. The motion of a heterogeneous particle under a low frequency AC field was investigated by Gangwal *et al*. [39]. According to their results, the strength and direction of the AC electric field determines the ICEP motion of a heterogeneous spherical particle.

Compared to the research that has been performed on fully conducting material, the study of heterogeneous materials is at its early stages. So far, there has been no systematic theoretical or numerical study characterizing the motion of a heterogeneous particle under applied DC electric fields. There is a lack of experimental evidence for the ICEK around a "non-electrode" heterogeneous particle under the DC electric field. Such studied could be used in eliminating the current drawbacks of classical electrokinetics or induced-charge electrokinetics. They could also be used to design novel microfluidic systems and future Lab-on-a-chip (LOC) devices (e.g. micro-valves, micro-mixers, micro-motors, etc).

## 1-1. Micro-Valve: History, Improvements, Shortcomings

The main function of a micro-valve is switching the direction of the flow at the desired time to control and regulate the fluid stream. Micro-valves are one of the most important components of integrated LOC devices. Using micro-valves with high performance the sequential loading and washing processes could be performs accurately and fast. Thus, a micro-valve capable of switching fluid flow fast with no leakage and less dead-volume is highly recommended. The first micro-valve was introduced by Terry [40], in 1979, which was the first magnetic MEMS micro-valve. This micro-valve was improved in several ways [41-45], where among all of them the pinch-type micro-valves became the most commonly used one. The pinch-type micro-valves had several advantages such as absolutely no leakage, zero dead volume, short response time, easy replacement of tubing. The characteristic that make it more practical compared to the other types of MEMS micro-valves. However, the difficult fabrication of the pinch-type micro-valves made the researchers to search for alternatives. In 1987 the first thermal micro-valve was introduced and fabricated [46], and its functionality was later improved [47].

Thermo-pneumatic [48-54], shape memory alloy [55-57], and bimetallic [58-62], are the different types of thermal micro-valves that use the actuated micro-valve technique. The important drawback of using thermal micro-valves is the response time; thus, the thermal micro-valves might have cause difficulties in operation control. In 1994 electrostatic micro-valves were introduced to solve some of the common shortcomings of former micro-valves. Sato and Shikida [63] used flexible membranes while many others used rigid silicon membranes [64-68] in an electrokinetic system to control the flow regulation. To operate these types of micro-valves high voltage is required which causes electrolyte problem if aqueous electrolyte solutions are involved. Thus, the applications of such micro-valves were limited to gas flow regulators.

Around the year 2000 a revolution in fabrication of micro-valves happened. This revolution solved the problems of the various MEMS-based micro-valves. As a result, new types of micro-valves were introduced: external pneumatic [51, 69-71], phase change [72-74], and passive capillary micro-valves [62, 75, 76, 76-78]. However, the existing micro-valves still have lots of serious problems which are unsolved. Such as: (i) using moving parts which cause additional problems and difficulties, (ii) external actuation means, (iii) complex fabrication and installation processes, (iv) resistible flow and pressure, (v) considerable dead volume, (vi) long response time, (vii) leakage, and (viii) stability. Thus, new design is highly required to develop practical and efficient micro-valves and overcome the current problems. Such a micro-valve could be a great step towards developing integrated LOC devices. In this thesis we developed a new ICEK micro-valve using a heterogeneous particle inside a micro-chamber. This ICEK micro-valve is easily controlled by applying two perpendicular electric fields. Our stable ICEK micro-valve is fast has small dead volume, no leakage, short response time, and easy to fabricate. Thus, it can be considered as an applicable alternative for exciting micro-valves.

### 1-2. Micro-Mixer: History, Improvements, Shortcomings

Mixing different solutions to obtain a homogeneous mixture in a short period of time is a key feature for many LOC applications; which is not easily achievable. Poor mixing process produces a heterogeneous mixture and consequently influences the accuracy of the results. Mixing two or more fluid streams in microchannels without using micro-stirrer or mechanical micro-mixers depends on their molecular diffusions; since, the nature of flow in microchannels is laminar (no convective term assists the mixing process).

To improve the mixing results, some researchers proposed using microchannels with specific geometries [79, 80], sequential grooves on the channel base [81], a sequential injection into an expansion chamber [82], or inserting non-conducting obstacles into the microchannel [83]. A special pattern of the heterogeneous surface charge is used along the microchannel walls by Biddiss *et al.* [84], to induce the local micro-vortices and produce a more homogeneous mixture.

Disturbing flow to change the flow regime from laminar to turbulent is a practical approach to develop a reliable mixing process. Changing the flow pattern can be achieved in different ways. Using mechanical micro-stirrers to agitate the flow and produce a good mixture was followed by Zhang *et al.* [85] and, Kim and Beskok [86]. However, using the stirrer introduces moving parts in the micro-systems and has many operational drawbacks and fabrication difficulties. The alternative solution (to avoid moving parts) was implementing electrokinetic methods for mixing. AC electric field is used to agitate the electrokinetic micro-mixer [87-89] which result in periodic disturbance of the flow streams. The induced-charge electrokinetics concept and induced micro-vortices can be employed to design an electric micro-mixer with high performance [36, 37, 90-92]. The simplicity of such an ICEK mixing method has attracted considerable attention in the fields of microfluidics and LOC [93, 94].

Zhao and Bau [95] induced vortices near a circular conducting metal cylinder and introduced an ICEK micro-mixer where they periodically switched between electric fields in oblique and vertical directions in a closed chamber. However, in many practical microfluidic applications, mixing must be performed in a continuous flow system; thus their proposed micro-mixer was limited to very few cases which dealt with closed micro-chambers. To improve their work some researchers used the conducting surface attached to the base of the microchannel [96, 97] or inserted the conducting surface into the microchannel walls [36, 37, 90, 91]. In all cases they

took the advantages of induced vortices around the conducting surface for mixing different types of fluids.

Typically AC electric field is applied to operate such systems and less attention has been paid to DC electrokinetic micro-mixers during the past decades. So far, there is no micro-mixer which operates on the basis of induced-charge electrokinetic motion of a conducting particle under an externally applied DC electric field. In this thesis we develop a new ICEK micro-mixer using conducting a particle inside a micro-chamber. Two perpendicular DC electric fields with the same magnitude control the proposed ICEK micro-mixer. Our ICEK micro-mixer which employs the induced vortices around the moving conducting particle is easy to be fabricated and is shown to produce 100% homogeneous mixture at the downstream of the fluid. This ICEK micro-mixer can be considered as a simple high-performance and accurate solution for problems of current micro-mixers.

### 1-3. Micro-Motor: History, Improvements, Shortcomings

Motor is a device that creates motion by converting the power (electric, aquatic, magnetic, etc) that it receives from an external source into mechanical energy. Faraday was the first person who could convert the electrical energy into mechanical energy by electromagnetic means in 1821 [98]. The first electromagnetic self-rotor was introduced in 1827 by Jedlik which used electromagnetic coils [98]. Such devices were unable to rotate continuously until Jedlik solved this problem by inventing commutator. One year later he introduced the first device which had the three main components of a practical DC motor: the rotor, the stator and the commutator. His invention then was used by many scientists even in micro-scales by developing the required manufacturing processes.

However according to Gad-el-Hak [99] the first micro-motor did not move even when large electric current was applied due to significant friction effect in small scales. To solve this problem, Fan *et al.* [100] introduced the integrated movable micro-structures which could be used for actuators and sensors. Based on their micro-mechanical structures, they reduced the area between rotor and the substrate using dimples on the rotor's surface [100]. Since fabrication of coils and iron cores for rotor/stator type mixer in small scales had not been developed yet, scientists were looking for an alternative. In 1987, Trimmer and Gabriel [101] proposed practical designs for an electrostatic micro-motor based on electrostatic-drive principles. An electrostatic motor works based on the attraction and repulsion of electric charges and for the first time were developed by Gordon [102] and Franklin [103] in the 1750s.

Using an electrostatic micro-mixer seems easier compared to former types of micro-motors. Controlling and moving the charged plates in an electrostatic micro-motor is much easier than fabricating coils and iron cores. In 1989, Brat *et al.* [104] described the principles that have to be considered in fabricating such an electrostatic micro-motor. In the same year, Tai and Muller [105] introduced an electrostatic synchronous micro-motor using the IC manufacturing technology. Muller's group [105, 106] fabricated and tested several rotating motors which are driven electrostatically.

Today, considering the developments in the manufacturing processes, the electrostatic micro-motors are frequently used in small sized systems to manipulate cells in microfluidic applications. Despite the important role of electrostatic micro-motors in micro-scale systems, they are unable to generate sufficient output torques. This small output torque is the result of using flat plates and the small dimensions of electrostatic micro-motors. To solve this problem many other micro-motors were developed, such as the ultrasonic or in general the piezoelectric

micro-motors [107]. These micro-motors on the other hand are difficult to fabricate in small scales. Employing induced-charge electrokinetics is a promising method to develop a practical micro-motor. It was found that the vortices induced on the conducting surface of a particle generate forces on the particle. These forces push the particle to have transitional and rotational motion depending on the force balance on the particle [108]. Utilizing this phenomenon, we were able to design a heterogeneous particle that rotates as long as a DC electric field is applied. This particular heterogeneous particle is used to develop a novel non-stop micro-motor using ICEK phenomenon.

In this thesis, we will numerically design and experimentally validate an ICEK micro-motor which is comprised of a triangular heterogeneous particle in a micro-chamber. The key point in generating and controlling the continuous rotation of this THP micro-motor under an applied DC field is the particular design of its geometry. This triangular heterogeneous particle (THP) has an electrically non-conducting body and three electrically conducting corners. The configuration of the THP conducting and non-conducting sections must be such that the applied to the particle are unbalanced all the time. Thus the THP micro-motor rotates as long as the DC electric field is being applied.

### 1-4. Thesis Layout

This thesis is divided into nine Chapters. In the first chapter the background study of electrokinetics is reviewed as well as the characteristics of the classical electrokinetics (EK when a non-conducting material is involved) and induced-charge electrokinetics (ICEK when a conducting material is involved). There are only a few studies that have reported the induced-charge electrokinetics using a heterogeneous particle. Thus, it essentially required to characterize the behavior of ICEK using a heterogeneous particle.

In the second chapter we introduce the electric double layer and zeta potential in details. The electro-osmosis and electrophoresis are explained. Differences between classical electrokinetics and induced-charge electrokinetics are completely described. Relative formulations of each type are listed.

In Chapter 3 the governing equations of transitional and rotational ICEP of a heterogeneous particle are defined in details. These equations are used for three dimensional numerical modeling later in chapter 4.

Chapter 4 conducts three dimensional numerical simulations of time dependent motion of a heterogeneous particle in a microchannel using a moving mesh strategy. Transient motion of a Janus particle is compared to the motion of a non-conducting particle (Classical EK), and also to a fully conducting particle. Effects of different factors (such as: electric field strength, particle size, zeta potential, and orientation of the heterogeneous particle) on the motion of a heterogeneous particle are investigated. The rotation of a heterogeneous particle which aligns itself with the direction of the applied DC electric field is also numerically simulated [108].

In chapter 5, we report the experimental visualization of the four induced vortices around a fully conducting spherical particle under an applied DC electric field. This is the first report of induced vortices under applied DC electric field. An experimental comparison between the velocity of a heterogeneous particle and a non-conducting particle with the same size is conducted. The results show that the heterogeneous particle moves much faster than the non-conducting particle. We also recorded the motion of heterogeneous particle and show that it moves in different directions when oriented different directions. Our experimental results [109] verify the numerical simulation results that we have already reported in chapter 4.

Chapter 6 is the introduction of a novel ICEK micro-valve. This proposed ICEK micro-valve works based on ICEK motion of a Janus particle immersed into a micro-chamber and controlled by applying two perpendicular DC electric fields. The flow rate and flow direction can be controlled by different configurations and magnitudes of these DC electric fields. We have conducted a time dependent, three dimensional numerical modeling, using the moving mesh technique. Different types of particles (non-conducting or fully conducting) are tested to be employed instead of a heterogeneous particle for the proposed micro-valve. The results illustrate that this micro-valve shows instability and leakage problems if non-conducting or fully conducting are used. However the ICEK micro-valve using the heterogeneous particle is stable, fast, easy to fabricate and has no leakage [108].

In chapter 7 we numerically conducted the simulation of a novel ICEK micro-mixer. Its designee contains a fully conducting spherical particle in a cylindrical micro-chamber. The micro-chamber is connected to two rectangular microchannels. The upstream microchannel delivers two unmixed fluids into the chamber and the downstream channel let the mixture flow out. Once the DC electric fields are applied perpendicular to each other, vortices are induced on the surface of the conducting particle. The applied DC electric fields also manipulate the motion of the particle. The vortices enhance the mixing of the two fluid streams in the micro-chamber as the fluid streams are flowing through the micro-chamber. We demonstrated that this proposed micro-mixer can be operated in low-voltage ranges to satisfy the requirement for miniaturization. The size and the strength of the vortices depend on the applied electric field. The effects of the strength and direction of the applied electric field are examined in this chapter. The results show that at one particular configuration of the position of the conducting particle we can obtain 100% heterogeneous mixture at the downstream of the ICEK micro-mixer [110].

In chapter 8, we develop a non-stop induced-charge electrokinetic micro-mixer using a triangular shaped heterogeneous particle. This triangular heterogeneous particle (THP) is made of a non-conducting sheet and its three corners are conducting materials. A method to generate and control the continuous rotation of this particle under a DC field is numerically investigated and experimentally developed in this thesis. We also investigate the effects of changing the model parameters such as particle size, electric field, etc. to determine the facts that affect the rotation of this heterogeneous particle. We experimentally proved that such a particular triangular heterogeneous particle can be used as a non-stop ICEK micro-motor.

The last chapter of this thesis is the conclusion of the conducted study on induced-charge electrokinetic motion of a heterogeneous particle moving in a microfluidic system. Our numerical and experimental results are compared in this chapter. Three new applications for induced-charge electrokinetic phenomena (using induced vortices in the system) are also briefly introduced.

# CHAPTER II: Theory

## Fundamentals of Electrokinetics: Classics and Induced-Charge

The main objective of this thesis is to perform a theoretical, numerical and experimental study on the induced-charge electrokinetic (ICEK) behavior of a heterogeneous particle under applied DC electric field. The way a heterogeneous particle reacts to an applied DC electric field depends on its conductivity. In this thesis we will investigate different aspects of the ICEK phenomena when a heterogeneous particle is involved. In this chapter, we will review the important terms and definitions that are related to the electrokinetics and induced-charge phenomena. We will discuss the formation of an electric double layer on a solid surface which is in contact with an aqueous electrolyte solution. The definitions of zeta potential, electro-osmotic flow and electrokinetic velocity are explained. We will also cover the basic characteristics of "Classical Electrokinetics" and "Induced-charge Electrokinetics", then will explain how the conductivity of the solid surface determines the type of its corresponding electrokinetic phenomena. Moreover, different types of particles which are categorized based on the conductivity of their materials will be introduced in this charter.

## 2-1. Electric Double Layer (EDL) and Zeta Potential

A solid surface carries electric charge when it is in contact with aqueous solution e.g. glass carries positive electric charge while plastic carries negative electric charge. Once this solid surface contacts an electrically neutral aqueous solution (the electrolyte), the charges on its surface attract counter-ions in the fluid. As a result, the arrangements of free ions of the aqueous solution change. A layer of these counter-ions forms immediately next to the charged solid surface and binds strongly to the solid surface. This layer produces a nonzero charge region in the electrolyte. This nonzero charge region balances the charges at the solid surface. This layer is called a "compact layer". Since the charge of the bulk aqueous solution is zero, as we move away from the compact layer, the net charge density gradually decreases from compact layer to the electrically neutral bulk fluid. The distance between the compact layer and the neutral bulk fluid is layer is called a "diffuse layer". Unlike the ions in compact layer that are bound to the solid surface, the ions in the diffuse layer are mobile. These two layers, compact and diffuse layers, are called the electric double layer (EDL) [111]. The boundary between the layers of EDL is known as the shear plane and the electric potential at this boundary is called the zeta potential, $\zeta$. The zeta potential is an approximate measurement to the surface potential in most electrokinetic models. In classical electrokinetics zeta potential is considered as a constant value [11, 13, and 29]. Zeta potential could be defined as

$$\zeta = \frac{Q}{\varepsilon\, \varepsilon_0\, \kappa} \tag{2-1}$$

where Q is the net surface charge, and $\kappa^{-1}$ is the Debye–Hückel parameter and is given by

$$\kappa^{-1} = \lambda_D = \sqrt{\frac{\varepsilon\, \varepsilon_0\, K_B\, T}{2 n_0\, (ze)^2}} \tag{2-2}$$

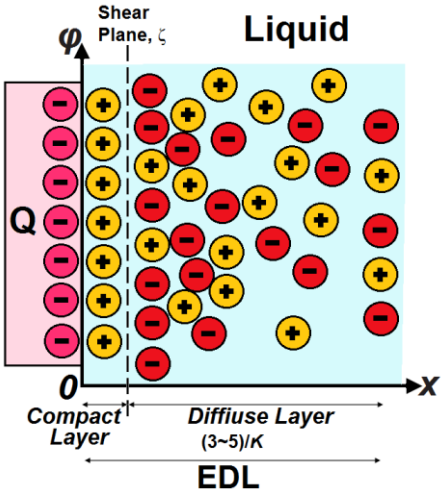


**Figure 2-1.** Schematic diagram of electric double layer, shear plane and zeta potential

where $K_B$ is the Boltzmann constant, $T$ is the temperature and $n_0$ is the bulk ionic concentration. The Debye EDL thickness, $\kappa^{-1}$, only depends on the fluid properties (such as: bulk ionic concentrations, the valence of the electrolyte, etc). And, the Debye length does not depend on the properties of the solid surface. Figure 2-1 shows the arrangements of the different layers of electric double layer and zeta potential location. We are assuming that in the outer region of the electric double layer, the ionic concentrations are uniform and the local volume net charge density is zero. That is why we can use the Laplace equation to calculate the distribution of the applied electric field through the bulk liquid.

## 2-2. Electro-osmotic and Electrophoretic

EDL forms around an object with electrically non-conductive surface in contact with an aqueous solution. Once an external electric field is applied - the positive ions in the EDL get be attracted towards the negative side of the electric field. Conversely the negative ions get attracted towards the positive side of the applied electric field. This movement of ions towards their counter signs drags their surround fluid molecules and thus moves the bulk fluid. , This motion is called electro-osmotic flow (EOF). Moreover, if an electrically non-conductive particle with

initial charge immersed to an aqueous solution and external electric field is applied, the particle moves as a result of applied electric body force and the flow friction force on the particle. Balance of these two forces determines the electrophoretic (EP) velocity of the particle. Figure 2-2 shows the electro-osmotic flow and electrophoresis of a non-conducting particle in contact with aqueous solution and under applied electric field. For thin Debye EDL thickness, $\kappa^{-1} = \lambda_D$ , it seems the flow slips over the outside of the double layer and causes a plug like flow profile. According to the Helmholtz-Smoluchowski formula [112] the slip velocity is given by

$$\vec{U}_{eo} = -\frac{\varepsilon\, \varepsilon_0\, \zeta_w}{\mu} \overrightarrow{E_e} = -\mu_{eo}\ \overrightarrow{E_e} \tag{2-3}$$

and electrophoretic velocity of a charged particle in an aqueous solution, under the applied electric field is also is given by Helmholtz-Smoluchowski formula [112]

$$\vec{U}_{ep} = \frac{\varepsilon\, \varepsilon_0\, \zeta_p}{\mu} \overrightarrow{E_e} = \mu_{ep}\ \overrightarrow{E_e} \tag{2-4}$$

where $\mu$ is the viscosity of the fluid, $\zeta_w$ and $\zeta_p$ represents the zeta potential at the shear plane of solid surface and particle. $\mu_{eo}$ and $\mu_{ep}$ are referred to the electro-osmotic mobility of the fluid and the electrophoretic mobility of particle respectively.

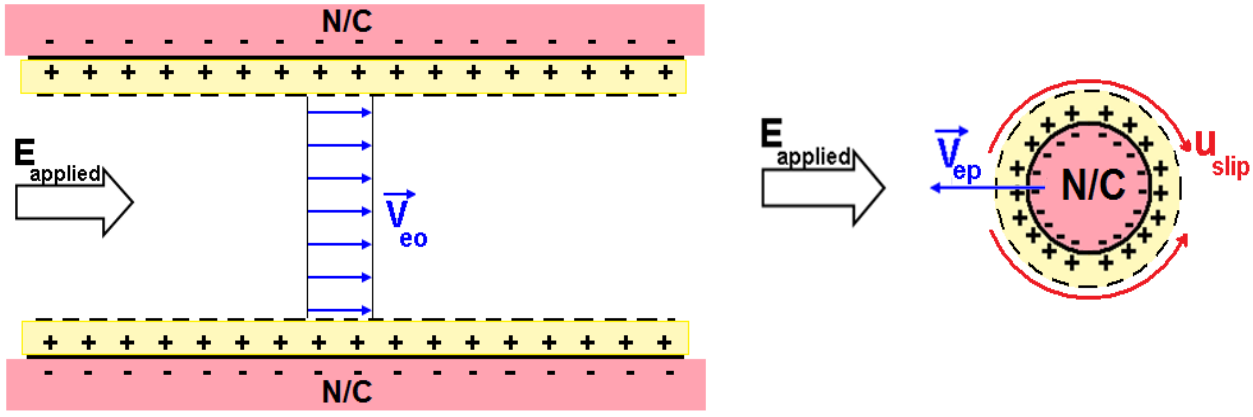


(a) (b)

**Figure 2-2.** Schematic illustration of (a) electro-osmotic flow over a non-conducting surface (b) electrophoresis of a non-conducting (N/C) particle.

Helmholtz-Smoluchowski formula is based on the following assumptions

- The electric double layer thickness is not too large (i.e., $\kappa >> 1$) compared to the microchannel diameter or particle size.
- The surface of microchannel or particle is non-conducting and the EDL is not polarizable.
- The surface of microchannel or particle is homogeneous in properties.

### 2-3. Classical Electrokinetics

Electrokinetics is the interaction between an externally applied electric field (DC or AC) and the electric double layer on the solid surface. If the electric double layer has formed on a non-conducting solid surface or a particle with fixed electric charge, the zeta potential at shear plane will be fixed. This case is called "Classical Electrokinetics (EK)". According to section 2-2 the electrokinetic velocity in classical electrokinetics study is fixed since the zeta potential of the surface is unchanged. According to Eqs. (2-3) and (2-4) the electro-osmotic velocity of the bulk fluid and electrophoretic velocity of the particle are linearly proportional to the applied electric field, $\vec{E}$. As a result, the classical electrokinetic phenomenon is referred to as the linear electrokinetics since the velocity has direct relationship with applied electric field.

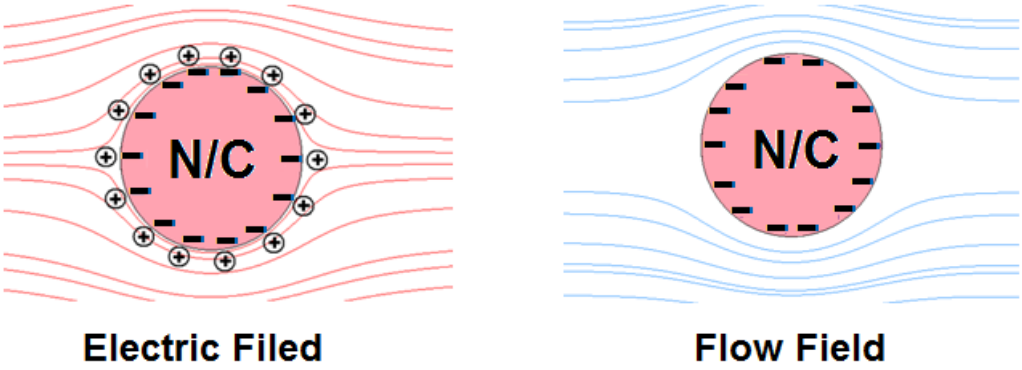


**Figure 2-3.** Schematic illustration of electric field and flow field around a negatively charged non-conducting (N/C) particle which is immersed in an aqueous solution

The theory of Classical Electrokinetics has been formed based on many assumptions to model an electrokinetic phenomenon. In this theory the aqueous solution is considered a homogeneous dilute electrolyte which is uniformly charged and non-conducting. Also it is assumed that the electrolyte is unbounded, the electric field is uniform, EDL is thin, and surface charge is fixed. Additionally, the particle is rigid with homogeneous and non-polarizable material which is uniformly charged. Under these assumptions the velocity of the particle is linear to the applied DC electric field. However, in real case most of the assumptions of the classical electrokinetics are not valid, for example most of the materials are partially conducting and, as a result, the surface charge of those materials is not fixed. Therefore the classical electrokinetics is unable to model every electrokinetic phenomenon. To solve the classical EK drawbacks a class of non-linear electrokinetic phenomena has been introduced. Based on the non-linear electrokinetic theory the electric field induces surface charge when a conducting surface is in contact with an aqueous solution. The external electric field, then, interacts with the electric double layer of the induced charges. Since the induced zeta potential and local electric field vary along the conducting surface, the produced slip velocity will be non-linear, $\vec{u} = \mathcal{F}(\overrightarrow{\mathrm{E}})$.

**2-4. Induced-Charge Electrokinetics**

One of the fundamental equations to evaluate the distribution of electric potential in a dielectric medium is the Poisson equation

$$\nabla^2 \phi_e = \frac{\rho_e}{\varepsilon_0 \, \varepsilon} \tag{2-5}$$

where $\phi_e$ is the distribution of the applied electric potential, $\varepsilon_0$ and $\varepsilon$ are the dielectric constant in the vacuum and in the medium, respectively. The $\rho_e$ is the free charge density. Assuming

there is no free charge (e.g. pure fluids, or electrically neutral aqueous solutions) then $\rho_e \approx 0$ and the Poisson equation becomes the Laplace's equation

$$\nabla^2 \phi_e = 0 \tag{2-6}$$

Thus the distribution of the applied electric potential, $\phi_e$ , in the fluid can be obtained by solving the Laplace's equation.

Consider a neutral electrically conducting particle with arbitrary geometry, immersed in an aqueous solution. Once an electric field is applied, the electric field passes through the conducting particle (Figure 2-4a) and drags the charges inside the particle to its conducting surface. Shortly after (on the order of $10^{-4}$s), the negative charges migrate to that side of the particle which is closer to the higher voltage; while the positive charges move to the opposite side (Figure 2-4b). Consequently an internal electric field is generated around the particle which acts like a shield and resists the external electric field from passing the conducting particle. Meanwhile, the induced surface charges of the conducting particle attract the counter-ions of the aqueous solution and EDL forms around it. At this stage, the particle behaves like an insulator and the electric field around the particle reaches steady-state condition (Figure 2-4c). The established configuration of the charges and EDL on the conducting particle is equivalent to the non-flux electrostatic boundary condition. Because the induced charges under the surface of the conducting particle have an opposite sign to that of the ions attracted on the surface of the particle (from the aqueous electrolyte solution), the induced electric field on the particle–electrolyte interface should be in the opposite direction to that of the external field, that is

$$\vec{E}_{induced} = -\vec{E}_{applied} \tag{2-7}$$

In other words, the strength of the local induced electric field $E_{induced}$ of the fully conducting surface is the same as the externally applied electrical field $E_{applied}$ but in the opposite direction

$$\vec{E}_{induced} = -\vec{E}_{applied} \tag{2-8}$$

or

$$\nabla \zeta_{induced} = -\nabla \phi_e \tag{2-9}$$

where $\zeta_{induced}$ is the local induced zeta potential on the surface of the conducting particle. $\phi_e$ is given by Eq. (2-9).The above mentioned particle was initially neutral and did not have any surface charge. Therefore, the integration of the induced charges over the conducting surface should be zero. Consequently the induced zeta potential is

$$\oint_S \zeta_{induced}\, \mathrm{dS} = 0 \tag{2-10}$$

where S is the conducting surface under the applied electric field. Integrating Eq. (2-10) the following relation will be obtained

$$\zeta_{induced} = -\phi_e + \phi_c \tag{2-11}$$

where $\phi_c$ is a constant for an electrical conducting surface under an applied electric field. Substituting Eq. (2-11) into Eq. (2-10), $\phi_c$ can be calculated as

$$\phi_c = \frac{\oint_S \phi_e \mathrm{dS}}{\mathrm{S}} \tag{2-12}$$

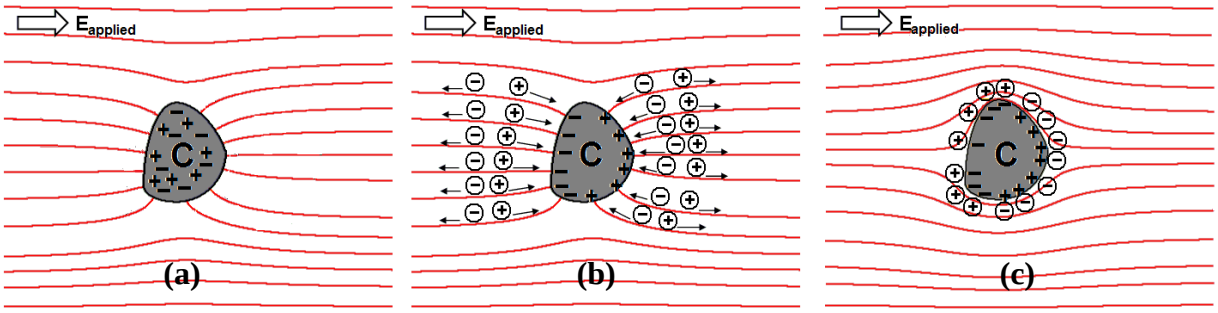


**Figure 2-4.** Charging process of an arbitrary shape conducting particle under a uniform applied electric field: (a) initial electric field passing throw the conducting particle, (b) induced charges under the surface of the conducting particle attracts the electric ions of the aqueous solution, and (c) steady-state electric field and the induced dipolar EDL. "C" represents conducting material.

The EDL sign changes along the surface of the particle from positive in the upstream side of the flow to negative at the downstream side of the flow (Figure 2-5a). Also, the distribution of the local net charges under the surface of the conducting particle, and hence, the EDL is not uniform around the particle. As a result, the slip velocity varies as a function of the local electric field in different directions and causes micro-vortices around the particle (Figure 2-5b). According to the Helmholtz-Smoluchowski formula [112]

$$\vec{U}_i = -\frac{\varepsilon \varepsilon_0 \zeta_{induced}}{\mu} \vec{E}_{applied} \tag{2-13}$$

Knowing the exact distribution of the induced zeta potential is the key to calculating the induced electro-osmotic velocity around the conducting particle and electrophoretic motion of the particle. However the induced zeta potential is proportional to the local electric field strength and varies with the position on the surface of the conducting particle. As a result, the induced-charge electrokinetic velocity is non-linear and depends on the local induced zeta potential. Eq. (2-9) gives the distribution of the induced zeta potential; though, its exact solution is not available except for relatively simple geometries (such as a two dimensional circular cylinder). However, for irregular complex geometries there is no analytical or exact solution for Eq. (2-9); thus the distribution of the induced zeta potential (and hence ICEK velocity) on such geometries is unknown.

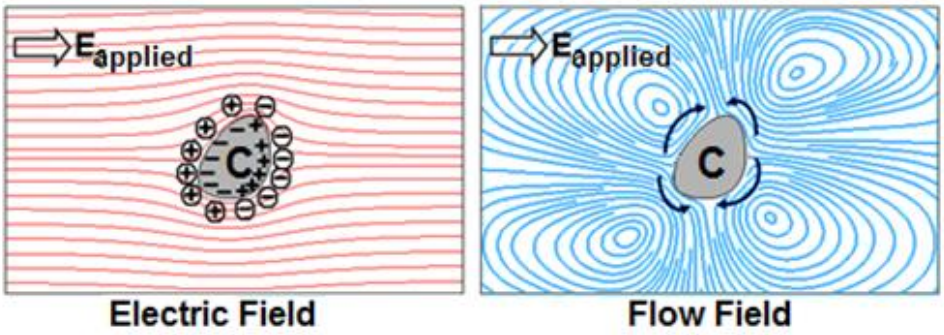


**Figure 2-5.** Electric lines and Induced-charge electrokinetic flow field around a conducting particle.

Thus a numerical method which is capable of relating the induced zeta potential to the external applied electric field is highly necessary. Wu and Li [34-37] introduced a computational method to simply calculate the induced zeta potential, ICEK velocity, electrical and flow fields numerically. Using Eq. (2-8) to (2-12) allows a simple numerical method to calculate the final distribution of the steady state induced zeta potential on the conducting particle of an arbitrary geometry. The ICEK velocity can then be calculated over the entire study domain.

The induced-charge electrokinetics has some unique characteristics which can be used to develop new microfluidic and LOC equipments; such as controlling zeta potential, and having nonlinear relationship with the applied DC electric field. Eq. (2-11) shows that induced zeta potential is directly related to the applied DC electric field. Controlling the applied electric field results in inducing desired $\zeta_{induced}$ and manipulating the motion (transitional and rotational) of a particle with conducting surface as well as controlling its speed.

**2-5. Heterogeneous Particle**

The classical electrokinetics (EK) and induced-charge electrokinetics (ICEK) are categorized as two totally different electrokinetic theories because of the origins of their surface charges. The classical EK deals with materials with fixed surface charge; while, the surface charge is induced by applied electric field in IECK theory.

Up to now, we have only considered two extreme cases: (i) the material is totally non-conducting and the charge on the solid material is fixed and unchangeable; (ii) the material is fully conducting and will be completely polarized under the applied electric field. However there are a large number of materials that do not satisfy the characteristics of these two categories. Such materials are partially conducting thus; they do not fit in the first category (non-conducting)

or the second category (fully conducting). These heterogeneous materials cover a large range of conductivities and configurations and are extensively used in microfluidics and electrokinetics devices. Thus it is necessary to study and understand how a heterogeneous particle acts in an electrokinetic micro-system.

Consider a heterogeneous particle which is consisted of some fully conducting and some non-conducting sections. To study such a heterogeneous particle, in this thesis, we have applied the ICEK theory and equations to model the conducting sections; and the classical EK is used to model the non-conducting parts.

As a simple case, consider a Janus particle[1] as Figure 2-6 shows. The Eq.(2-8) to (2-13) are used to calculate the induced-charge zeta potential on the conducting hemisphere. While the slip velocity over the non-conducting half of the Janus particle, is calculated by the classical EK formula, Helmholtz-Smoluchowski equation. Since the induced zeta potential on conducting surface varies in different positions, $\zeta_{induced} = F(\vec{E}_{applied})$, the ICEK velocity changes in direction and value along the conducting sections of the Janus particle.

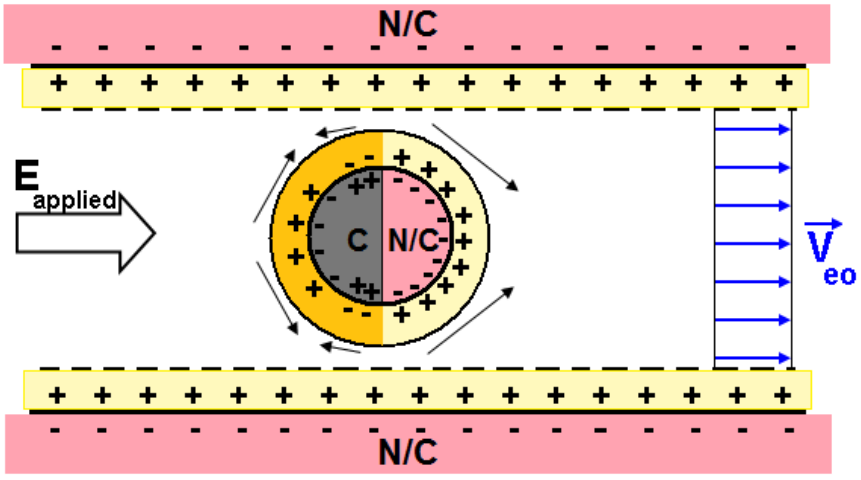


**Figure 2-6.** The electro-osmotic flow around a Janus Particle in a straight microchannel. The

[1] "Janus" is the name of Roman God who has two faces looking into opposite directions. In this study, a spherical Janus particle refers to a sphere with two hemispheres, with different conducting materials, connected to each other. One hemisphere is a fully conducting material (such as gold, aluminium, etc) and another hemisphere has non-conducting characteristics (such as polymer, glass, etc.).

arrows represent the direction of electro-osmotic velocity of the particle surface. "C" and N/C" represents conducting and non-conducting material respectively.

The charges on non-conducting hemisphere might be the opposite of the charges induced on the conducting section. Thus the sings of the induced EDL and EDL over the non-conducting section at the interface of two hemispheres change. As a result, the slip velocity on the non-conducting half will be in different direction than that of the conducting part. Different micro-vortices in opposite directions form near the solid-fluid interface due to these velocity variations. On the other hand electrophoretic motion of the particle is caused as a result of the interactions between applied electric field and induced-charge on the conducting hemisphere of this heterogeneous Janus particle as well as the interactions between applied electric field and electrostatic chargers of non-conducting hemisphere of the heterogeneous Janus particle. Figure 2-6 shows that electro-osmotic flow in the microchannel is caused by electrostatic charges on the non-conducting microchannel walls. The net velocity of the particle will be determined by the bulk fluid EOF, the electrophoretic motion of the particle, and the complex flow field (vortices) around the Janus particle. It will be more complicated once the heterogeneous Janus particle has not a regular pattern like the heterogeneous Janus particle where the conducting and non-conducting parts are hemispheres.

The electro-osmotic flow around the conducting section of a Janus particle has different values due to the variation of the local induced zeta potential. The value and direction of this electro-osmotic flow changes from location to location around the surface of the conducting particle. The sign and consequently the direction of this electro-osmotic velocity is opposite in specific locations. This resultant electrokinetic flow slips outside the electric double layer and varies proportionally to the local tangential electric field. Thus, the non-uniform electro-osmotic flow (vortex) results in vortices near the solid–liquid interface (as shown in Fig. 2-7).

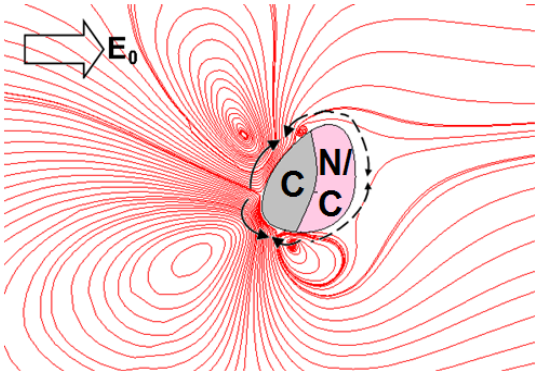


**Figure 2-7.** The induced vortices around a Janus Particle. The arrows represent the direction of electro-osmotic velocity of the particle surface. "C" and N/C" represents conducting and non-conducting material respectively.

## 2-6. Summary and Conclusions

In this chapter we introduced the electric double layer, zeta potential, classical electrokinetics and induced-charge electrokinetics. The shortcomings of the classical electrokinetics to be used in the electrokinetics studies of all particle types are highlighted. Induced-charge electrokinetics that is a new branch of the electrokinetic phenomena that deals with electric systems containing fully conducting materials was also introduced.

Studying the behaviour of a heterogeneous particle requires additional investigations. New techniques must be used to characterize the motion of a heterogeneous particle in a microchannel. To calculate the net velocity of a heterogeneous particle with arbitrary geometry in an irregularly shaped microchannel we used a complete 3D multi-physics numerical method which is set up based on the above mentioned equations. Our 3D numerical model simulates the electric field, the flow field and the motion of a heterogeneous particle for the first time. We studied the induced-zeta potential on a heterogeneous particle surface with an arbitrary geometry, and its effect on slip velocity on the particle surface. We used the moving grid technique to fulfill the particle-fluid simulation as described in the next section.

The governing equations dealing with such problems are discussed in details in the next chapter. In chapter 4 we will simulate the motion of a heterogeneous particle in a microchannel using (i) the three-dimensional method that was introduced in this chapter and (ii) the governing equations of electric field, flow field, concentration and forces applied to the particle (discussed in chapter 3). This simulation is disused in detail in chapter 4 and is verified by our experimental results in chapter 5. Using the numerical and experimental results presented in chapters 4 and 5, then, we conducted a number of numerical modeling of an induced-charge electrokinetic components, i.e. ICEK micro-valve (chapter 6), micro-mixer (chapter 7), and micro-motor (chapter 8).

## CHAPTER III: Methods

# Three dimensional Governing Equations

In chapter 2 it was described that when a conducting object is in contact with aqueous solution, once the electric field is applied, surface charges will be induced on the surface of the conducting object. The induced surface charges interact with the applied electric field and micro-vortices will be induced. Consider a heterogeneous particle with arbitrary shape that has one conducting section and one non-conducting section. Such a particle can freely move in a microchannel (see Figure 3-1) and two different streams of fluids will be dragged to the main microchannel by electro-osmotic flow once the DC electric field is applied from left to right. The motion of this heterogeneous particle is coupled with the (i) applied DC electric field, (ii) the time-dependent flow field, (iii) particle-fluids interaction, and (iv) the concentration of species of different fluids. The net velocity of the particle will be determined by the bulk fluid electro-osmotic force (EOF), the electrophoretic motion of the particle and, the complex flow field (vortices) around the heterogeneous particle. Three-dimensional numerical simulation of the motion of this particle requires solving the equations with the boundary conditions and initial conditions described as follows. The assumptions used in the system of equations for this project are listed in Table 3-1.

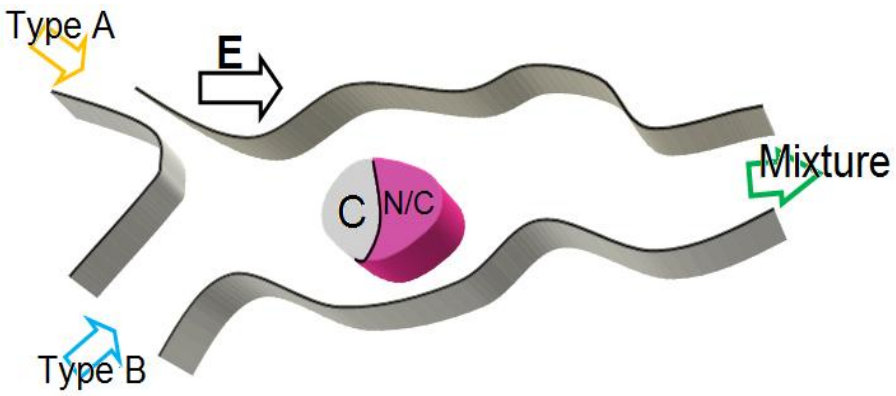


**Figure 3-1.** Schematic of an arbitrary geometry representing a microchannel inside which there is a moving heterogeneous particle. Two types of fluid streams are driven into the microchannel by the applied electric field and the mixture of these fluids leaves through the outlet. "C" represents the conducting material and "N/C" represents the non-conducting material and the DC electric field is applied from left to right.

**Table 3-1:** The list of assumption used for modeling and simulations

| **Assumptions:** |
|---|
| The Laplace's equation is valid in this study since the ionic concentrations in the outer region of the EDL are uniform and the local volume net charge density is zero. |
| A constant DC electric field is applied externally |
| Slipping flow boundary condition is valid based on thin[2] EDL. |
| The initial polarization process is fast enough (as an order of $\mathbf{10^{-4}s}$) to be neglected. |
| The non-conducting part of the particle is electrostatically charged. |
| The fully conducting part of the particle is initially electrically neutral. |
| The fully conducting part of the heterogeneous particle is completely polarized. |
| The fluid in the microchannel is considered as a Newtonian incompressible fluid. |
| The Holmholtz-Smoluchowski equation can be used for calculating the slip velocity. |
| The steady state condition is valid for induced-charge conducting sections of the heterogeneous particle. |
| The Debye length is negligible (in comparison with the size of the particle and the size of the microchannel). |

[2] As mentioned in chapter 2, the Debye length, 1/κ, is the characteristic thickness of EDL and is a function of the concentration of the electrolyte. As an example the range of Debye length for KCL solution, varies between 9.6nm at $10^{-3}M$ to 304.0nm at $10^{-6}M$. Also, the Debye length for pure water, varies between 3.0nm at $10^{-2}M$ to 304.0nm at $10^{-6}M$.

As discussed earlier, the induced electric double layer around the conducting particle acts like a shield in a very short time ($10^{-4}$s). Thus a conducting surface become like a non-conducting surface under the applied electric field in $10^{-4}$s . The only difference is that (i) a non-conducting surface has a fixed zeta potential on its surface and thus constant slip velocity on its boundaries. (ii) a conducting surface has variable zeta potential which is induced on the surface of the conducting surface. As a result the slipping velocity on the boundaries of a conducting surface is variable from one location to the other location. However, the Neumann boundary condition is valid for both conducting and non-conducting surfaces since the both acts similar with respect to applied electric field and fluid flow.

**3-1. DC Electric Field in a Dielectric Medium**

One of the fundamental equations to evaluate the distribution of electric potential in a dielectric medium is the Poisson equation

$$\nabla^2 \phi_e = \frac{\rho_e}{\varepsilon_0 \varepsilon} \tag{3-1}$$

where $\phi_e$ is the distribution of the applied electric potential, $\varepsilon_0$ and $\varepsilon$ are the dielectric constant in the vacuum and in the medium, respectively. The $\rho_e$ is the free charge density. Assuming there is no free charge (e.g. pure fluids, or electrically neutral aqueous solutions) then $\rho_e \approx 0$ and the Poisson equation becomes the Laplace's equation

$$\nabla^2 \phi_e = 0 \tag{3-2}$$

Thus the distribution of the applied electric potential, $\phi_e$ , in the fluid can be obtained by solving Laplace's equation. To solve Laplace's equation, as listed in Table 3-1, we assume that

the conducting section of the heterogeneous particle is completely polarized (fully conducting material) and this polarization happened fast enough to ignore the polarization (adjustment) period. Thus, a steady state induced dipolar electric double layer (EDL) forms on the fully conducting section of the heterogeneous particle. The boundary conditions subjected to this case are as follows

$\vec{n} \cdot \vec{\nabla} \phi = 0$ at channel wall and particle surface (3-3a)

$\phi = \phi_0$ at channel inlet(s) (3-3b)

$\phi = 0$ at channel outlet (3-3c)

where $\vec{n}$ is the unit normal vector pointing into the liquid phase.

**3-2. Flow Field**

We consider a Newtonian incompressible fluid continuously that flows in the microchannels. The continuity equation and the Navier-Stokes equation are the governing equations which are required to be solved to have the flow distribution in the microchannel.

$$\nabla \cdot \vec{U} = 0 \tag{3-4}$$

$$\rho \left[ \frac{\partial \vec{U}}{\partial t} + \vec{U} \cdot \vec{\nabla} \vec{U} \right] = -\vec{\nabla} P + \mu \nabla^2 \vec{U} + \vec{E} \rho_e \tag{3-5}$$

where $\mu$ and $\rho$ are the viscosity and density of the fluid, $\vec{U}$ is the velocity, and $\vec{\nabla} P$ is the pressure gradient. Since the Reynolds number for the fluid in micro-scales is less than one (Re<<1), the convection term at the left hand side of the momentum equation can be canceled; thus we can write Eq. (3-5) in the following format

$$\rho \frac{\partial \vec{U}}{\partial t} = -\vec{\nabla} P + \mu \nabla^2 \vec{U} + \vec{E} \rho_e \tag{3-6}$$

Considering a steady flow and no pressure driven force inside the EDL, the local net charge density is not zero. Thus, the driving force for electro-osmotic flow, $\vec{E}\rho_e$, exists only inside the EDL. For very thin EDL the driving force for electro-osmotic flow can be replaced by the slip boundary condition on the surface. The boundary conditions associated with our case are as follows

$\vec{n}\cdot\vec{\nabla}\vec{U}=0$ and $P=P_a$ at the inlet and outlets (3-7a)

$\vec{U}_{slip\_w}=-\frac{\varepsilon_0\varepsilon\zeta_w}{\mu}\vec{E}$ and $\vec{n}.\vec{\nabla}P=0$ at the microchannel wall (3-7b)

$\vec{U}_{slip\_N/C}=\vec{V}_p+\vec{\omega}_p\times\left(\vec{x}_p-\vec{X}_p\right)-\frac{\varepsilon_0\varepsilon\zeta_{p\_NC}}{\mu}\vec{E}$ at the non-conducting surface of the heterogeneous particle (3-7c)

and $\vec{n}.\vec{\nabla}P=0$

$\vec{U}_{slip\_C}=\vec{V}_p+\vec{\omega}_p\times\left(\vec{x}_p-\vec{X}_p\right)-\frac{\varepsilon_0\varepsilon\zeta_{induced}}{\mu}\vec{E}$ at the conducting surface of the heterogeneous particle (3-7d)

and $\vec{n}.\vec{\nabla}P=0$

where we consider the fluids in the microchannel are fully electrokinetically driven and there is no pressure gradient along the microchannel. $\vec{E}=-\vec{\nabla}\phi_e$ is the local applied electric field whose distribution is already calculated using Eq. (3-2). $\zeta_w$ and $\zeta_{p\_N/C}$ are the zeta potentials on the microchannel wall and on the non-conducting section of the heterogeneous particle respectively. The $\zeta_{induced}$ is the induced zeta potential on the conducting section of the heterogeneous particle which can be calculated using Eq. (2-8). $\vec{V}_p$ and $\vec{\omega}_p$ are the transitional and the rotational velocities of the heterogeneous particle respectively. The position vector on the surface of the

heterogeneous particle is represented by $\vec{x}_p$. The position vector of the center of the heterogeneous particle is shown with $\vec{X}_p$.

We are modeling the three-dimensional motion of the heterogeneous particle which is physically time-dependent. Consequently, the transient term in Eq. (3-6), $\partial\vec{U}/\partial t$, cannot be dropped. A fully coupled transient particle-fluid interaction strategy is used to simulate the influence of the bulk fluid flow on the motion of the heterogeneous particle, as well as the effect of the particle motion on the flow field.

### 3-3. Particle motion

The applied DC electric field exerts electrostatic force to the heterogeneous particle since the particle carries induced surface charges. In addition, hydrodynamic force is applied to the heterogeneous particle by the flow field. The resultant acting force on the heterogeneous particle is given by [113, 114]

$$\vec{F}_{total} = \vec{F}_E + \vec{F}_h \tag{3-8}$$

where $\vec{F}_E$ and $\vec{F}_h$ are electrostatic force and total hydrodynamic force respectively. The hydrodynamic force, includes two components [113, 114]

$$\vec{F}_h = \vec{F}_{h\_out} + \vec{F}_{h\_in} \tag{3-9}$$

where $\vec{F}_{h\_out}$ represents the hydrodynamic force acting on the heterogeneous particle by the fluid flow in the region outside and $\vec{F}_{h\_in}$ represents the hydrodynamic force inside the electrical double layer (EDL). In this study the electrical double layer is assumed to be very thin (Table 3-1). This assumption is valid when the Debye length is negligible in comparison with the size of the microchannel and the size of the heterogeneous particle. Ignoring this thin EDL, the flow

field in the region inside the electrical double layer ($\vec{F}_{h\_in}$) will not be considered and instead, the effect of the flow field inside the electrical double layer ($\vec{F}_{h\_in}$) is then substituted by the electro-osmotic velocity. This electro-osmotic velocity inside the EDL is then used as the slip boundary condition on the solid surface outside the electrical double layer.

On the other hand, the flow field around the heterogeneous particle is originated outside the EDL. This flow is subjected to slip boundary condition (as mentioned in section 3-2) at the surface of the heterogeneous particle. According to Chapter 2, the electrostatic force applied to the heterogeneous particle, $F_E$, is balanced by the hydrodynamic force ($\vec{F}_{h\_out}$) acting on the particle. This hydrodynamic force is produced by the fluid flow in the region outside EDL, The resultant force on the particle (Eq. (3-7)) is thus given by[113, 114]

$$\vec{F}_{total} = \vec{F}_E + \vec{F}_{h\_out} + \vec{F}_{h\_in} \quad and \quad \left|\vec{F}_E\right| = -\left|\vec{F}_{h\_in}\right| \tag{3-10}$$

thus

$$\vec{F}_{total} = \vec{F}_{h\_out} = \vec{G} - \oint_\Gamma \bar{\bar{\sigma}}_P .\vec{n}dS = (\rho - \rho_P)g\forall_P - \oint_\Gamma \bar{\bar{\sigma}}_P .\vec{n}dS \tag{3-10a}$$

where $g$ is the acceleration due to gravity, $\vec{G}$ is the total body force, $\forall_P$ is the volume of the particle and, $\rho_p$ is the density of the particle. The total torque acting on the particle is given by [113, 114]

$$\vec{T}_{net} = -\oint_\Gamma (\vec{x}_p - \vec{X}_p) \times (\bar{\bar{\sigma}}_P \cdot \vec{n})\mathrm{dS} \tag{3-11}$$

The stress tensor which is represented by $\sigma_p$ can be calculated using

$$\bar{\bar{\sigma}}_P = -p\bar{\bar{I}} + \mu\left[(\vec{\nabla}\vec{U}) + (\vec{\nabla}\vec{U})^T\right] \tag{3-12}$$

where $\bar{\bar{I}}$ is the identity tensor. The equations governing the particle motion are based on the Newton's second law and are given as follows

$$m_p \frac{\mathrm{d}\vec{V}_p}{\mathrm{d}t} = \vec{F}_{net} \tag{3-13}$$

$$J_p \frac{\mathrm{d}\vec{\omega}_p}{\mathrm{d}t} = \vec{T}_{net} \tag{3-14}$$

where $m_p$ is the mass of the heterogeneous particle, and $J_p$ is the moment of the heterogeneous particle. The displacement of the center of the heterogeneous particle can be calculated as follows

$$\frac{\mathrm{d}\vec{X}_p}{\mathrm{d}t} = \vec{V}_p \tag{3-15}$$

The initial conditions of the fluid velocity and the motion of the heterogeneous particle are set up as zero

$$\vec{V}_p\big|_{t=0} = 0,\ \vec{\omega}_p\big|_{t=0} = 0 \text{ and } \vec{u}\big|_{t=0} = 0 \tag{3-16}$$

### 3-4. Concentration Field

In this study the concentration field of different fluid streams is described by the concentration equation

$$\frac{\partial C_i}{\partial t} + \vec{U} \cdot \vec{\nabla} C_i = D_i \nabla^2 C_i \qquad \text{i=1,...,n} \tag{3-17}$$

where $C_i$ is the concentration of the fluid stream i and $D_i$ is its diffusion coefficient. The boundary conditions are

$$C = C_i^* \qquad \text{at inlet } i,\ \text{i=1,...,n} \tag{3-18a}$$

$$\left.\frac{\partial C_i}{\partial n}\right|_{t\geq 0} = 0 \qquad \text{at all the walls} \tag{3-18b}$$

and the initial concentration in the system is

$$C_i\big|_{t=0} = 0 \qquad \text{through the microchannel} \tag{3-19}$$

## 3-5. Summery and Conclusions

In this chapter the required governing equations to model the time dependent motion of a heterogeneous particle with an arbitrary geometry, in a microchannel under applied DC electric field are categorized. The initial and boundary conditions subjected to the corresponding equations are also defined for each system of equations. Using the governing equations described in this chapter and appropriate boundary conditions we will have a fully coupled transient particle-fluid interaction strategy. Using this system we can numerically model the interactions between the electric field, flow field and the motion of the heterogeneous particle.

In next chapters, first, we will numerically model the motion of a heterogeneous particle in a microchannel. The effects of the applied DC electric field, the size and the orientation of the particle on generation of the induced vortices and their size will be investigated. Then, in chapter 5, we will experimentally visualize the existence of the induced vortices near a conducting surface. We will also experimentally validate our numerical results. The last three chapters of this thesis will describe novel applications of induced-charge electrokinetics in microfluidics and Lab-on-a-chip (LOC) devises, i.e. ICEK micro-valve, ICEK micro-mixer, and ICEK micro-motor.

## CHAPTER IV: Induced-charge Electrokinetics

# Motion of Heterogeneous Particle: Transitional and Rotational

In chapter 2 we introduced the induced-charge electrokinetic phenomena and its characteristics. In Chapter 3 we explained the governing equations which are required to numerically simulate the induced-charge electrokinetic motion of a heterogeneous particle. In this chapter, using those equations and initial and boundary conditions we will model the motion of a heterogeneous particle with arbitrary shape in a microchannel under an applied DC electric field. The motion of the heterogeneous particle in the microchannel is numerically simulated using a complete 3-D multi-physics model. We used a spherical particle where one half of it is an ideally conducting material and the other half is a non-conducting (dielectric) material. This heterogeneous particle is called "Janus particle". The distribution of induced surface charge varies on the conducting hemisphere of the Janus particle. Under an externally applied DC electric field, these surface charges generate induced micro-vortices in the fluid. In this chapter we compared the effects of micro-vortices on the motion of the Janus particle. The effects of size and orientation of the Janus particle, the electrical field as well as the zeta potential of the non-conducting part on the motion of Janus particle are also investigated.

**4-1. Geometry and Computational Domain**

Transitional and rotational motion of a spherical Janus particle is investigated in this chapter. The Janus particle, with diameter $D_p$ , is suspended initially at $x = 3 \times D_p$ , $y = 1.5 \times D_p$, and $z = 1.5 \times D_p$ in a microchannel whose length, width and height are $L = 15 \times D_p$ , $W = H = 2 \times D_p$ respectively. The system is symmetrical with respect to z-plane and y-plane. As shown in Figure 4-1 the origin of the coordinate system is chosen to be the point O. The wall parallel to the x-plane in the upstream of the system is defined as the inlet while the wall in the downstream is selected to be the outlet. Both the inlet and the outlet are defined as open boundaries; thus, there is no pressure gradient along the length of the microchannel. The electrolyte that completely fills the microchannel is water with density of 998(kg/m$^3$), viscosity of $0.9 \times 10^{-3}$(kg/m.s), dielectric constant of $\varepsilon = 80$, and regular permittivity of vacuum $\varepsilon_0 = 8.854 \times 10^{-12}$(C/V.m). To avoid the gravity effects we have considered the density of the particle to be equal to the density of the electrolyte. DC electric field is applied from left to right through the microchannel to agitate the electro-osmotic motion of the electrolyte and electrophoretic motion of the particle. The non-conducting hemisphere of the Janus particle ($\zeta_P = -60\,mV$) and the microchannel walls ($\zeta_w = -15\,mV$ ) are considered to carry a constant zeta potential since they have uniformed negative electric charges.

Our computational domain is fully covered by unstructured three-dimensional tetra meshes to increase the accuracy of the simulation. Using the commercial software FLUENT 12 and visual C to run the prepared UDF (User-Defined Function) file, we could simulate the motion of the Janus particle in the microchannel. The UDF file was written for solving the particle motion in three-dimensions using a moving grid technique to model the interaction between the fluid and the particle and the generation of micro-vortices in a coupled multi-physics system under

different conditions. For the purpose of this study we developed the UDF file (written by Wu and Gao [34]) to be able to simulate the local electric field around a heterogeneous particle in a microchannel and solve the motion of heterogeneous particle (some parts conducting some parts non-conducing) in the computational domain. Conducting grid independency method, the total number of cells (that gave accurate results, independent of the number and size of the cells, while minimizing the required computational time and CPU) converged to 217647 cells.

Since the particle moves in the microchannel the mesh will be deformed after a while. To avoid the error and non-physical results we used the re-meshing option of the dynamic mesh module of the FUENT. We activated the "Smoothing" and "Re-meshing" options, to let the FLUENT automatically refresh the stretched meshes while the particle is moving. In addition to this preparation, at some steps, it was required to stop the run and manually re-mesh the system. Then continue the program from the last location of the particle.

The development length of a laminar flow in our microchannel can be calculated by [115]

$$L_{development} = 0.06 \times \mathrm{Re} \times W \tag{4-1}$$

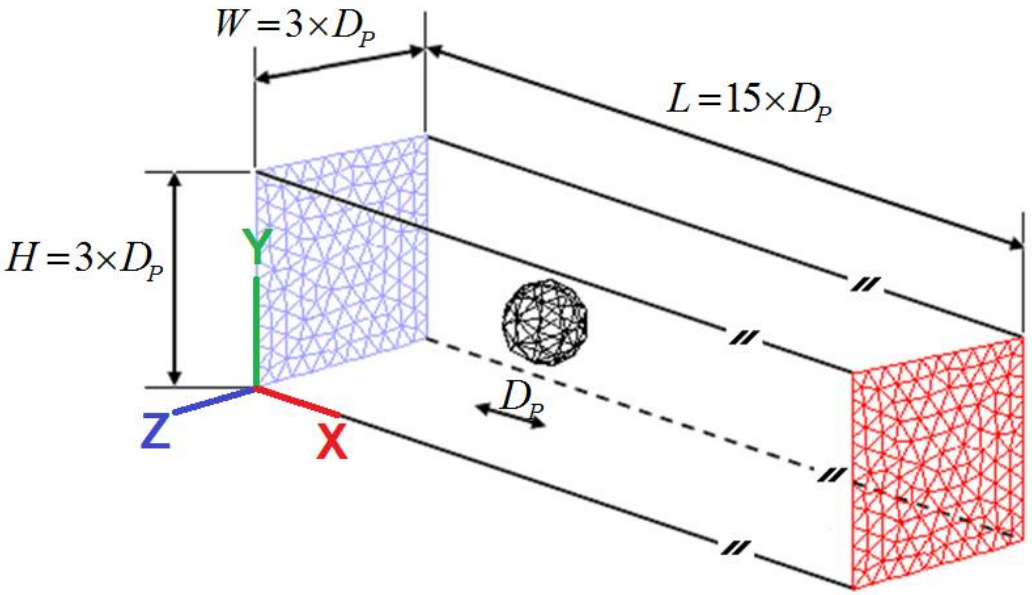


**Figure 4-1.** Schematic computational domain, Janus particle is suspended in a microchannel

Where $L_{development}$ is the development length of the flow, Re is the Reynolds number and W is the weight of the microchannel. For A microchannel described in Figure 4-1 we can calculate the Reynolds number as follow

$$\mathrm{Re} = \rho u_{eo} L_R / \mu \qquad (4\text{-}2)$$

Where $r$ is the fluid density, $u_{eo}$ is the electro-osmotic velocity of the flow, $L_R$ is the most relevant length scale, $\mu$ is the viscosity, for many microchannels, $L_R$ is equal to

$$L_R = 4A / P_{wetted} \qquad (4\text{-}3)$$

4A/P where A is the cross sectional area of the channel and $P_{wetted}$ is the wetted perimeter of the channel. For the microchannel of Figure 4-1 the length scale is equal to $L_R = 4\times(2D_p)^2/(4D_p) = 4D_p$ . The electro-osmotic velocity of this geometry (Figure 4-1) can be calculated using Eq.(2-3); when the applied electric field is 30V/cm and zeta potential on the microchannel walls is 15mV. The electro-osmotic velocity of above mentioned microchannel is in x direction

$$\vec{u}_{eo} = \frac{\varepsilon \varepsilon_0 \zeta_w}{\mu}\vec{E} = \left(\frac{80\times 8.54\times 10^{-12}\times 15\times 10^{-3}}{10^{-3}}\times 30\times 10^2\right)\vec{e}_1 = 3.07\times 10^{-5}\,\vec{e}_1 \quad (m/s) \qquad (4\text{-}4)$$

where $\vec{e}_1 = (1,0,0)$, is the unit vector in x direction. Knowing the values of electro-osmotic velocity and length scale and substituting them in Eq.(4-2), the Reynolds number can be calculated as $\mathrm{Re} = \frac{\rho u_{eo} L_R}{\mu} = \frac{998\times 3.07\times 10^{-5}\times 4\times 20\times 10^{-6}}{0.9\times 10^{-3}} = 27.23\times 10^{-2}$ while $\rho = 998(Kg/m^3)$ , $D_p = 20\mu m$, , and $\mu = 0.9\times 10^{-3}\,(Kg.m^{-1}.s^{-1})$. Thus**,** the developed length scale for this microchannel, using Eq. (4-1) is

$$L_{development} = 0.06 \times \mathrm{Re} \times W = 0.06 \times 27.23 \times 10^{-2} \times 2D_p = 0.654 \times 10^{-6} \ (m) \quad (4\text{-}5)$$

This means that the developing length for a microchannel with weight of $40\mu m$ is only $0.654\mu m$ which is negligible compare to the length of this microchannel ($300\mu m$).

The distribution the electric field in the computational domain is calculated using Laplace equation (Eq. (3-2)). The boundary conditions subjected to this study for Laplace equation are Eq. (3-3a, b, and c). The continuity condition is valid all over the microchannel domain (Eq. (3-4)). To solve the Navier-Stokes Equation (Eq. (3-5)) we used the boundary conditions which mentioned in chapter 3 as follow: Eq. (3-6a to d) which present the no-gradient pressure in the microchannel when the inlet and lout let of the microchannel have the same constant value of $P=P_a$. The Walls are not permeable to fluid therefore there is no fluid flux perpendicular to the microchannel walls and surface of the particle. The Helmholtz-Smoluchowski relation is valid on the microchannel walls and the non-conducting surface of the particle. The slipping velocity on the conducting surface of the particle is calculated base on the numerical simulation of the induced-zeta potential on the surface.

**4-2. Three-Dimensional Numerical Simulation**

Using the equations presented in chapter 2 and 3, the zeta potential around a spherical Janus particle can be calculated. As a result of variable local electric field, and thus the non-uniform induced zeta potential, the fluid motion on the conducting hemisphere will also be non-uniform and in opposite directions. Consequently, the vortexes will be indeed near the conducting hemisphere. The three-dimensional streamlines in a microchannel (presented in Figure 4-1) and around a non-conducting particle and a Janus particle is shown in Figure 4-2.

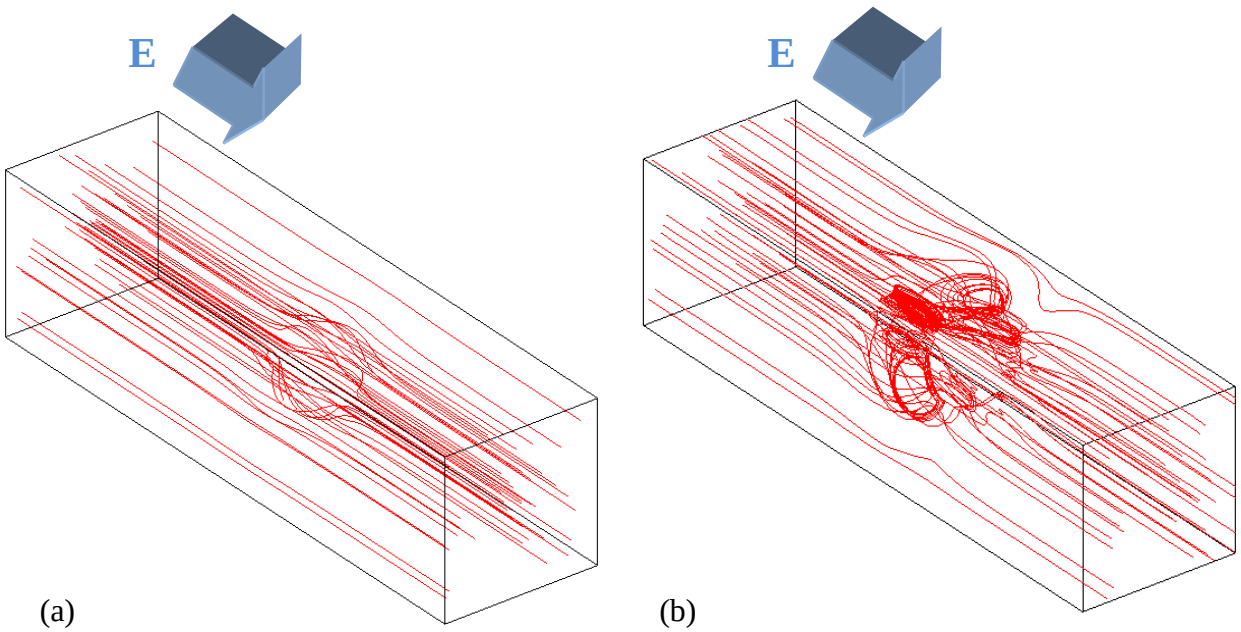


**Figure 4.2.** 3D streamlines in a straight microchannel with a (a) non-conducting particle, (b) Janus particle suspended in the middle of this microchannel. Vortices are induced around the conducting hemisphere of the Janus particle. The particle of $D_p$=20μm suspended in a microchannel. The zeta potential on the microchannel wall is -15 mV. A uniform zeta potential of -60mV on the non-conducting surfaces of non-conducting sphere and Janus particle. The DC electric field of E=30V/cm is applied from left to write. The conducting hemisphere of the Janus particle faces the upstream of the fluid. The electro-osmotic flow is from left to right.

### 4-3. Induced Micro-Vortex Generation and Motion of a Janus Particle

Using the governing equations mentioned in chapter 3 subjected to appropriate boundary conditions; we could numerically study the induced-charge electrokinetic phenomena and the behavior of a Janus particle under an applied DC electric field.

To understand the behavior of each particle type under the applied DC electric field, we have conducted three different simulations where (i) a non-conducting particle, (ii) a conducting particle, and (iii) a Janus particle are involved. We used the exact same initial and boundary conditions for all three cases, to make the results comparable. The flow fields around the spherical particles are shown in Figure 4-3.

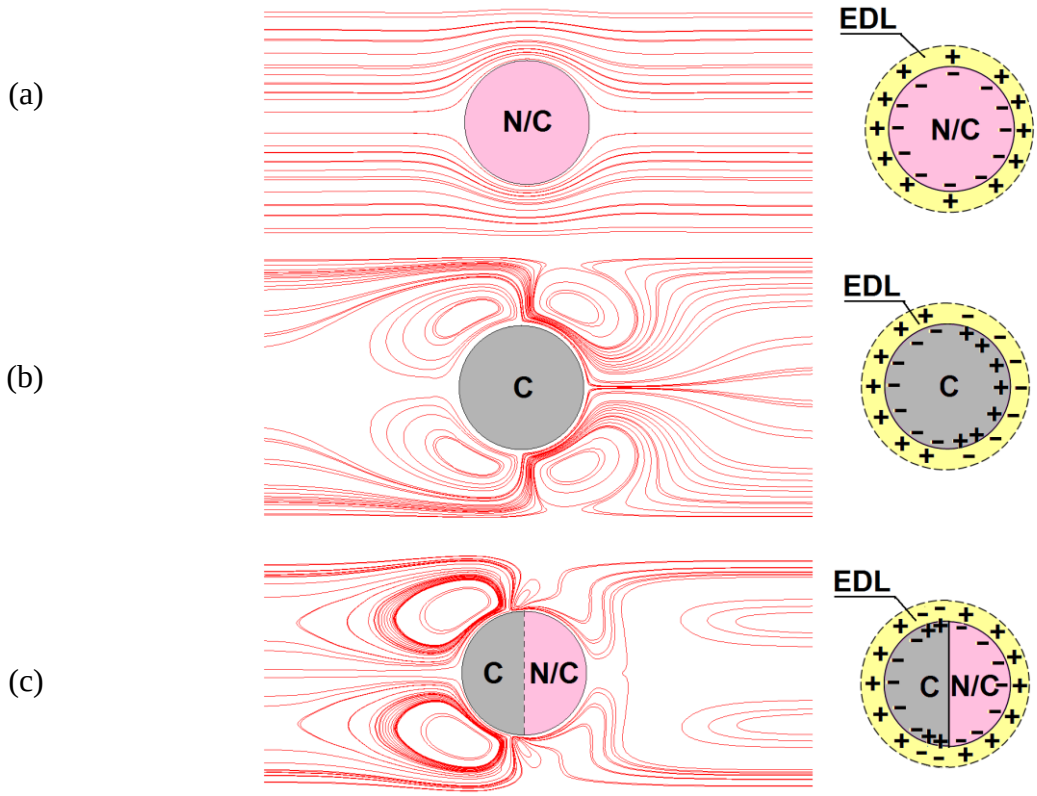


**Figure 4-3.** Electrokinetic Flow pattern around (a) non-conducting (b) fully conducting (c) Janus particle; sphere with $D_p$=20μm suspended in a microchannel. The zeta potential on the microchannel wall is -15 mV. A uniform zeta potential of -60mV on the non-conducting surfaces of non-conducting sphere and Janus particle. The DC electric field of E=30V/cm is applied from left to write. "C": conducting material and "N/C": non-conducting material.

In the case of non-conducting sphere, the zeta potential at any point on the surface of the particle is uniform and constant. Thus the streamlines smoothly follow the surface of the non-conducting particle and pass it without distortion (Figure 4-3a). Four vortices are induced around the fully conducting particle once the external DC electric field is applied (Figure 4-3b). This is the result of forming EDL around the conducting particle and non-uniform induced zeta potential on the surface of the particle; thus, the direction of the flow changes along the conducting particle and consequently four vortices are induced around the particle. This will be experimentally validated in the next chapter (chapter 5) where we will experimentally visualize these four induced micro-vortices around a fully conducting spherical particle. Similarly, four

vortices on the conducting hemisphere of a Janus particle are induced once the DC electric field is applied (Figure 4-3c). The EDL formed around the Janus particle consisted of a large portion of positive charges (which is responsible for two big vortices) and a small portion of negative charges on conducting side of the Janus particle. Meanwhile, the non-conducting hemisphere of Janus particle of our study is considered a dielectric material with constant negative charge; thus, the net charge in EDL on the non-conducting section of the Janus particle has positive sign. Since the net charge in the EDL of the non-conducting part has the opposite sign to the net charge in the EDL on the conducting part, this difference causes two other vortices on the conducting part near the interface of the two hemispheres. This figure shows that even small change on particle property (conducting / non-conducting) will changes the electrokinetic pattern of the flow around the particle. The deformed streamlines produce vortices with opposite rotation.

As Figure 4-3 shows the upstream of conducting particle and Janus particle are pretty the same since at theta=180 for both of these cases the conducting hemispheres are faced to the electric field (similar cases); and vortices are formed around the conducting section. However the pattern of vortices for conducting particle and Janus particle is different when theta gets close to 90 degrees (270 degrees). Since we have two small vortices about 100degrees (260degrees) and we now that the fluid flow is continuous; thus the flow pattern on the non-conducting section of the Janus particle first disturbed by those small vortices and then followed the solid boundaries of the non-conducting hemisphere. Obviously, the flow pattern at the downstream of this Janus particle is different from the flow pattern at the theta=0 of the non-conducting sphere; while the flow smoothly followed the boundaries of non-conducting sphere once reached it and passed this sphere in the absence of any external distortion.

We have investigated the effects of induced vortices around a spherical particle on the motion of the particle. Results of simulating the motion of the (i) non-conducting sphere (ii) conducting

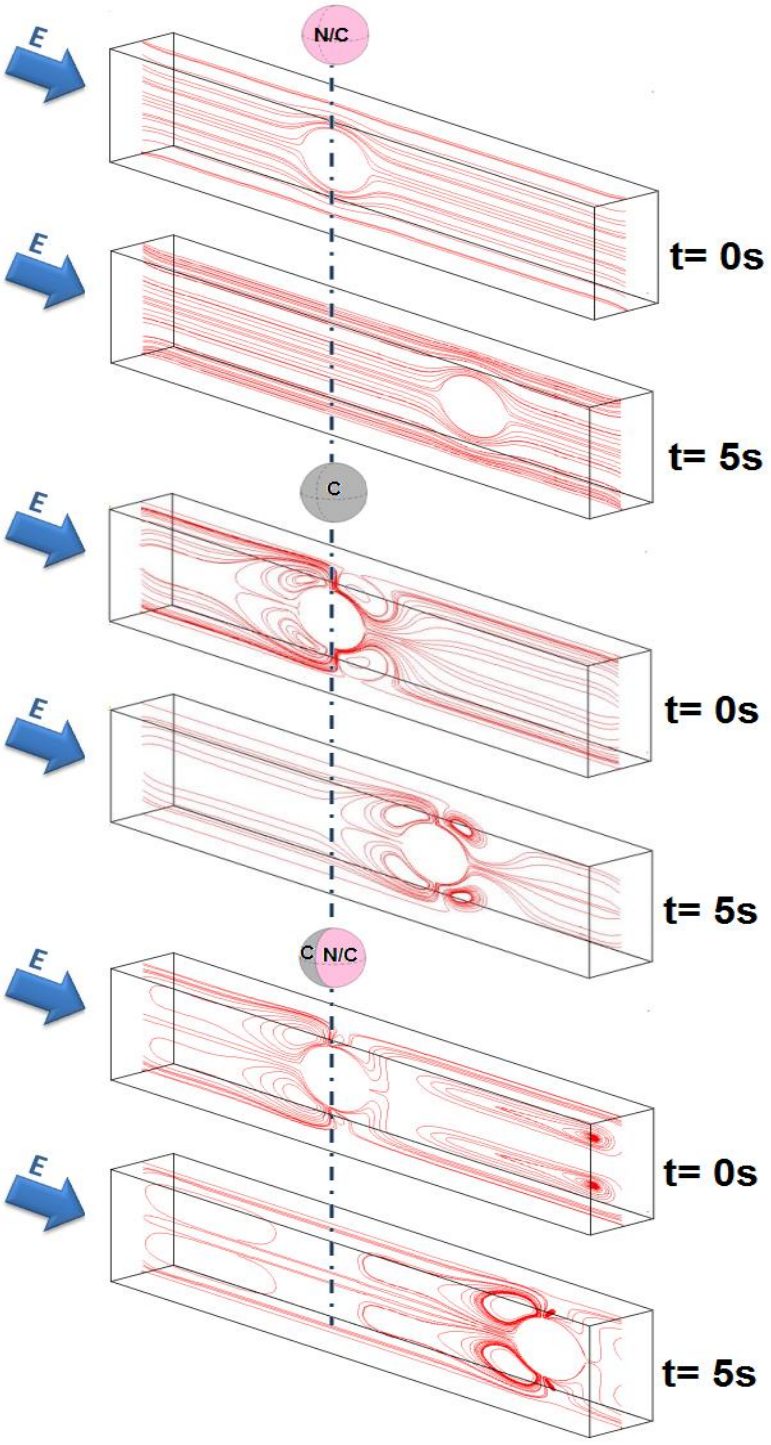


**Figure 4-4.** Three dimensional steady-state electrophoretic motions of a non-conducting particle, a fully conducting particle, and a Janus particle for a period of 5sec. For all cases the zeta potential on the microchannel walls is chosen -15mV and on the non-conducting surface of the particle is -60mV. The DC electric field of E=30V/cm is applied from left to write. "C" and "N/C" represent conducting and non-conducting material respectively.

sphere and (iii) Janus particle in a straight microchannel are illustrated in Figure 4-4. Comparing the motion of these three particle types under the same conditions we realized that the Janus particle moves faster than the other two and the conducting particle is the slowest of the three particles. These three particles are releases from the same initial position and exactly the same DC electric field is applied to generate electro-osmotic flow, electrophoretic motion and induced vortices. After 5second the destination of the Janus particle - whose conducting section faces the positive voltage - is further in comparison to the other two particles. It seems the two big vortices around the Janus particle act like an engine and boosts the displacement of the Janus particle. In the next chapter we will experimentally validate the numerical results presented in this section. It will be shown that the Janus particle moves much faster in comparison with the non-conducting particle.

We have conducted an investigation of the velocity of the particle with respect to the applied DC electric field. According to Figure 4-5 the non-conducting particle has a direct and linear relationship with different magnitudes of the applied DC electric field. The graph which represents the velocity of a 20μm non-conducting sphere in a microchannel follows the classical electrokinetic theory. The Janus particle moves faster than the two other particle types while its conducting section faces the positive voltage of current system. Both Janus particle and fully conducting particle plots clearly show that the classical electrokinetics theory is no longer valid when conducting materials are engaged in an electrokinetic system. Thus, the induced-charge electrokinetic has a nonlinear relation with the applied electric field.

Figure 4-6 shows the net applied forces to a 20μm non-conducting particle and the same size Janus particle for different values of external DC electric fields. This net force is caused by electro-osmotic force and electrophoretic motion of the particle; also in case on conducting

particle the force generated by the complicated flow pattern (vortices) will be added to the system. Figure 4-6 shows that the non confuting particle moves slower than a Janus particle since the applied forces to a Janus particle is much stronger. Also increasing the electric field will increase the strength of net applied forces to both types of particle.

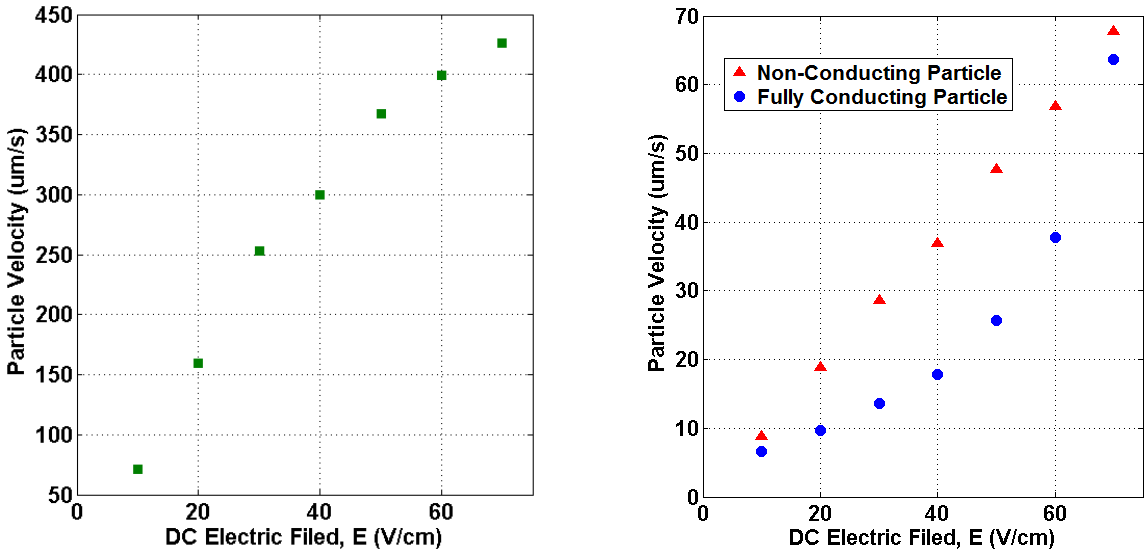


**Figure 4-5.** The relationship between the velocity of different types of particles and the applied DC eclectic fields, 20µm in diameter (a) Janus particles and (b) non-conducting and fully conducting particles.

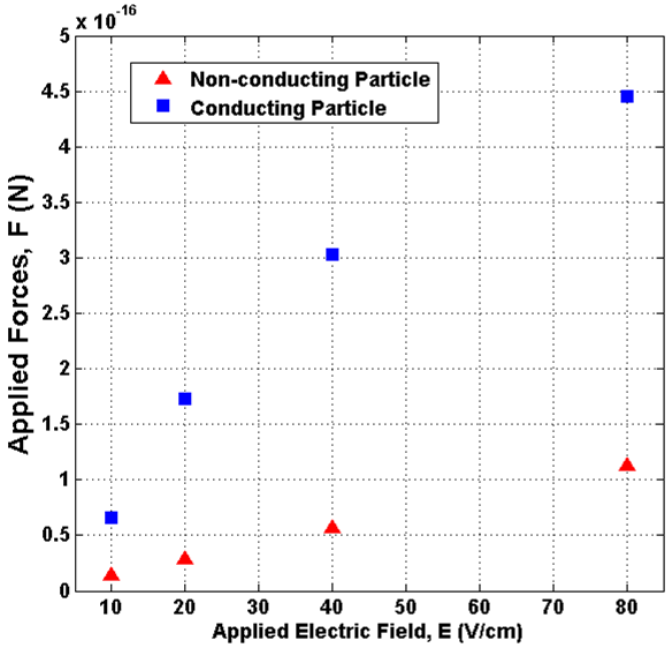


**Figure 4-6.** The relationship between the net applied forces to the different types of particles and the applied DC eclectic fields, 20µm in diameter Janus particles and non-conducting and fully conducting particles.

Effect of the size of the Janus particle on its transitional motion is investigated using two different size Janus particles. The conducting hemispheres of both Janus particles are facing the positive voltage. The diameter of one of the Janus particles is half of the other one. Applying the DC electric field one can clearly see that the Janus particle with larger diameter moves faster than the smaller Janus particle in the same period of time (Figure 4-7). This can be explained by considering the origin of the ICEP velocity. Under the same conditions the local electric field strength in the gap between the Janus particle surface and microchannel wall has an inverse relationship with the size of this gap. The larger Janus particle blocks a larger portion of the flow channel; thus the gap in this case is smaller. Consequently, the local electric field in the smaller gap region is stronger. Therefore, the driving force for the larger Janus particle is stronger and the bigger Janus particle is pushed forward faster. On top of that, the larger Janus particle has

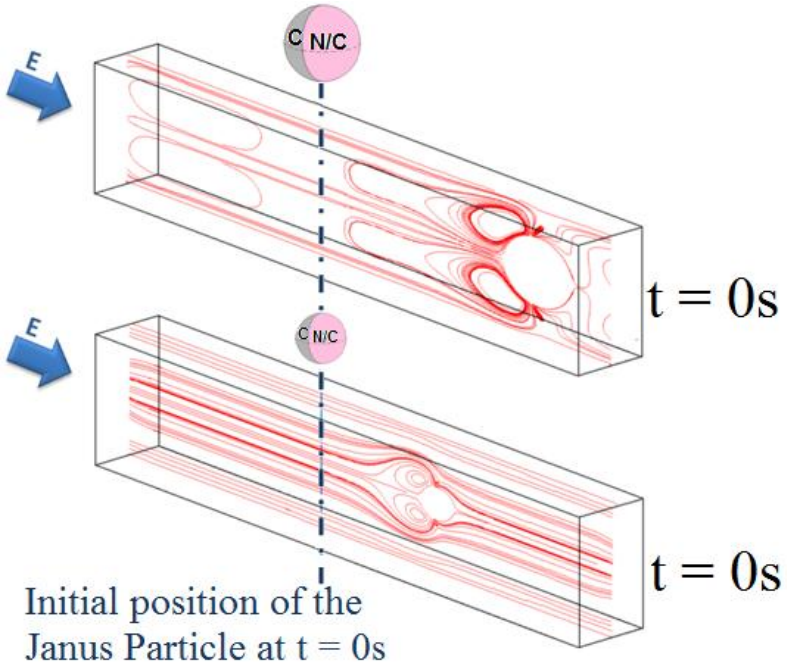


**Figure 4-7.** Three dimensional steady-state electrophoretic motion of two different size Janus particles. The diameter of larger Janus particle is $D_p$=20μm and the diameter of small Janus particle is $D_p/2$=10μm. For all cases the zeta potential on the microchannel walls is chosen $\zeta_w = -15mV$ and on the $\zeta_{p\_N/C} = -60mV$. The DC electric field of E=30V/cm is applied from left to write. "C" and "N/C" represent conducting and non-conducting material respectively.

larger conducting hemisphere which means there are more charges inside the conducting section to be polarized by the external electric field once the DC electric field is applied. The excess charges have more surface area to migrate under the conducting surface skin; and consequently affect the electric body forces. Stronger vortices will generate as a result of that and push the larger Janus particle to move faster than the smaller one.

### 4-4. Different Orientation of a Janus particle and its 3-Dimensional Transitional Motion

Consider two Janus particles that are exactly the same but oriented in opposite directions: the conducting hemisphere of one of them is facing the right hand side of the microchannel (case A) while that of the other Janus particle is facing the left hand side (case B). Both Janus particles are released at the same initial position in the microchannels. Once the DC electric field is applied the vortices induce around the conducting section of each particle and push the particle to move. Thus, the Janus particle of case B is pushed to move forward in the downstream of the

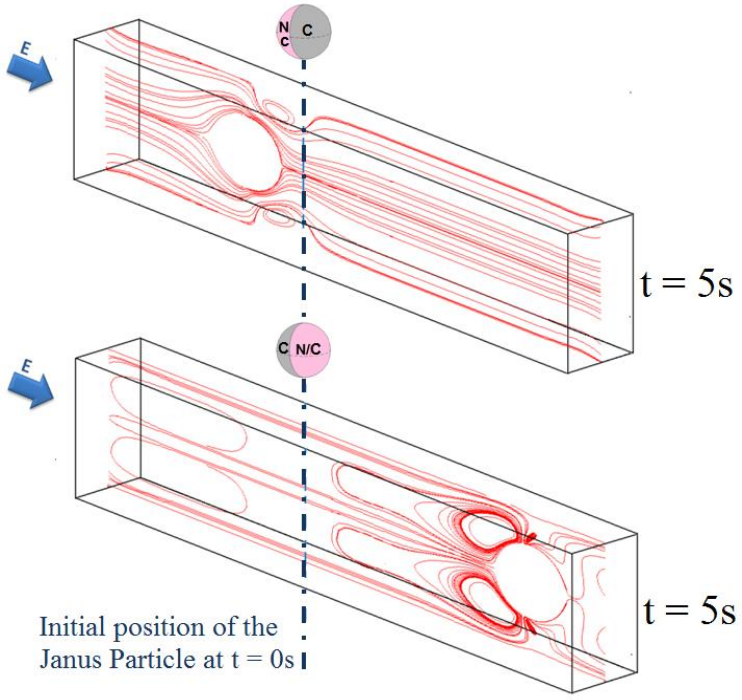


◄ **Figure 4-8.** Three-dimensional electrokinetic motion of two Janus particles in opposite directions (a) conducting part facing downstream (b) conducting part facing upstream. The Janus diameter of both particles are $D_p$=20μm. For both cases $\zeta_w = -15mV$ and $\zeta_{p\_N/C} = -60mV$. A DC electric field (E=30V/cm) is applied from left to write. "N/C" and "C" represent non-conducting and conducting materials respectively.

system (from left to right). While, the induced vortices on the conducting surface of the Janus particle of case A push the particle to move in the opposite direction of the electro-osmotic flow towards the upstream of the flow. However, as Figure 4-8 shows the Janus particle moves faster in case B than in case A. This means the orientation of the Janus particle plays an important role in the particle motion, direction, and speed. This is experimentally investigated in chapter 5 and it is shown that Janus particles in different orientations move in opposite directions.

### 4-5. The Effect of Zeta positional of Non-Conducting Hemisphere

To investigate the effect of the zeta positional of the non-conducting hemisphere on the motion of the Janus particle we have considered three similar Janus particles with the same size but different zeta potentials on the non-conducting section, $\zeta_p$. Figure 4-9 represents the electrokinetic flow pattern around the Janus particles with different zeta potential values (i) $\zeta_p = -15\text{mV}$ (ii) $\zeta_p = -60\text{mV}$ and (iii) $\zeta_p = -90\text{mV}$ on non-conducting sections of the sphere. The vortex size has a direct relation with the zeta potential, $\zeta_p$; since only two big vortices in front of the Janus particle is visible when the $\zeta_p = -15\text{mV}$ and it is difficult to see the two other small vortices, near the interface of the non-conducting and conducting hemispheres. As discussed in Figure 4-2c, the charge sign along the electric double layer around the Janus particle varies three times. The EDL sign is positive (refer to Figure 4-2c) at theta=0(rad) and this sign will change to negative when getting close to the interface of the two hemispheres; again, the negative sign will be positive on the non-conducting hemisphere. This sign change along the EDL around the Janus particle causes vortices in opposite directions with various strengths. Increasing the zeta potential on the non-conducting hemisphere of a Janus particle, $\zeta_p$, amplifies

the opposite forces near the interface of conducting and non-conducting hemispheres. Consequently a bigger and stronger vortex forms at this region. This demonstrates that the electrostatic charge (zeta potential) of the non-conducting hemisphere of the Janus particle has significant influence on the flow field pattern and the vortices around the Janus particle. Figure 4-9 shows that higher $\zeta_p$ will resulted in larger size and stronger induced vortices.

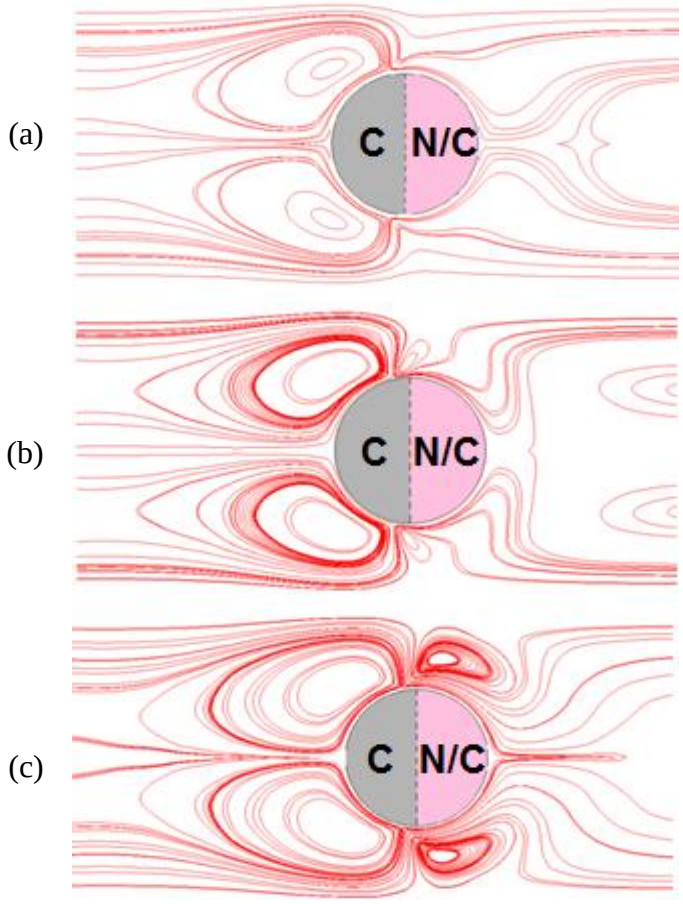


**Figure 4-9.** The effect of the electrostatic charge (zeta potential) of the non-conducting hemisphere of the Janus particle on flow field pattern and vortices' size (a) $\zeta_{p\_N/C} = -15\text{mV}$ (b) $\zeta_{p\_N/C} = -60\text{mV}$ (c) $\zeta_{p\_N/C} = -90\text{mV}$. The diameter of the Janus particles is $D_p$=20μm. The zeta potential on the microchannel wall is -15 mV. The DC electric field (E=30V/cm) is applied from left to write. "C" and "N/C" represent conducting and non-conducting materials respectively.

### 4-6. the Effect of Conducting Portion of Heterogeneous Particle

As mentioned in section 4-5 the size of the conducting section has a significant effect on the motion of the Janus particle. To investigate this effect in this section we compared two spherical heterogeneous particles where the ratio of the conducting section to the non-conducting section for each one is as follows: (i) case A: Janus particle: 1:1 (ii) case B: 1:3. Figure 4-10 demonstrates that in case B where only a quarter of the sphere is conductive the induced vortices around this section are smaller and weaker than case A (Janus Particle). Consequently the motion of particle in case B is slower in comparison with a spherical Janus particle. A close look at the vortex region demonstrates that the small vortices close to the interface of conducting and non-conducting sections for case A are bigger than case B. The force balance in the electric double layer explains this fact. Since the zeta potential on the non-conducting surface of the particles are the same, when the bigger vortices at the upstream of the particle become weaker, less opposite force is required to balance the total force in EDL. Thus, the second pair of vortices close to the interface shrinks and become smaller in case B.

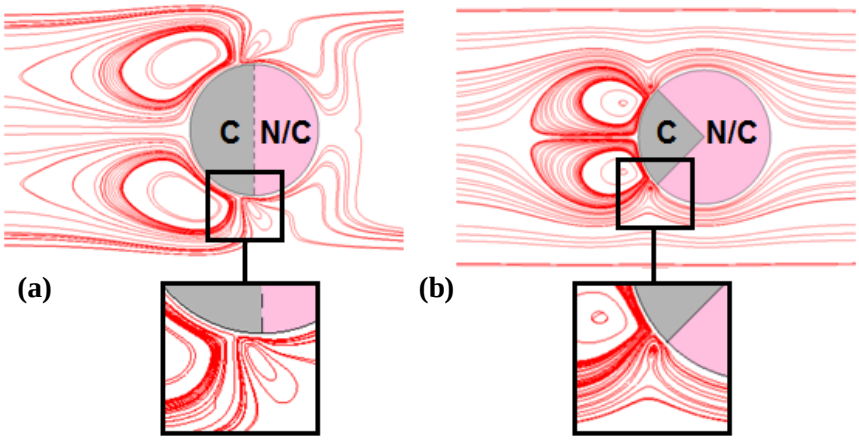


**Figure 4-10.** Vortex size around heterogeneous particles with different proportions of the conducting material. The ratios of the conducting section to the non-conducting section are (a) 1:1 (case A), (b) 1:3 (case B). Both particles have the same diameters, $D_p$=20µm. All other conditions are the same. The zeta potential on the microchannel wall is -15 mV. The DC electric field of E=30V/cm is applied from left to write. "C": conducting and "N/C":Non-conducting.

## 4-7. Alignment and Rotational Motion of a Janus Particle

Up to this step, we assumed the interface surface of the two hemispheres of a spherical Janus particle is perpendicular to the direction of the applied DC electric field. Based on this assumption the Janus particle only has a transitional motion towards the downstream or upstream of the fluid depending on the initial orientation of Janus particle (for more information please refer to section 4-4). However, when the normal vector to the interface of two hemispheres of a spherical Janus particle has a non-zero angle with respect to the direction of the applied DC electric field, the Janus particle rotates to align itself due to the electric field force. Consider a spherical Janus particle whose normal vector has 90 degree angle with the positive direction of the applied DC electric field (Figure 4-11b, t=0s). Two vortices are formed around the conducting hemisphere (facing the top wall of the microchannel) and generate complex fluid flow; while the electro-osmotic flow passes the non-conducting section of Janus particle smoothly at the bottom of the sphere. Due to the unbalanced forces at the top and bottom of the sphere the Janus particle rotates to balance the forces. The size and the position of the vortices change as the particle rotates. The creation of the vortices is because the local electric field on the conducting surface changes; and the induced dipolar EDL also changes due to the variation of the local electric field. The Janus particle has small transitional motion while it is rotating to align itself. Once the applied forces to the surface of this hemisphere become balanced, the Janus particle does not rotate any longer. This is the stable position for Janus particle and after that the particle continues its transitional motion as long as the DC electric field is applied.

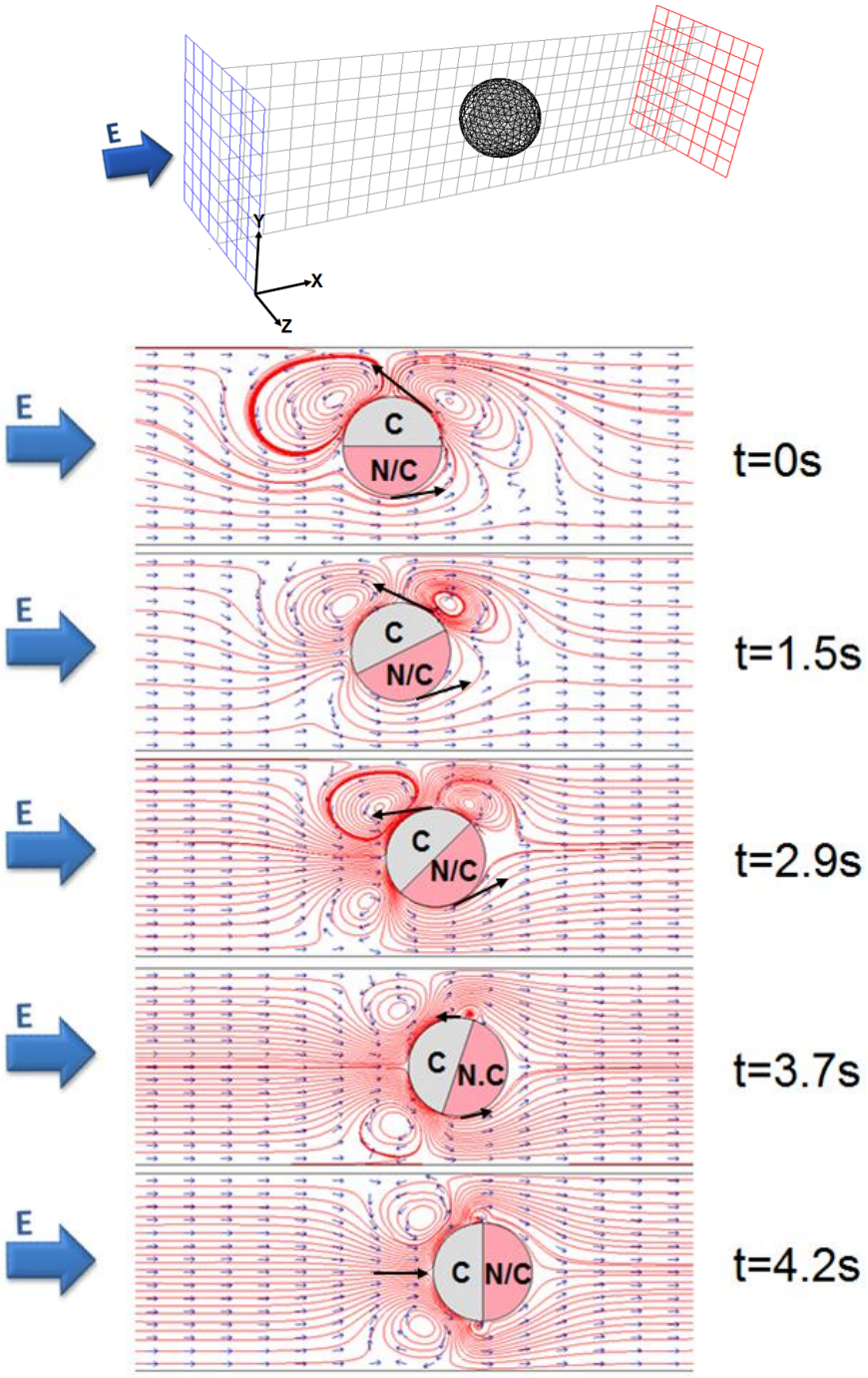


**Figure 4-11.** Three-dimensional rotational and transitional motion of a Janus particle in a straight microchannel for a 90 degree alignment movement. Streamlines and arrows show the flow pattern and flow direction in the microchannel around the Janus particle. The Janus particles diameter is $D_p$=20µm. The length of microchannel is 200µm and the dimension of the channel cross-section is W=H=40µm. The zeta potential on the microchannel wall and on the non-conducting sections of the Janus particle is -50 mV. The DC electric field of E=50V/cm is applied from left to write. "C" and "N/C" represent conducting and non-conducting materials respectively. The arrows represent the net forces applied to each hemisphere of the Janus Particle.

## 4-8. Summery and Conclusions

Induced-charge electrokinetic (ICEK) phenomenon is numerically investigated in this chapter. The induced-charge electrokinetics deals with the interaction of applied electric field with its induced-charge on conducting materials. We have numerically demonstrated that vortices forms around conducting surfaces in contact with aqueous solution under the applied electric field. According to our numerical results the induced-charge and the induced zeta potential have direct relation with the applied electric field but not linear relation like classical electrokinetic theory. Three-dimensional electrokinetic (transitional and rotational) motion of a heterogeneous particle in a microchannel is numerically modeled in this chapter. Results show that induced vortices have a significant role in motion of heterogeneous particles:

- Janus particles move faster than non-conducting spheres or fully conducting particles under the same condition.
- The bigger the Janus particle is the faster the motion of the particle.
- The orientation of the Janus particle is critical in direction of its transitional motion.
- The Janus particle rotates to align itself with the direction of applied DC electric field.

The induced vortices act like engine and boost the transitional motion of the heterogeneous particle or its rotational movement to reach its stable condition.

We will experimentally investigate the induced-charge electrokinetic phenomena in chapter 5. The induced vortices around a fully conducting sphere will be experimentally visualized in the next chapter. We will also compare the velocities of Janus particles and non-conducting particles experimentally and show that the orientation of the Janus particles affect the indirection of their motion. In chapter 6 we will introduce a new application for ICEK in microfluidic devises, i.e., ICEK micro-valve for flow regulation and control. In chapter 7 a novel ICEK micro-mixer will

be numerically simulated. This ICEK micro-mixer with 100% performance provides a fully homogeneous mixture at the downstream of the system. The last chapter will numerically and experimentally investigate the functionality of a non-stop ICEK micro-motor which is driven electrokinetically. This ICEK micro-motor results from using a triangular heterogeneous particle with a specific design under applied DC electric field which rotates as long as the electric field is applied.

# CHAPTER V: Experimental Validation

## Experimental Visualization of Induced-charge Electrokinetic Phenomena

Vortex induces around a conducting surface (which is in contact with aqueous solution and is under an applied electric field). Induced vortices are the main characteristic of induced-charge phenomenon. The interaction between the applied electric field and the induced EDL around the conducting particle, induces vortices which can disturb the flow pattern around the conducting surface and make the particle (with conducting surface) move. The existence of these vortices was numerically predicted [34, 35, 108, 116]. However, very few experimental evidences of their existence have since been reported, particularly when a non-electrode conducting objects is involved and a DC electric field is applied. According to the literature, the AC field was/is the most common agitating force for induced-charge electrokinetic experiments. Moreover, former studies had mostly reported the vortices around active electrode, used as a conducting surface. For the first time we have shown that four vortices form around a spherical conducting particle which is "not an active electrode" under a DC electric field. Our experimental results show that there is a significant difference between the motions of a Janus particle when a DC electric field is involved compared to the cases where an AC electric field is applied. Our results demonstrate that a Janus particle moves faster than a non-conducting (polymer) particle under the same experimental conditions. The induced vortices that will be visualized in this chapter can be used

in many critical aspects of electrokinetic microfluidics applications; such as mixing in microfluidic devices which are used for biochemical, medicine, biology applications.

### 5-1. Micro-Chip Fabrication

Using soft lithography method we bonded a polydimethylsiloxane (PDMS) micro-chip on a glass substrate. To fabricate the PDMS micro-chip, first, we coated a film of SU-8 25 negative photo-resist onto a silicon wafer using a spin coater device (Figure 5-1a) and pre-baked it. Next, we placed a photo-mask (which bears the microchannel) on top of the coated wafer, and exposed it to UV light. See Figure 5-1b for different photo-masks and Figure 5-1c for UV exposure device. Our Master, then, is ready after post-baking and developing. Then, a 12:1 (w/w) mixture of PDMS polymer and the curing agent was poured over the Master (Figure 5-1d). The master which is covered with a mixture of PDMS and curing agent, first, is left into the vacuum oven to become degassed the mixture; and then is cured at 75°C for 3hr in oven (Figure 5-1e). We need to peel off the PDMS layer which has the microchannel structure (Figure 5-2a); and, cut the section that has the desired microchannel required for our experiment (Figure 5-2b). Two holes will be punched at the locations that are assigned for wells (Figure 5-2c). Placing the PDMS with the desired microchannel structure up-side-down on a glass slide (Figure 5-2d); the next step is putting it in an oxygen plasma discharger (Figure 5-2e) with another glass slide and waiting for 35 seconds. The final step is to place the PDMS layer on top of the glass slide exposed to the oxygen plasma (Figure 5-2f) to form permanent bonding which prevents leakage, pressure drop and error during the experiment. The micro-chip is now ready to be used (Figure 5-2g). More details regarding the micro-fabrication and soft lithography could be find in an article by Biddiss *et al.* [84].

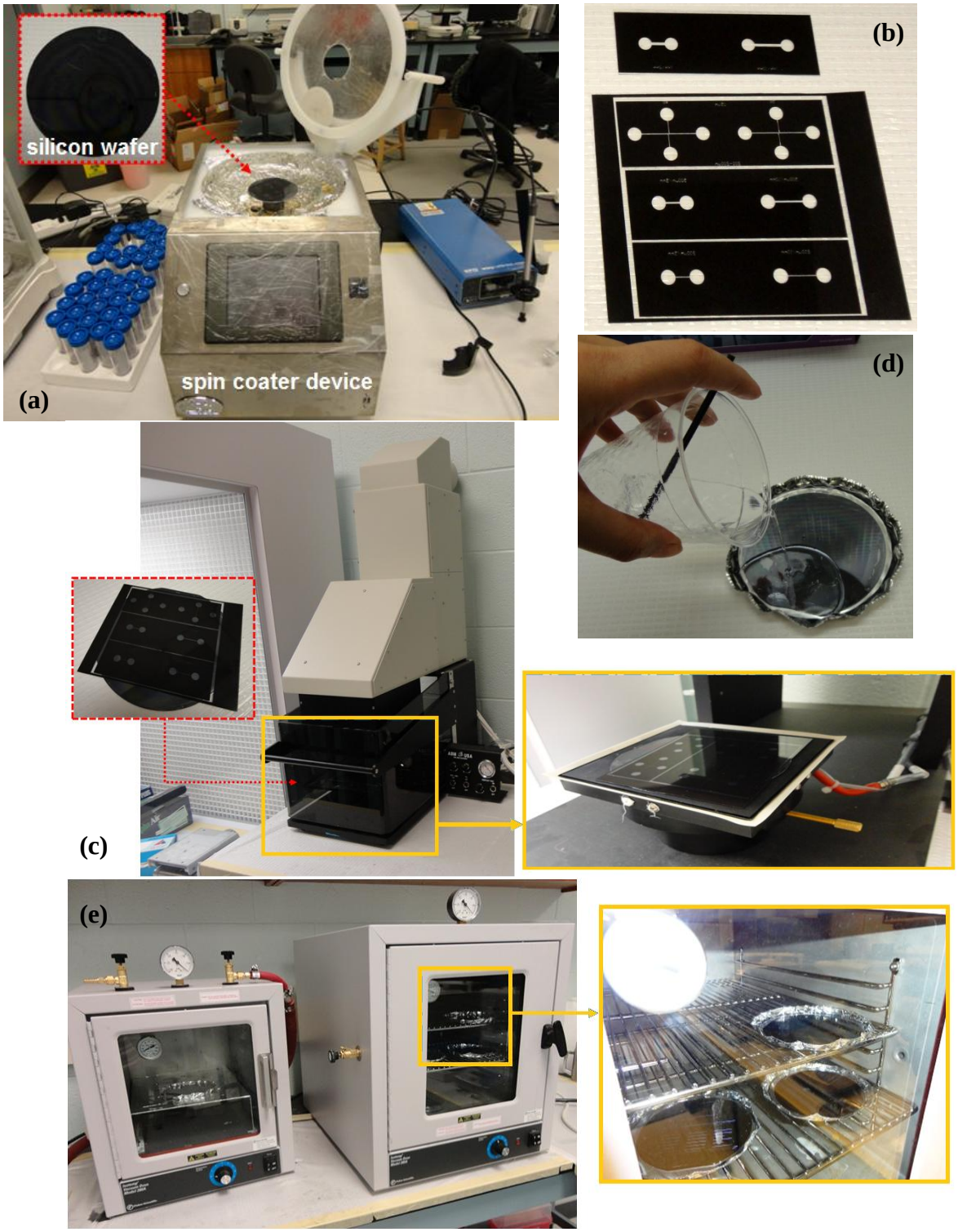


**Figure 5-1.** Steps 1 to 5 (out of 12) of soft lithography method to fabricate a micro-chip. (a) the raw silicon wafer placed in a spin coater device to be coated, (b) the printed sheet of the desired microchannels, (c) the coated wafer covered by the printed sheet of desired microchannels and located under the UV light in a UV exposure device, (d) the master covered with a mixture of PDMS and curing agent, (e) degassing of the mixture using vacuum oven, and then, baking the mixture in a heat oven.

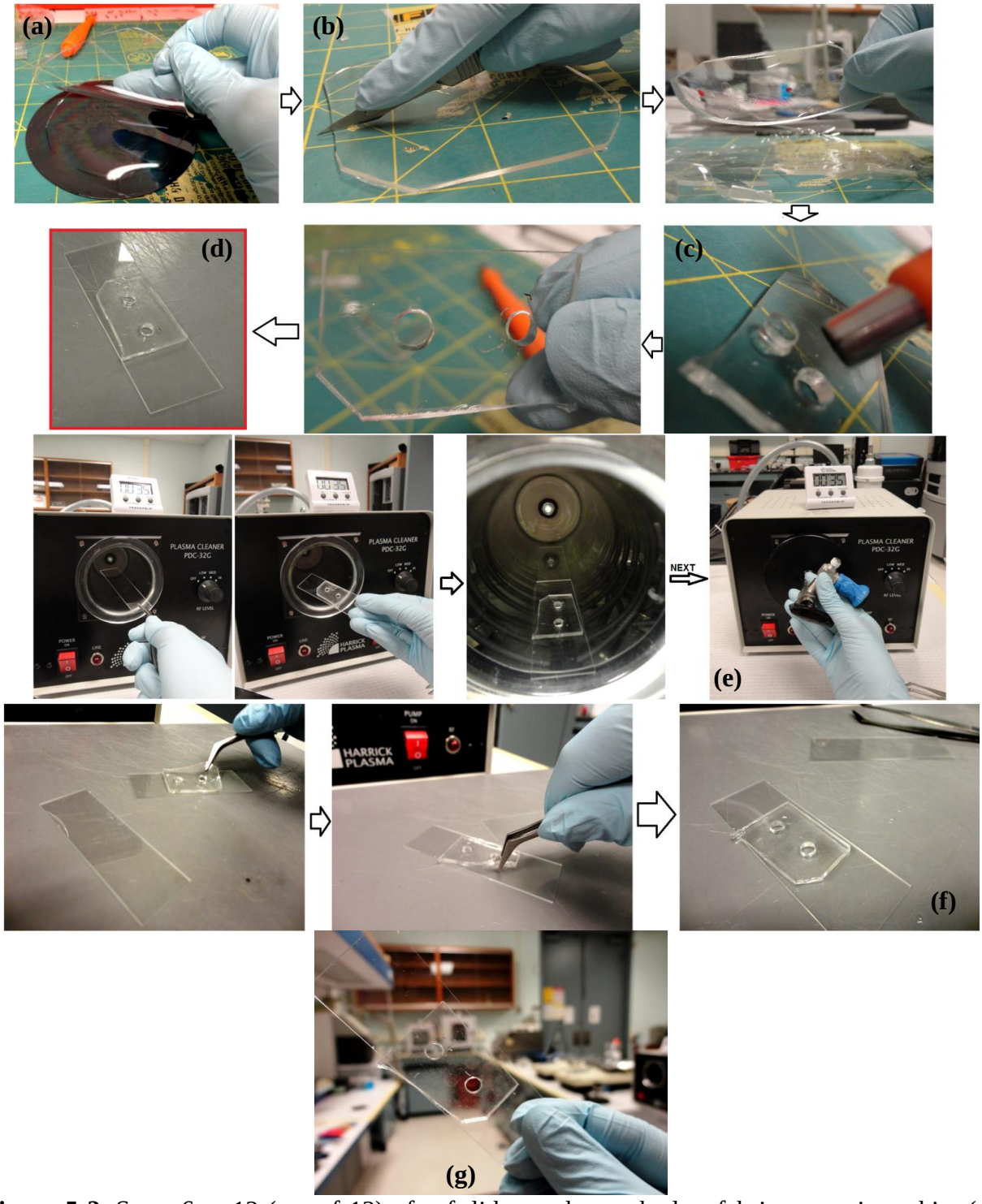


**Figure 5-2.** Steps 6 to 12 (out of 12) of soft lithography method to fabricate a micro-chip. (a) peeling off the backed PDMS layer, (b) cutting the PDMS layer to use the microchannel which is required for our experiment, (c) punching two holes at desired locations to make the wells, (d) putting the microchannel on a glass slide (where there is not a tight seal between the PDMS and the glass), (e) placing one new and cleaned glass and also the microchannel on a glass slide in the plasma cleaner for 35s, (f) turning the PDMS and placing it on top of the glass slide for tight bonding, (g) the prepared micro-chip is ready to be used.

To investigate the induced micro-vortices around a conducting surface and their effects on the particle motion we fabricated (A) a micro-chamber and (B) a single straight microchannel connecting two wells. To visualize the experiment we used a general system as shown in Figure 5-2. In case (A) the rectangular micro-chamber is opened to the air and had a width of 2.5cm, a length of 3.5cm, and a depth of 2.5mm. In case (B) the channel has a width 200µm, length 1.5mm, and depth 20µm. The diameter of both wells is 5 mm.

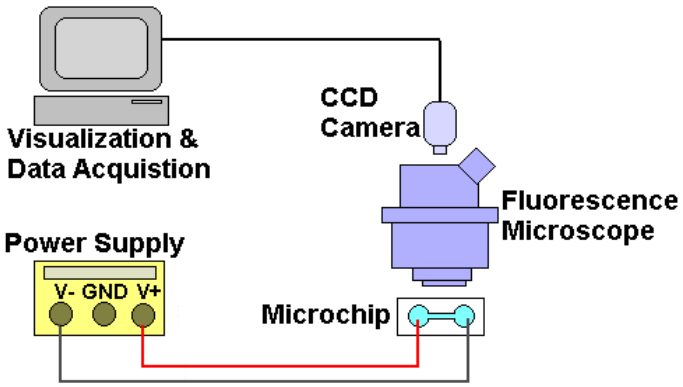


**Figure 5-3.** Illustration of the experimental system.

### 5-2. Materials and Experimental Setup

We are using a spherical carbon-steel particle (1.2mm diameter) as the fully conducting three-dimensional surface. This carbon-steel sphere is located in the middle of the prepared micro-chip filled with de-ionized (DI) water. The carbon-steel sphere density is much higher than that of water and thus sinks into the electrolyte remains stationary under the applied electric field during the experiments. Our experimental system consists of a data acquisition system, a fluorescence microscope and an imaging system, a micro-chip, and a DC-regulated power supply (CSI12001X, Circuit Specialists Inc., USA) as illustrated in its schematic in Figure 5-3. The microfluidic chip was fixed on the observation platform of the microscope (TE2000-E, Nikon). To visualize the flow pattern around a conducting particle we used 1.90µm dragon green fluorescent particles (Bangs Laboratories Inc) with excitation and emission light wavelengths of

the fluorescence particles being 480nm and 520nm, respectively. Two platinum wires were used as electrodes and the applied voltages were controlled by the DC-regulated power supply. Using fluorescent microscope, a high-intensity illumination system, and a CCD camera (DS-QilMc, Nikon) we were capable of monitoring the motion of the florescent particle and illustrating the flow pattern around the carbon-steel sphere. The microscope images captured by the CCD camera were digitized by the computer software (NIS-Elements BR 3.0) to be stored and analyzed. To investigate the electrokinetic motion of the Janus particle and the non-conducting particle, case (B), we used a set up similar to case (A). The only difference was that the micro-chip for this case is a straight microchannel with two wells at the ends. To avoid the pressure driven flow, each well is loaded with 20μL of DI water to maintain the same level of fluid in both wells. The particle solution is pre-diluted and a small droplet of that is released into the left well. Once the DC electric field is applied, the displacement of the particle is recorded using the microscope imaging system. Knowing the period that images are captured and calculating the traveling distance by the image analysis software, we could determine the velocity of each individual particle.

For case (B), two types of particles have been used: a Janus particle and a homogeneous non-conducting particle. Polystyrene particles with a diameter of 10μm that are coated with Ni film of 100nm thickness on one half of the particles are our heterogeneous Janus particles. These particles are fabricated at Kopelman's laboratory at the University of Michigan. The 9.82μm polymer particles (fluorescent carboxyl polymers microspheres- Bangs Laboratories Inc) are chosen as our homogeneous non-conducting particles.

To fabricate the Janus particles the 10μm polystyrene (NIST particle standards: Polysciences, Inc., Warrington, PA) are suspended in methanol at 1% w/v. After spin-coating 500μL of the

solution at 600rpm for 10s onto a 4" glass wafer; 100nm Ni was coated on to the wafer surface by vapor deposition method. Removing the coated particles from glass (with a damp acrylic paintbrush) and placing them in De-ionized (DI) water is the last step of fabricating Janus particles which have been used in our studies. For more information about fabricating these Janus particles please refer to [117].

To minimize the experimental error and increase the reliability of our results we repeated each experiment ten times using ten new micro-chips under the same conditions. Moreover, during each set of calculations we recorded the motions of over forty particles. Finally, for every applied DC electric field, the particle velocity was determined by averaging obtained results.

## 5-3. Flow Pattern around a Conducting Sphere

### 5-3-1. Vortex Visualization

Consider a 1.2mm in diameter spherical carbon steel particle that is placed in the middle of an open to air micro-chamber (3.5 cm in length, 2.5 cm in width, and 2.5mm in height) and in contact with DI water. Two platinum electrodes located at the ends of the micro-chamber apply the desired voltages and produce 40V/cm DC electric field from left to right. Releasing a droplet of dragon green fluorescent particles close to the particle and recording the images with the TE2000-E Nikon microscope, the first captured image at t=0.0224s is shown in Figure 5-4. It can be seen in this figure that the fluorescent particles are affected by the forces around the conducting sphere and are dragged to move in two opposite directions. A dark line can be seen at the middle of the image which shows the forces are divided into two equal and opposite directions and thus cause the motion of the fluorescent particles. The red dash lines represent the area of the carbon-steel particle.

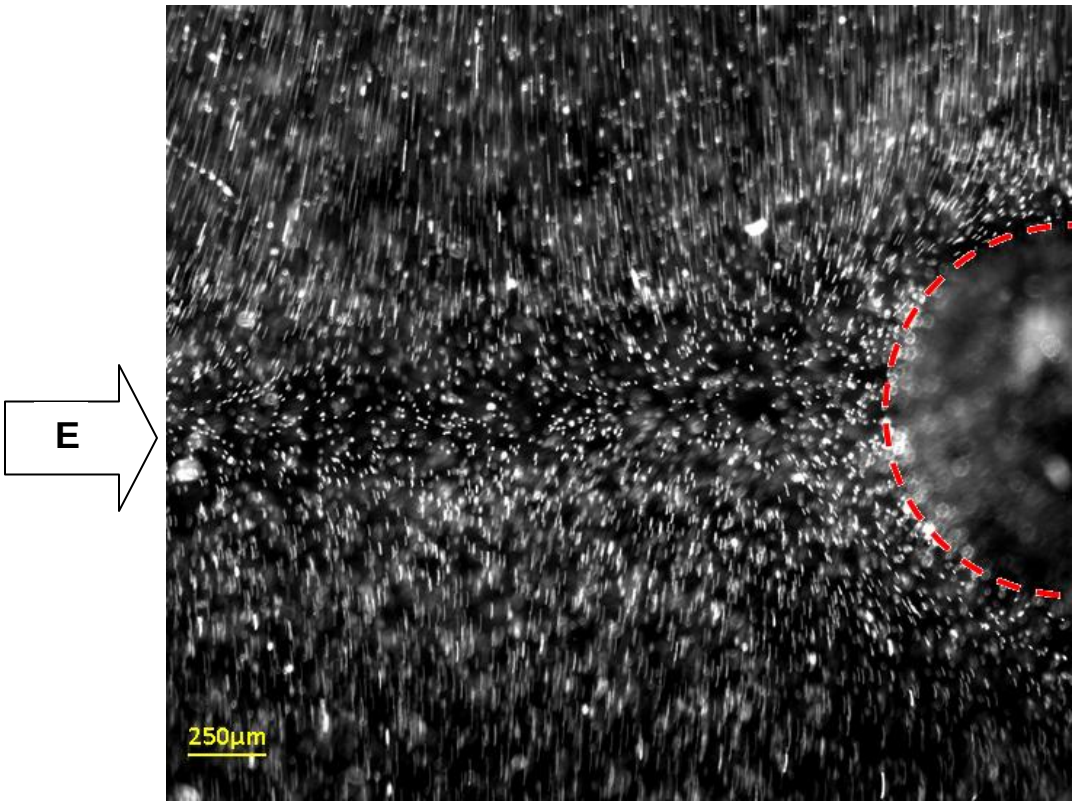


**Figure 5-4**. The induced-charge electrokinetic forces which push the fluorescent particles in two opposite directions. A DC electric field (E=40V/cm) is applied from left to right. The image is captured at t=0.0224s. The red dash line shows the carbon-steel particles limits.

As we continue capturing images of the above mentioned system, at time equal to two seconds four clear vortices are induced around the carbon-steel sphere (Figure 5-5). The particular microscope (TE2000-E Nikon) has a limited field of view and is unable to images the entire region of interest (a region that covers all four vortices) around the particle. Thus, we were not able to capture the whole RIO in one acquisition. And obtained the image shown in Figure 5-5 in two steps by dividing the ROI into two sections: the left and, then, the right hemispheres of the particle. For both experiments we recorded the flow pattern around the each hemisphere at t=2s, while E= 40V/cm is applied from left to right and the other conditions are kept unchanged.

The four vortices shown in Figure 5-5 are under-developing vortices and have not reached their final position in 2seconds. Recording the flow pattern for more a longer period, we were

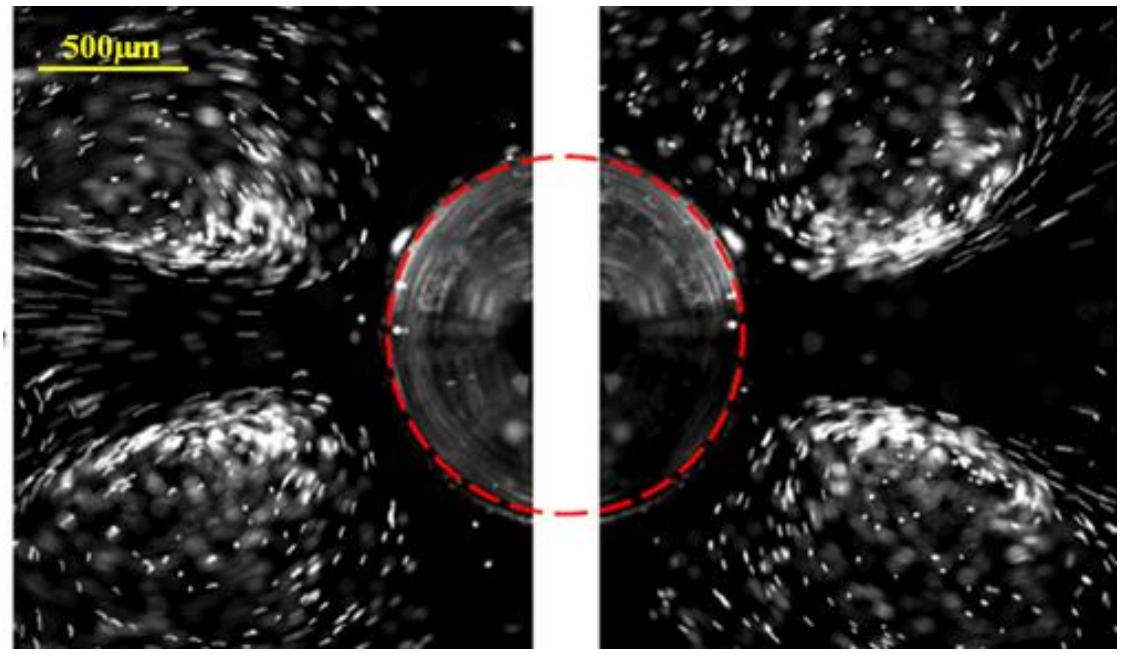


**Figure 5-5**. Fluorescent particles with a diameter of 1.90µm are used to visualize the induced-charge electrokinetic flow pattern around a carbon-steel sphere (diameter=1.2mm). The DC electric field (40V/cm) is applied from left to right. Dash line represents the particle boundary. The image is captured by TE2000-E Nikon microscope at t=2s.

able to show that the vortices expand and move away from the particles and thus do not fit in the field of view of the TE2000-E Nikon microscope. Repeating the same experiment with a different fluorescent microscope (AZ100 Nikon) with wider field of view (but lower resolution) we could capture all four vortices around the 1.2mm carbon-steel sphere in one acquisition at t=10s (Figure 5-6). These four vortices are stabilized and fully developed at t=10s and will not expand more.

### 5-3-2. DC Electric Field Effect on Vortices

The relationship between the vortex size and the applied DC electric field is investigated. Several DC electric fields are applied to the system with the 1.2mm carbon-steel sphere located in the middle of the micro-chamber. Figure 5-7 shows one fully conducting vortex on top-right hand side of the conducting sphere (facing the positive electrode) at t=10s for different DC electric

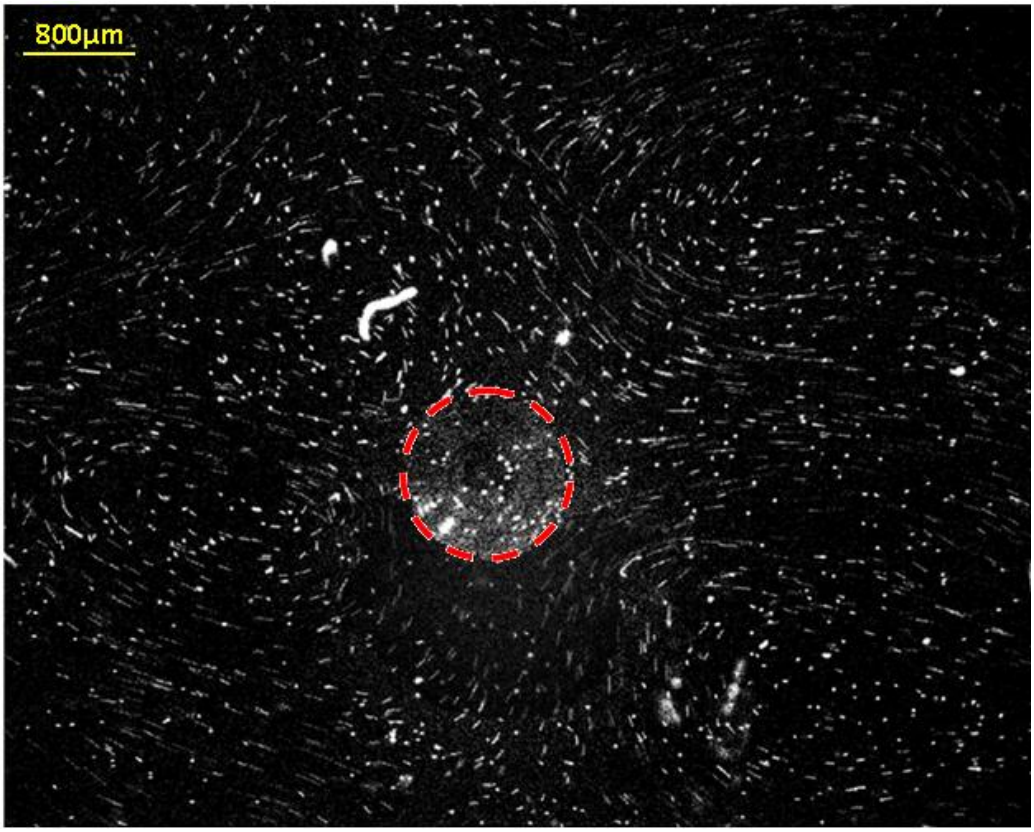


**Figure 5-6.** Four developed vortices induced around a 1.2mm carbon-steel sphere placed in a micro-chamber that is filled with DI water. A DC electric field of 40V/cm is applied from left to right. Dash line represents the particle boundary. The image is captured by AZ100 Nikon microscope at t=10s.

fields. This limited field of view is due to the limited field of view of TE2000-E Nikon microscope. It can clearly be seen that increasing the electric field has a direct effect on the strength and size of the induced vortices around the conducting particle. The vortex grows with increasing the external electric field. The larger vortex (Figure 5-7c) produces a large "sinkhole" in its center and circulates the fluid faster. Figure 5-8 represents a three-dimensional vortex at the upstream of the flow while a DC electric field of 15V/cm is applied from left to right. Using TE2000-E Nikon microscope and decreasing the CCD camera's shutter speed we were able to trace the motion of 1.9µm fluorescent particles.

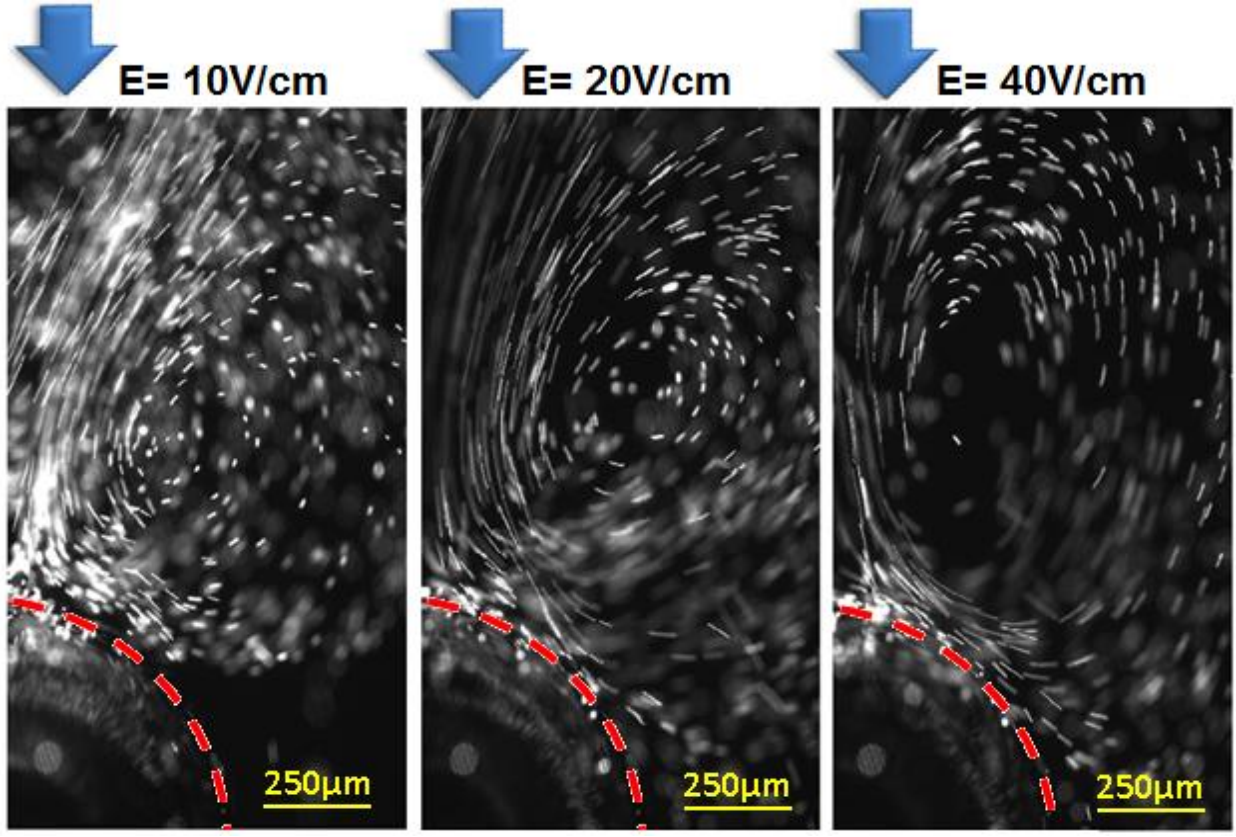


(a) (b) (c)

**Figure 5-7.** Vortex distributions for various applied DC electric fields. Dash line represents the particle boundary. The images are captured by AZ100 Nikon microscope at t=10s.


**Figure 5-8.** One induced vortex near the 1.2mm carbon-steel sphere. A DC electric field of 15V/cm is applied from left to right. Dash line represents the particle boundary. The image is captured by TE2000-E Nikon microscope. The image captured by increasing the exposure time of the CCD camera.

### 5-3-3. Particle Types and Their Movements

In section 4-3 we numerically investigated the effect of conductivity on particle motion. In this section we will experimentally verify that a Janus particle moves faster (as a result of induced vortices) than a non-conducting polymer particle when the sizes of both particles are the same (e.g., 10μm) and other experimental conditions are the same.

The SEM[3] photograph of 10μm Janus particles which are used for experiments are shown in Figure 5-9. The dark side is the coated section of the Janus particle. These particles are polystyrene particles coated with a 100nm thick Ni film. We are using the straight microchannels whose fabrication process was described in section 5-1-2 "Materials and Experimental Setup". The Janus particles are suspended in DI water and diluted before being placed in the microchannel. We released a droplet of this dilute solution into the left well of the microchannel and applied the voltage to the electrodes. We have traced the motion of one Janus particle in this straight microchannel and the position of this particle is shown for different time steps in Figure 5-10. For comparison, the positions of a carboxyl polymer particle under the same condition are also reported in Figure 5-10. This figure illustrates that the induced vortices on the conducting hemisphere of the Janus particle act like an engine and push the Janus particle to move faster than the polymer particle which has electrophoretic motion.

According to our experimental results, the induced-charge phenomena caused by low frequency AC is similar to applied DC electric field around a fully conducting particle. The main difference realized when we are dealing with a heterogeneous particle. A Janus Particle moves with the interface between conducting and none conducting hemispheres is parallel with the low frequency AC applied electric field [39].

[3] The scanning electron microscope (**SEM**): The captured images using this electron microscope are high resolution and have a 3D quality. The SEM images are useful for judging the surface structure of the sample.

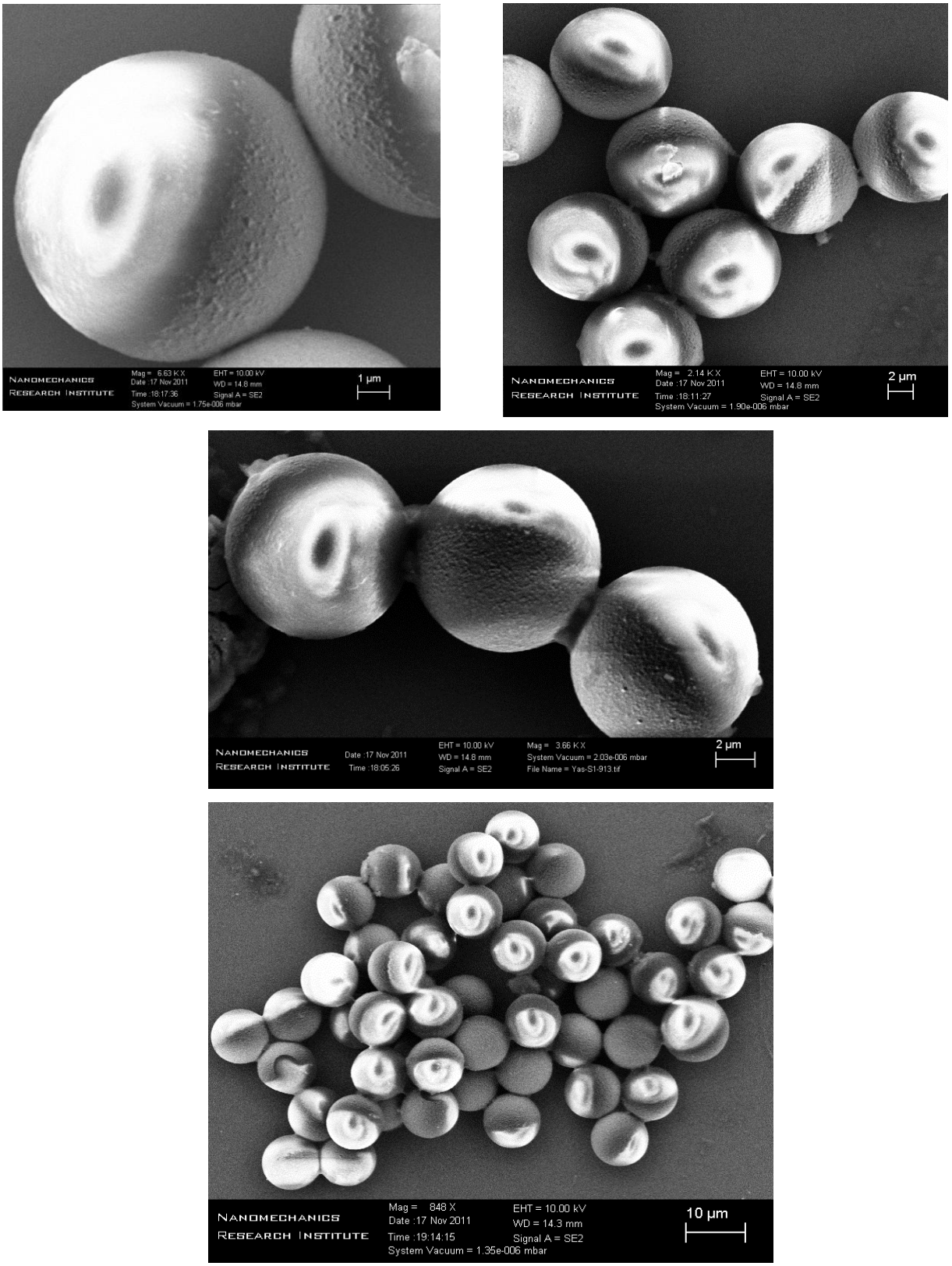


**Figure 5-9.** The SEM photograph of the 10µm polystyrene Janus particles coated with 100nm Nickel film on one hemisphere. The dark side is the coated section.

But this Janus particle moves in different direction when the DC Electric field is applied. The Janus particle moves with its interface perpendicular to the applied electric file direction when DC field is applied.

Releasing a diluted droplet of Janus particle in the left well and applying DC electric field, the Janus particle enters the straight microchannel. The movement of the Particle has been recorded using AZ100 Nikon microscope. To calculate the displacements of Janus particle we have used the following image analysis method: we traced the position of each particle over a period of time and then, knowing the displacement and the duration that took the particle to travel that distance, we could calculate the velocity of each particle.

Some of the Janus particles might not be aligned with the applied DC electric field at the initial time, t=0s. These particles will both rotate to align with the applied DC electric field and translate in the microchannel. To avoid including this rotation period in the travel duration, we traced the particle at times between t=10s to t=35s (giving the Janus particles enough time to rotate and reach their stabilized alignment with the field). In order to minimize the experimental error and increase the accuracy of the results we have calculated the velocity of more than 40 particles.

A similar process was followed when the non-conducting polymer particles were involved to calculate the velocity of the polymer particles. These experiments were repeated for different applied DC electric fields to investigate the effects of the electric field on the particles motion. The average velocity of the 40 Janus particles and the 40 polymer particles in the straight microchannel as functions of the various applied DC electric field are plotted in Figure 5-11.
This graph shows that the Janus particles move much faster compared to the polymer particle under the same applied DC electric fields (as shown in the results of our numerical simulations in

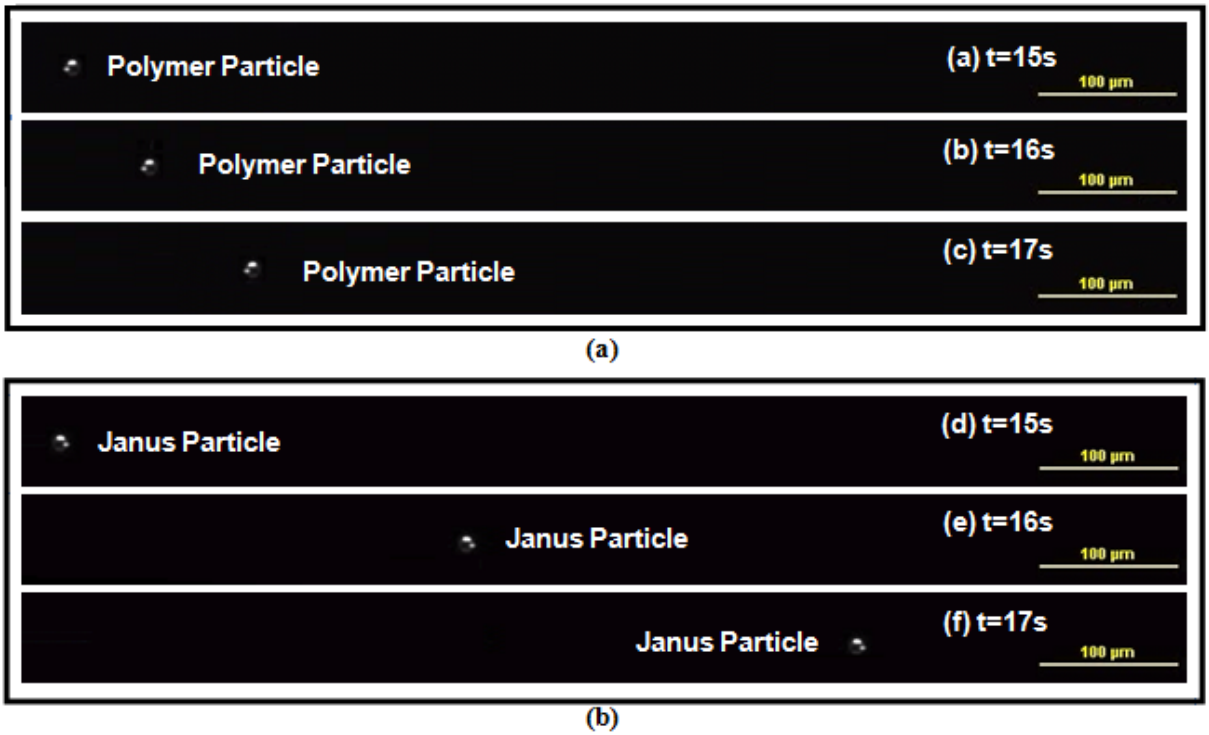


**Figure 5-10.** Tracing electrokinetic movement of the particle for (a) a non-conducting polymer particle (D=10μm) and (b) a Janus particle (D=10μm) with the conducting hemisphere facing the positive electrode. The external DC electric field of 80V/cm is applied from left to right.

chapter 4). The plot corresponding to the polymer particles also demonstrates that the velocity of polymer particles haves linear relationship with the applied electric field. This follows the previous findings in classical electrokinetics theory [11, 13]. However, the velocities of the Janus particles have nonlinear relationship with applied DC electric field which does not satisfy the classical electrokinetics theory. The correlation between the velocities of the Janus particles with the applied DC electric field may be better shown by a quadratic curve. It can be seen that the slop of the plot corresponding to the Janus particles decreases in higher electric field values. This might be related to the polarizability limit of the conducting section of the Janus particles. A conducting section of the Janus particles will be polarized under the applied electric field while the free charges inside the particle moves to the surface of the particle.

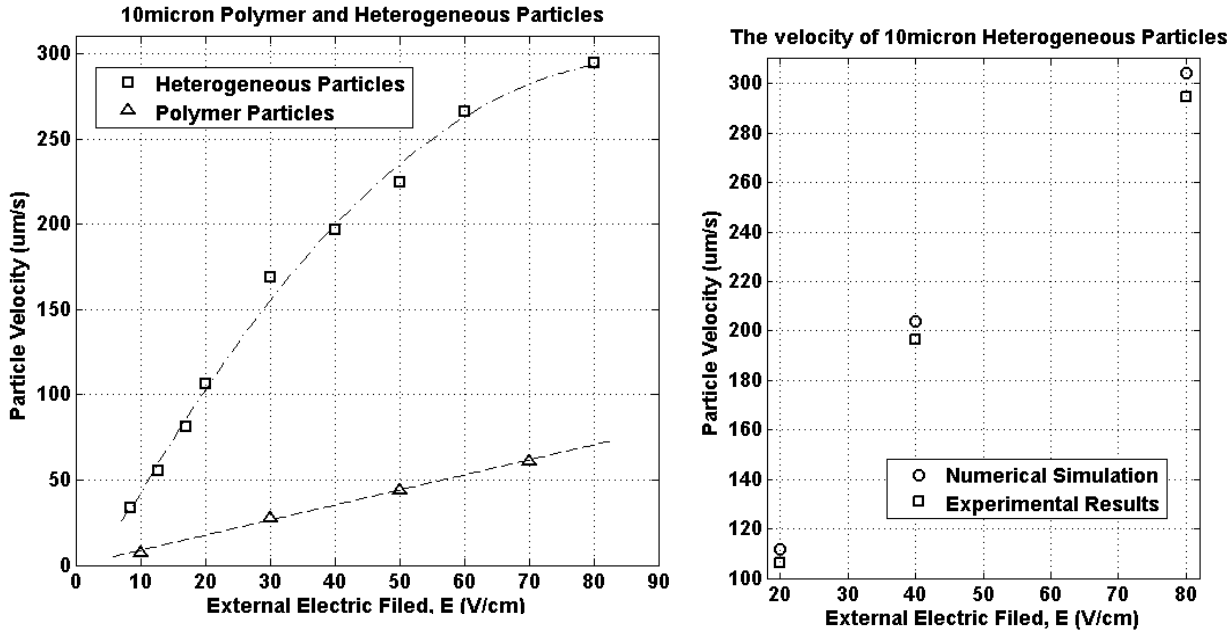


(a) (b)

**Figure 5-11.** (a) The electrokinetic velocities of 10µm Janus particles and polymer particles for variety of applied DC electric fields. (b) Validation of the velocity of Janus particle calculated by numerical simulation comparing with experimental data.

Increasing the electric field increases the number of migrated charges till the surface charge reaches an upper limit and saturates. Approaching this point, the conducting section of the Janus particle reaches it maximum polarizability and will not polarize more. At this point the strength of the induced vortices around the conducting section of the Janus particle is maximum; thus its velocity is maximum. Increasing the electric field beyond this limit has no additional effect on the polarizability of the particle; thus, its velocity remains constant. The reduction in the slope of Janus particle plot in Figure 5-11a at high electric field could be explained by this fact. To validate our numerical simulations (explained in chapter 4), the calculated velocities of a Janus particle (diameter=10µm) for different applied DC electric fields are compared with our experimental results in Figure 5-11b. The numerical results are in good agreement with the experimental data. The small difference between the numerical simulation and experimental data

might be the result of simplifying assumptions used in the numerical model and simulation, such as neglecting the gravity effect.

In chapter 4 it was demonstrated that when the Janus particle is unaligned with the direction of applied DC electric field, the particle is in an unstable position. This situation is due to the electric force and induced forces which are applied by the generated vortices. At this situation the unaligned Janus particle tents to rotate till its interface between the conducting and non-conducting hemispheres becomes perpendicular to the direction of applied DC electric field. However a Janus particle might be aligned in two positions: the conducting hemisphere faces the (i) positive voltage or (ii) negative voltage. In each case the induced vortices act like engine and push the particle. As a result of forces induced by the vortices the Janus particle could move towards the downstream of the flow (if the conducting section faces the positive voltage) or move towards the upstream of the flow (when the conducting section faces the negative voltage) against the direction of the electro-osmotic flow of the fluid.

Figure 5-12 shows three Janus particles in a straight microchannel. Once the electric field is applied two of these Janus particles move forward towards the downstream of the flow but one particle moves in the opposite direction (towards the upstream of the flow). Thus, the orientation of the Janus particle has a significant effect on the direction and velocity of its movement. The conducting section of the two of the Janus particles (shown in figure 5-12) which are moving in the same direction as the direction of the applied DC electric field are facing the positive voltage. While the Janus particle that is moving against the direction of the applied DC electric field has opposite orientation. These results confirm our numerical simulations which were explained in chapter 4. As Figure 5-12 demonstrates the particle with the opposite orientation (particle 3) moves slower than the two other particles. These findings, to our knowledge, are in accordance

with the first experimentally proven evidence of Janus particle motion under DC electric field. Note these results apply to DC electric field and the behavior of Janus particle under applied AC electric field is different where it moves with the interface plane parallel to the AC electric field axis [39].

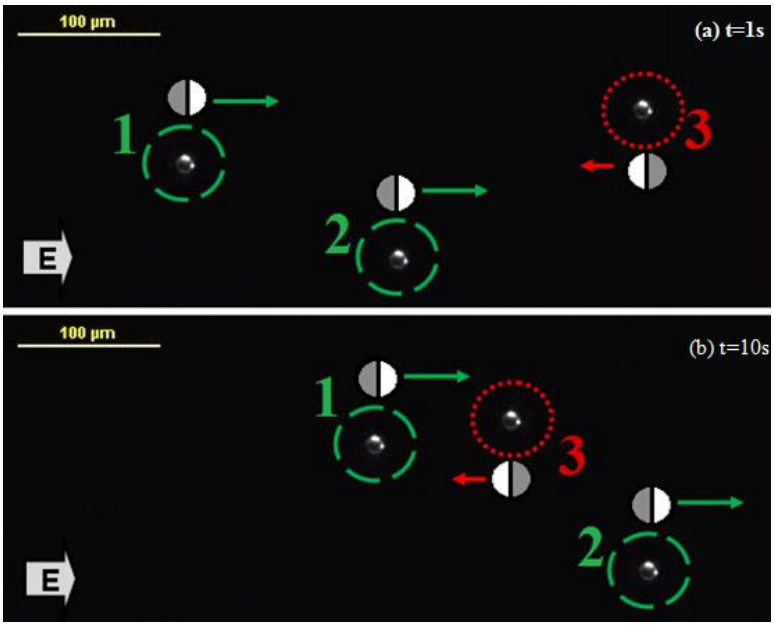


**Figure 5-12.** Investigating the relationship between the orientation of a Janus particle under an applied DC electric field with the velocity and direction of its motion. A DC electric field of 10V/cm is applied from left to right. The circles represents the heterogeneous particles where the gray side represents the conducting surface, while the bright section is non-conducting part.

### 5-4. Summary and Conclusions

We have experimentally demonstrated four vortices generate around a spherical conducting particle (which is immersed in an aqueous solution) once DC electric field is applied. This confirms a key theoretical finding in induced-charge electrokinetics phenomena (vortices) while a DC electric field is involved. We have experimentally investigated the effect of the applied DC electric field on the size and the strength of the induced vortices. We also determined the velocity of the Janus particles and compared it with the velocity of the same size polymer particles for a variety of applied DC electric fields. Results show that the Janus particle moves

faster than a polymer particle since the vortices around its conducting hemisphere push the particle and boosts its motion. The results are compared with the numerical simulation of chapter 4 and a good agreement between our numerical simulation and our experimental data is achieved. We have also showed that Janus particles with different orientations move in different directions; however they move along the applied DC electric field (in negative or positive directions of the field). Former studies all had reported the motion of the Janus particles under the applied AC electric field. Those studies showed that the interface of the two hemispheres of Janus particle is parallel to the direction of the applied AC field. Our experimental results for the first time showed the behavior of a Janus particle under the applied DC electric field, these results show that the Janus particle has a different behavior under DC electric field compared to the cases where an AC electric field is applied. The vortices that were shown in this chapter can be used for mixing in micro-devices of biochemical, medicine, and many other useful and critical aspects of electrokinetic devices. In the next chapters we will develop three practical applications of using ICEK in microfluidics and lab on chip devices.

## CHAPTER VI: Application (1)

# Induced-Charge Electrokinetic Micro-Valve

In previous chapters we numerically and experimentally demonstrated that one of the specific characteristics of induced-charge electrokinetics (ICEK) phenomena is vortex generation. These vortices form on the surface of a conducting material immersed in an aqueous solution, once the electric field is applied. We have shown that by controlling the direction and strength of the applied DC electric field we can manage the motion of a fully conducting homogeneous particle or a heterogeneous particle (such as Janus particle). Using the ICEK in different aspects of the microfluidics and lab-on-a-chip (LOC) devices could overcome many of the shortcomings of classical electrokinetics and improve the performance of the micro-devices.

In this chapter and the following two chapters we will introduce three novel applications of ICEK phenomena and could be considered as reliable solutions to the drawbacks of current electrokinetic micro-devices. A Micro-valve is one of the important components of microfluidic devices. The main application of a valve is switching the direction of the flow at the desired moment. Response time, dead volume and leakage are some of the significant parameters that determine the performance of a valve where the valve that minimizes all of these parameters is preferred.

Many former micro-valves suffered from some disadvantages such as leakage problems or complicated fabrication processes. In this chapter we will develop a new micro-valve using the electrokinetic motion of a Janus particle in a micro-chamber, which solves some of the drawbacks of the current micro-valves. Our numerical results will also demonstrate that using this ICEK micro-valve for switching and controlling the flow rate in a micro-device is feasible. The main advantages of this proposed ICEK micro-valve are: (i) it is easy to fabricate (ii) could be controlled easily (iii) has a short response time and (iv) and has a small dead volume. The operating demonstration of the proposed ICEK micro-valve will be tested when a Janus particle is employed or a fully conducting particle is involved. Moreover, the results are compared with a case that a non-conducting particle is used. We will show that only a Janus particle can fulfill the requirements of such a micro-valve.

### 6-1. Geometry and Computational Domain

The proposed ICEK micro-valve contains a Janus particle located in the middle of a cylindrical micro-chamber. The micro-chamber is connected to three microchannels with circular cross section of different sizes. The electric fields are applied (from left to right, $E_1$ , and from bottom to top, $E_2$ which is perpendicular to $E_1$ ) using four electrodes at desired location as shown in Figure 6-1b), vortices are induced at the conducting hemisphere of the Janus particle which push it forward to block the entrance of microchannel B; thus the fluid can only flow through the microchannel C. Switching the direction of the applied electric field, the configuration of the induced vortices changes; thus, the applied forces to the Janus particles changes. Consequently the Janus particle moves away from entrance of microchannel B and finally stops at the entrance

of microchannel C. Blocking the entrance of microchannel C, the fluid flow direction is now switched to the new direction through microchannel B.

To achieve this goal we have numerically modeled the three dimensional motion of a spherical Janus particle (which is initially placed at the center of the cylindrical micro-valve) using the mathematical model described in chapter 3. The diameter of the Janus particle is 20μm and the diameter of microchannels A, B, and C are 15μm, 10μm and 10μm respectively. The cross sections of the microchannels are chosen to be smaller than the size of the Janus particle to achieve full blocking of the microchannels. The proposed valve can be fabricated using the alignment methods. Such techniques are developed to fabricate microchannels with various cross sectional shapes (e.g. microchannels with star grooves, rhombus grooves [118], and cylinders [119-121] ). In our numerical study the length of each of the microchannels is 20μm. the height and the diameter of the micro-chamber are both 40μm to let the Janus particle move freely inside the micro-chamber. The boundary conditions at the end of the microchannels are set to be open boundaries; thus, there is no overall pressure gradient in this system.

The zeta potential on the non-conducting hemisphere of the Janus particle is set to -50mV; while the zeta potentials on the non-conducting microchannel and micro-chamber walls are set to -15mV. To avoid the gravity effect, the density of the fluid and the Janus particle are assumed to be equal[4]. To provide the electric field required for generating the driving forces, four electrodes are located at the locations shown in Figure 6-1c. Applying a voltage between electrodes 1 and 2 (or electrode 1 and 5) produces a potential difference and generates the electric field that is named E1 in Figure 6-1a. Electrodes 3 and 4 can be used to produce a second electric field, E2,

[4] For the particular type of Janus particles that we are using in our experiments (Chapter 5), we observed that the Janus particle floats in the fluid without sinking to the bottom or moving to the surface of the fluid. Which indicates the density of this Janus particle and fluid should be close to each other.

which is perpendicular to E1. Also at the desired moment we will apply voltage to electrode 3 and 6 to achieve electric field E2. The applied voltages to these electrodes can be set to any desired values, thus the applied electric fields can be controlled easily.

This computational domain is fully covered by three Dimensional hybrid meshes (Figure 6-1a) and the mesh independence study has been performed in this chapter. To solve the mathematical model described in chapter 3 over the present computational domain we used FLUENT12 (commercial software) which, in correlation with visual C, runs a UDF file that was written for solving the moving mesh and particle motion in 3D.

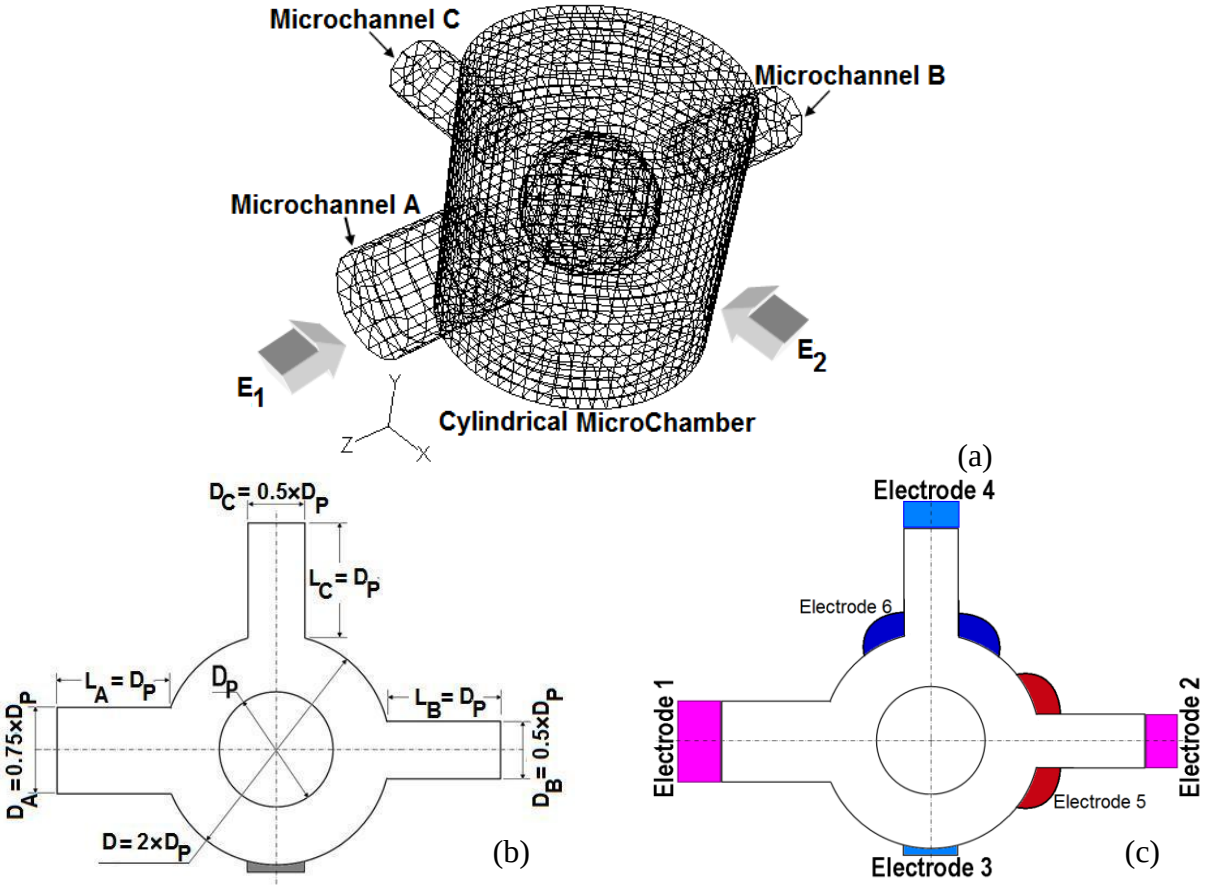


**Figure 6-1.** (a) Computational domain of the proposed ICEK micro-valve with three microchannels and one suspended Janus particle in it. $E_1$, and $E_2$, represent the external electric field directions, (b) Geometry and dimensions in a non-dimensional format, (c) The location of the four electrodes.

The Laplace equation (Eq. (3-2)) is solved to calculate the distribution the electric field in the computational domain. We used Eq. (3-3a, b, and c) to solve the Laplace equations as the boundary conditions subjected to this study. The continuity condition is valid all over the micro-valve domain (Eq. (3-4). To solve the Navier-Stokes Equation (Eq. (3-5)) we used the following boundary conditions as mentioned in chapter 3: Eq. (3-6a to d).

**6-2. ICEK Micro-Valve Using a Spherical Janus Particle**

The functionality of an ICEK micro-valve using a spherical Janus particle is shown in Figure 6-2. Consider a spherical Janus particle which is initially located at the center of the micro-chamber with its conducting side facing the positive voltage (which is applied by electrode 1). Applying positive voltage to electrode 1 and negative voltage to electrode 2, we could produce the electric field $E_1$ from left to right. As a result of applied electric field, vortices are induced around the conducting section of the Janus particle which push it to move towards the microchannel B (Figure 6-2a and b).

After approximately 3.3s, the Janus particle reaches the entrance of microchannel B and blocks it (Figure 6-2c). The Janus particle stays at the outlet of microchannel B and blocks it completely and does not move as long as the electric field $E_1$ is applied. We reached the goal of blocking the desired microchannel without leakage in short period of time; however, directing fluid into the desired microchannel is not discussed yet (Figure 6-2c).

At this stage, a second DC electric field (perpendicular to $E_1$ =200V/cm) is applied, $E_2^*$ =35V/cm. This second electric field is used to drive fluid flow through the microchannel C, and is chosen sufficiently weaker than $E_1$ so that it will not affect the blocking of microchannel B

(Figure 6-2d). As mentioned in chapter 4 and 5, the Janus particle tends to align itself with the direction of the resultant DC electric fields. This fact clearly can be seen in Figure 6-2d where the Janus particle rotates a little bit to align itself with the resultant electric field (sum of $E_1$ and $E_2^*$) but still blocks the microchannel B.

Now assume that we are interested in changing the flow direction by blocking microchannel C and letting the fluid flow through the microchannel B. To achieve this goal, we apply positive and negative voltages to electrodes 3 and 4 respectively which provides the DC electric field of $E_2$ =200V/cm. The electric field $E_1$ will also be simultaneously turned off.

Figure 6-3a to 6-2e show that the Janus particle rotates to align itself with the new applied DC electric field and moves towards the microchannel C and eventually blocks it (after approximately 3.7s). Once microchannel C is blocked, next, we need to direct the fluid into microchannel B. This is achieved by applying voltages to electrodes 1 and 2 to produce a weaker DC electric field, $E_1^*$ =50 V/cm, perpendicular to the dominant DC electric field of $E_2$ =200V/cm (Figure 6-3e).

The velocity vectors in Figure 6-2 and 6-3 show the direction of the flow. The size of these vectors are normalized, thus the arrows do not represent the strength of velocity vectors. The proposed ICEK micro-valve is controlled by applying different values of voltages to the electrodes at desired moment. Consider the Janus particle moves toward the microchannel B when electric field E1 is applied. This electric field is generated by applying voltage to Electrode 1 and electrode 2. Once the Janus particle blocks the microchannel B, we have to switch the electrodes. We still need the E1 being applied into the system to keep the Janus particle blocking the microchannel B, so we apply the voltages to electrode 1 and electrode 5 in a way that applied electric field be the same as that was generated by electrode 1 and electrode 2 (Figures 6-1c and

6-1d). The same arrangement happens in Figure 6-2d and 6-2e. We keep the applied electric field unchanged by switching the active electrodes from electrode 4 to electrode 6 please check Figure 6-1b for the position of the electrodes. The point is that electrode 5 and electrode 6 both are in contact with the electrolyte. Therefore the electric field E1 and E2 are applied to the system even when the Janus particle blocked the microchannel B or microchannel C.

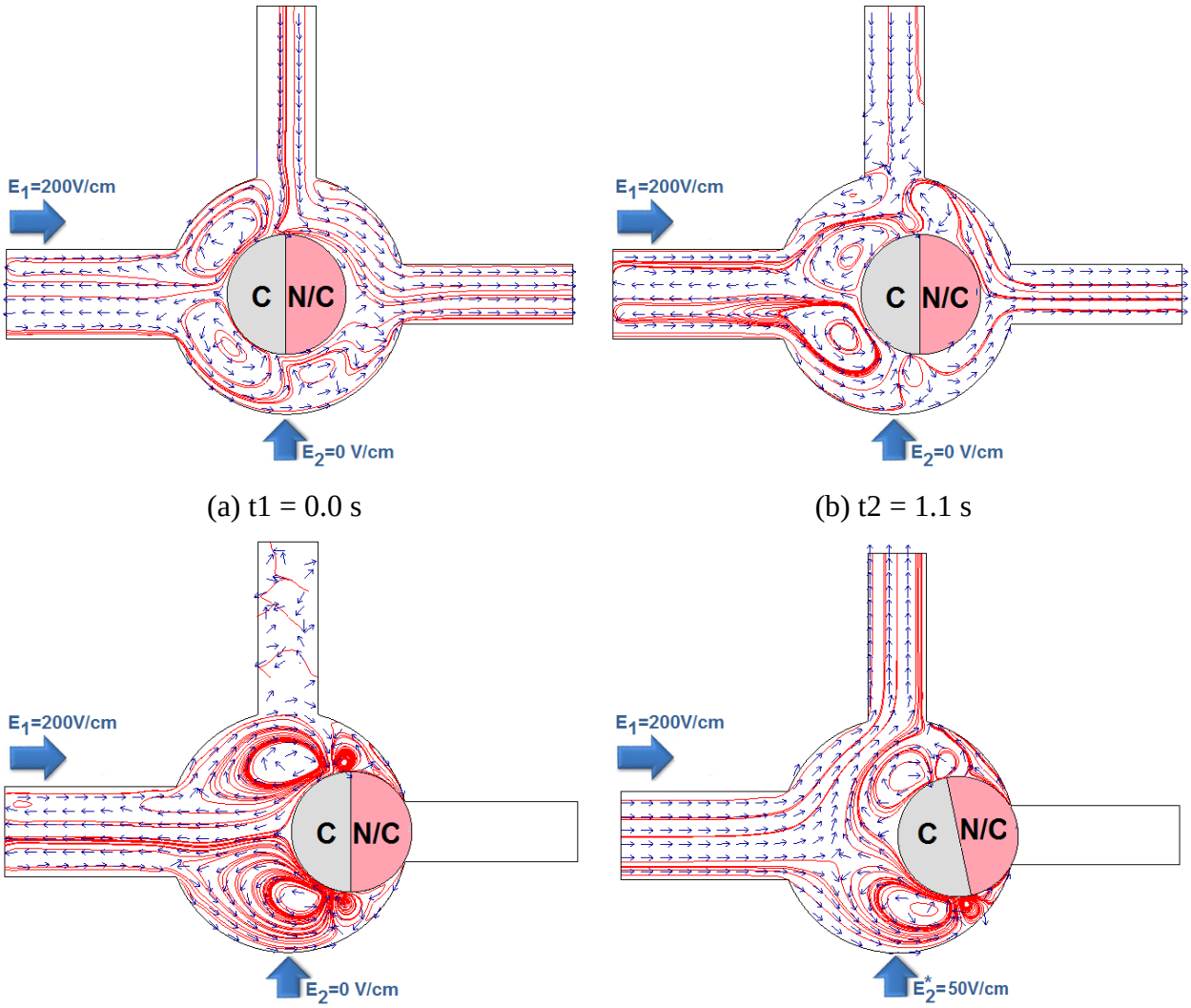


(a) t1 = 0.0 s (b) t2 = 1.1 s

(c) t3 = 3.3s (d) t4 = 3.6s

**Figure 6-2.** Sequences 1 to 4 (out of 9) of a micro-valve which is operated by induced-charge electrokinetics using a Janus particle inside it. The flow pattern and vortices are shown by plotted streamlines. The normalized vectors show the direction of the fluid. The diameter of the Janus particle and the micro-chamber are 20μm and 40μm respectively. The height of the micro-chamber is 40μm. The results are presented at the x-z plane crossing the middle of the 3D micro-valve at different time steps.

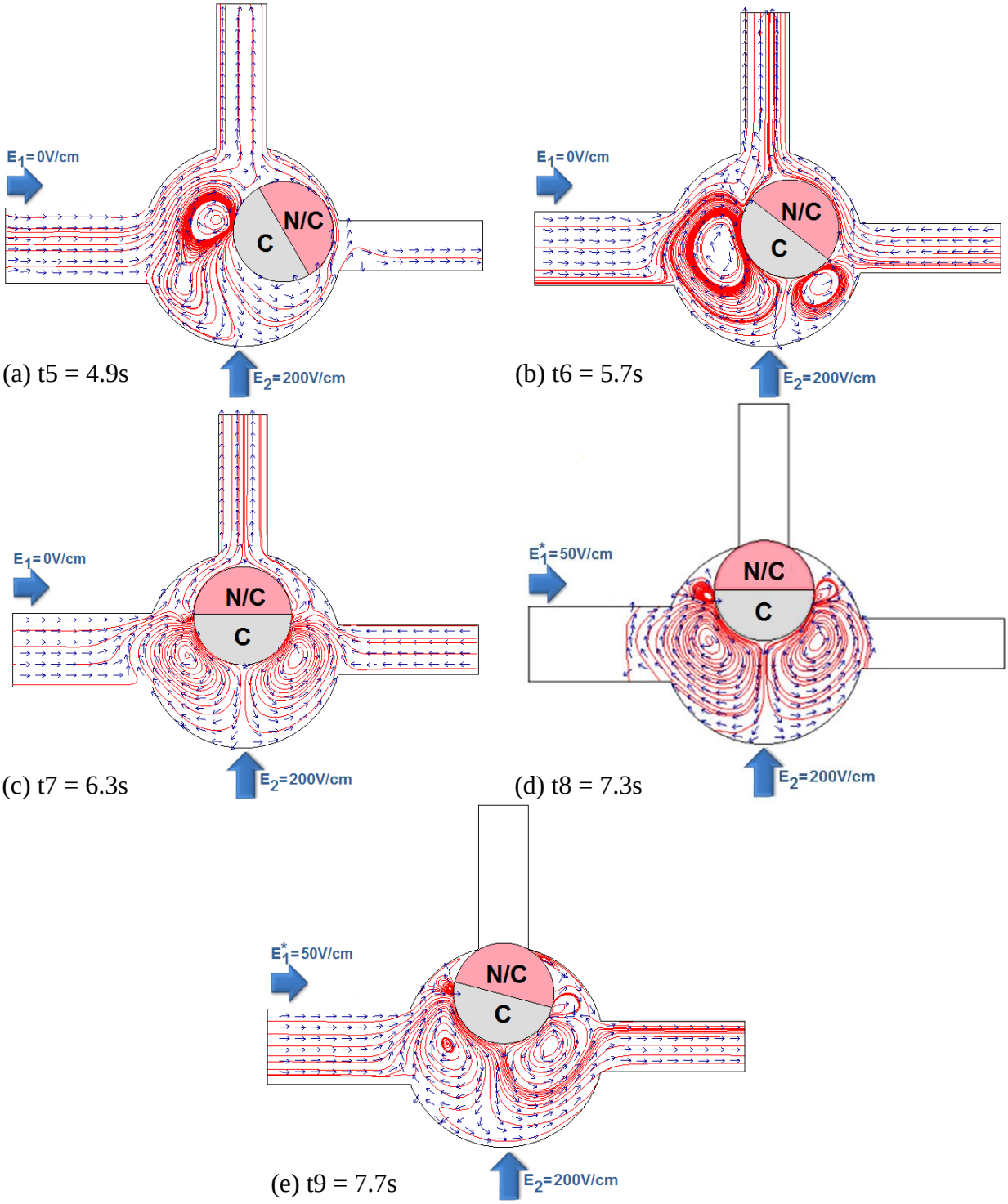


**Figure 6-3.** Sequences 5 to 9 (out of 9) of a micro-valve which is operated by induced-charge electrokinetics using a Janus particle inside it. The flow pattern and vortices are shown by plotted streamlines. The normalized vectors show the direction of the fluid. The diameter of the Janus particle and the micro-chamber are 20μm and 40μm respectively. The height of the micro-chamber is 40μm. The results are presented at the x-z plane crossing the middle of the 3D micro-valve at different time steps.

Our simulation study showed that under the applied DC electric field of 200V/cm the proposed ICEK micro-valve requires 3.7s to switch the flow direction without any leakage. This operation period can be reduced by increasing the applied electric field; e.g. when applying 400V/cm the micro-valve requires only 2.3s to switch the flow direction. The relationship between the applied DC electric field and required switching time is plotted in Figure 6-4. The comparison between other types of micro-valve and the presented ICEK micro-valve is summarized in Table 6-1.

It was explained that to pump the fluid trough the desired microchannel when the other one is blocked by Janus particle, another DC electric field (e.g. $E_1^*$ or $E_2^*$) in a different direction is required which is much weaker in comparison with the dominant DC electric field. There are variety of values that can be chosen within a range for this pumping DC electric field (e.g. $E_1^*$ or $E_2^*$). Thus, we can adjust the flow rate of the fluid pumped out of the valve, without affecting the blocking position of the Janus particle by using different values for $E_1^*$ or $E_2^*$ in the valid range. Applying $E_1$ =200V/cm for the dominant electric field, we can set the pumping electric field, $E_2^*$ to be between 29V/cm to 46V/cm without breaking the blockage and having the fluid flow through microchannel C. Similarly, applying the dominant DC electric field of $E_2$ =200V/cm, the pumping electric field, $E_1^*$, can vary from 49V/cm to73 V/cm to pump the flow towards microchannel B while blocking the microchannel C with the Janus particle.

Consider Figure 6-2b where there is a gap between the micro-chamber wall and the non-conducting hemisphere of the Janus particle (this gap gets smaller as the Janus particles moves closer to the entrance of microchannel B). The non-uniformity of the electric field in this gap produces dielectrophoresis (DEP) force on the Janus particle and affects motion of the particle.

**Table 6-1.** The comparison between the performance of the presented ICEK micro-valve and other types of active micro-valves

| Reference | Type | Mechanical part | Experimental or | Mode | Application | Fluid | Valving time (ms) | Flow regulation (μL $min^{-1}$) | On/off power | Leakage |
|---|---|---|---|---|---|---|---|---|---|---|
| Barth [58] | BM | M | E | NC | O/F S | air | 200 | N/R | N/R | N/R |
| Shikida *et al* [122] | ES | M | E | NO | R | Gas | N/R | 1000 | 200V | N/R |
| Goll *et al*[123] | ES | M | E | NO | O/F S | $N_2$ | N/R | 12000 | 60V | N/R |
| Fu *et al*[44] | EM | B | E | NO | R | Gas | 10 | 500000 | N/R | N/R |
| Takao *et al* [51, 124] | TP | M | E | NO | O/F S | DI | 5 s (O)<br>8 s (C) | N/R | 0.2W | 1 |
| Choi[125] | EM | I | E | NC | R | Gas | N/R | N/R | 0.25A | 5.6 |
| Rogge *et al* [126] | PE | M | E | NC | O/F S | $N_2$ | 2 | N/R | 245V | 30 |
| Peirs *et al* [127] | PE | B | E | NO | R | DI | N/R | N/R | N/R | 420 |
| Rogge *et al* [126] | PE | M | E | NC | O/F S | DI | N/R | N/R | N/R | 0.0133 |
| Oh *et al* [45] | EM | P | E | NC | O/F S | L | N/R | 836000 | 0.12A | 0 |
| Baechi *et al* [48, 128] | TP | M | E | NO | O/F S | L | 150 (C) | N/R | N/R | N/R |
| Kim *et al* [54] | TP | M | E | NO | O/F S | DI | 25 s (O)<br>20 s (C) | N/R | 0.2W | N/R |
| Reynaerts *et al* [60] | SMA | P | E | NC | O/F S | L | 660 (O) | N/R | N/R | N/R |
| Pemble and Towe [55] | SMA | P | E | NC | O/F S | L | 1 s (O) | 16800 | N/R | N/R |
| Presented Valve | ICEK | B | T | NO | O/F S | L | 4.1 s (S)<br>0 s (O) | 12 | 160V (S) | 0 |

**EM: electromagnetic;**
**ES: electrostatic;**
**BM: bimetallic;**
**TP: thermopneumatic;**
**SMA: shape memory alloy;**
**N/R:Not Reported**

**NC: normally closed micro-valve;**
**NO: normally open micro-valve;**
**O: opening; C: closing;**
**S: switching;**
**R: flow regulation;**
**O/F S: on/off switching;**
**M: membrane; I: Integrated;**

**L, liquid;**
**DI: de-ionized water;**
**E: experimental data;**
**T: theoretical data.**
**P: Pinch;**
**B: Ball;**

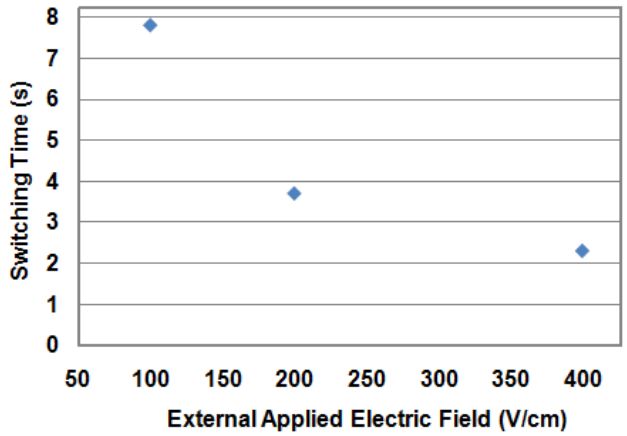


**Figure 6-4.** The valve switching time depending on the dominant applied DC electric field.

According to the theory of dielectrophoresis, the DEP force is a negative force and its strength is inversely proportional to the size of the gap. The DEP force applied to a sphere with diameter of $D_p$, under applied DC electric field of $E$ can be calculated as follows

$$F_{DEP} = -\pi\varepsilon\left(\frac{D_p}{2}\right)^3 \nabla\left|\vec{E}\right|^2 \qquad (6\text{-}1)$$

In our case, we numerically calculate the nun-uniform electric field in the gap region when the 20μm Janus particle gets closer to the micro-chamber wall (Figure 6-5). Using the Eq. (6-1) the DEP force (its direction is from right to left) for the Janus particle at the (x,y,z):(9.67,0,0)μm shown in figure 6-5 is calculated as $F_{DEP} = -50.2\times10^{-23}$N. We also numerically calculate the net force that results from the other forced (i.e. electrophoretic, vortices and electro-osmotic forces) which is being applied to the Janus particle at (x,y,z):(9.67,0,0)μm shown in Figure 6-5. The net force in our case is equal to $F_{applied} = 39.8\times10^{-19}$N and its direction is from left to right. The force applied by induced vortices near the conducting section of the Janus particle has a significant contribution and applies a strong force on the Janus particle. Since $F_{applied} = 39.8\times10^{-19}N$ and $F_{DEP} = -50.2\times10^{-23}N$ are applied to the particle in opposite directions

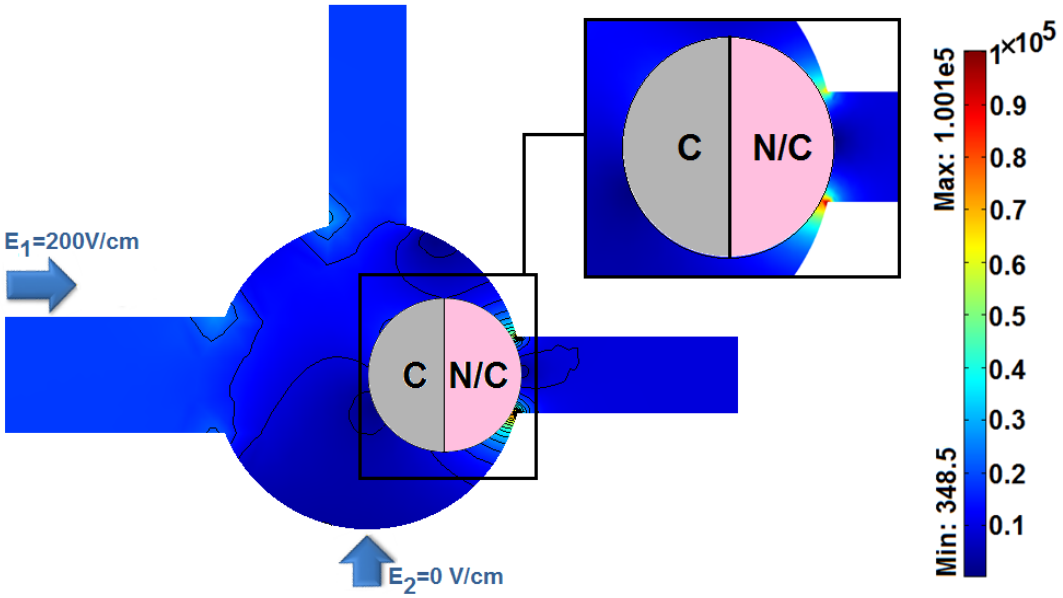


**Figure 6-5.** The distribution of the electric field and related contours in the micro-chamber when the Janus particle is very close to microchannel B. The diameter of the Janus particle and the micro-chamber are 20μm and 40μm respectively. The height of the micro-chamber is 40μm. The results are presented at the x-z plane crossing the middle of the 3D micro-valve when the particle is located at (x,y,z):(9.67,0,0)μm (the origin of the coordinate system is chosen the center of the micro-chamber).

the net force on the Janus particle is from left to right which pushes the particle towards microchannel B. Comparing $F_{applied}$ and $F_{DEP}$ illustrates that the applied force is about four orders of magnitude bigger than the DEP force so we can ignore the DEP force.

### 6-3. ICEK Micro-Valve Using a Spherical Fully Conducting Particle

To investigate the functionality of the proposed ICEK micro-valve the Janus particle is replaced with a fully conducting spherical particle. All other conditions are kept the same. Once the DC electric field of $E_1 = 200\,\text{V/cm}$ is applied, four vortices are induced around the conducting sphere and the particle moves towards microchannel B. The fully conducting particle stops after a short time, before reaching to the inlet of the microchannel B and does not move further to block its entrance (Figure 6-6). This results from the interaction between the two

vortices on the right hand side of the particle and the micro-chamber wall. As the fully conducting particle gets closer to the micro-chamber wall, the motion of the rotating fluid (vortex) is restricted by the solid wall of the micro-chamber. Thus, the momentum of the fluid motion converts to pressure, which results in a repellent force between the micro-chamber wall and the fully conducting particle. Thus, the fully conducting particle is pushed away from the micro-chamber wall. Consequently the fully conducting particle is unable to block the entrance of the microchannel B even after a long period of time. This result shows that the proposed ICEK micro-valve is not operational if a fully conducting particle is employed.

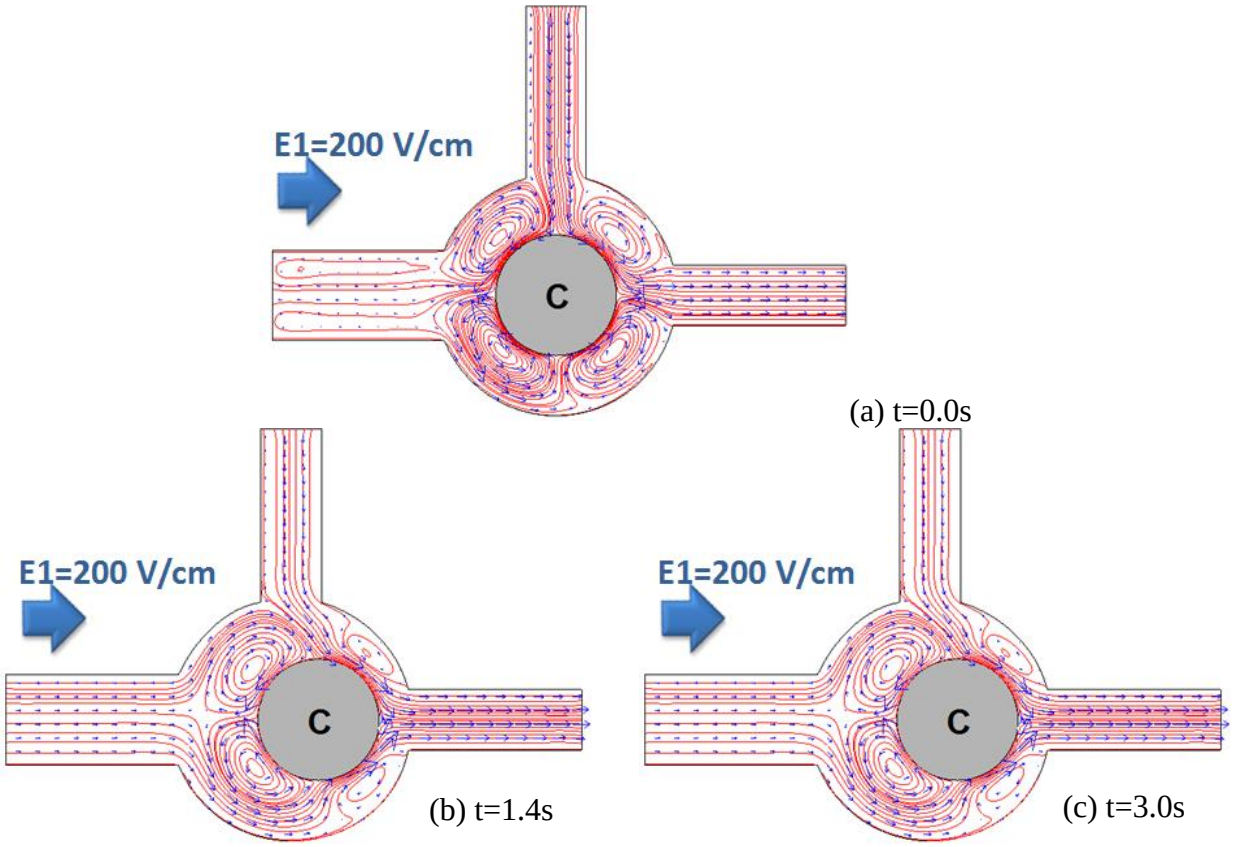


**Figure 6-6.** An ICEK micro-valve using a fully conducting particle. The particle stops moving after a while and will not block the microchannel. The streamlines show the flow pattern in the micro-chamber around the fully conducting particle. The arrows indicate the flow direction. The external DC electric field of 200V/cm is applied from left to right. The diameter of fully conducting particle and micro-chamber are 20μm and 40μm respectively. The height of micro-chamber is 40μm. The results are presented at the x-z plane crossing the middle of the 3D micro-valve at different time steps.

**6-4. Classical Electrokinetic (EK) Micro-valve Using a Spherical Non-Conducting Particle**

Using a spherical non-conducting particle instead of Janus particle for the proposed micro-valve and keeping all the other conditions the same we have an EK micro-valve (Figure 6-7). Applying the DC electric field of $E_1 = 200\,\text{V/cm}$, the electrophoretic motion of the particle moves the non-conducting particle towards microchannel B. The non-conducting particle blocks the entrance of microchannel B successfully (Figure 6-7a). To pump the fluid trough the microchannel C, as mentioned in section 6-2, we have to apply a weaker DC electric field, $E_2^*$, perpendicular to the dominant electric field, $E_1 = 200\,\text{V/cm}$. Applying $E_2^* = 50\,\text{V/cm}$ to pump the flow towards microchannel C, the non-conducting particle breaks the blockage and moves due to electrophoresis effects. Thus this EK micro-valve has leakage problem. Applying a second DC electric field of $E_2 = 200\,\text{V/cm}$ and turning off $E_1$, the non-conducting particle moves from its blocking position due to electrophoresis. Thus the non-conducting particle moves towards microchannel C and breaks the blocking (Figure 6-7b). The non-conducting particle moves with the streamlines and follows the micro-chamber wall to reach the microchannel C in 3.5s (Figure 6-7c). Comparing the switching time when Janus particle is involved (3.7s) one can conclude the response period for EK micro-mixer (with a non-conducting particle) is shorter than ICEK micro-valve (with a Janus particle). Applying $E_1^* = 50\,\text{V/cm}$ to pump the flow towards microchannel B, the non-conducting particle again breaks the blockage and moves due to electrophoresis (Figure 6-7d). Comparing this step (Figure 6-7d) with Figure 5-3e one can see that the vortices around the Janus particle apply forces to the particle and prevents the Janus particle from leaving the entrance of microchannel C. The results show that using a non-conducting particle to operate the micro-valve reduces the response time in comparison with

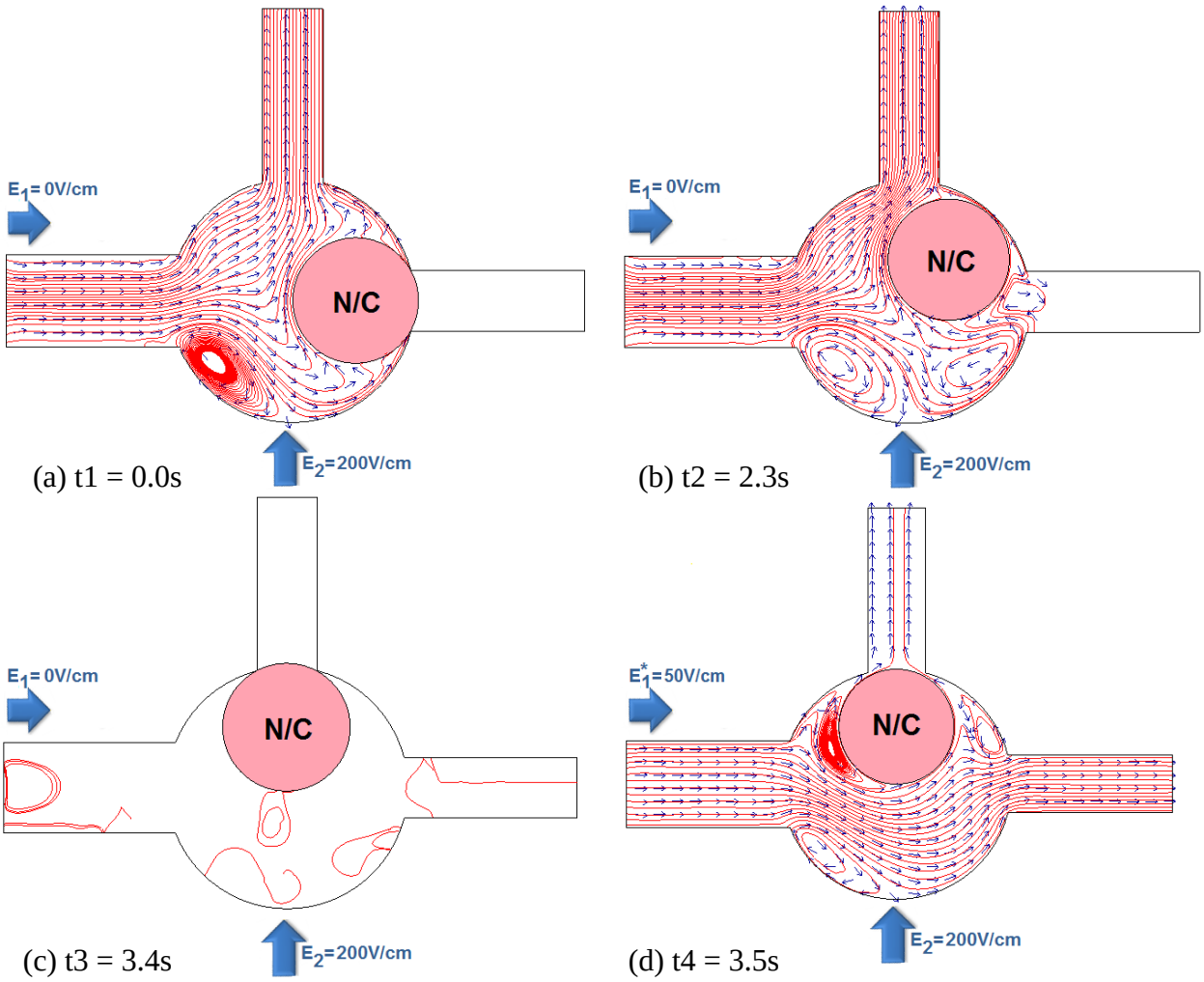


**Figure 6-7.** An EK micro-valve using a non-conducting particle. This valve always has leakage problem. The streamlines show the flow pattern in the micro-chamber around the fully conducting particle. The arrows indicate the flow direction. The diameter of the non-conducting particle and the micro-chamber are 20µm and 40µm respectively. The height of micro-chamber is 40µm. The results are presented at the x-z plane crossing the middle of the 3D micro-valve at different time steps.

using a Janus particle (which is an improvement) but the main drawbacks is leakage problem with this system. Thus an EK micro-valve using a non-conducting particle dose not satisfy the requirements of a reliable micro-valve.

The DEP force was shown that can be ignored in case of using a Janus particle for micro-valve. Since there are no vortices acting on the non-conducting particle, calculations can show that the DEP force will be comparable with the net force arising from electro-osmotic and

electrophoretic effects. Therefore, the DEP force will prevent the non-conducting particle from getting very close to the entrance of microchannel C. This means considering DEP force in our modeling of an EK micro-valve using a non-conducting particle shows such a valve always has leakage problem and using it for flow control is not feasible.

### 6-5. Summary and Conclusion

In this chapter we have proposed a novel application (ICEK micro-valve) for induced-charge electrokinetic phenomena for microfluidic devices and Lab-on-a-Chip (LOC) components. This ICEK micro-valve is easy to operate by controlling the motion of a spherical Janus particle (which is placed in a micro-chamber) using appropriate DC electric fields at specific times.

In chapters 4 and 5 we demonstrated that the orientation of a Janus particle is sensitive to the direction of the applied DC electric field. Taking advantage of this characteristic, the Janus particle can quickly block or open the inlet of the desired branch of a micro-valve by switching the direction of the main DC electric field. The flow rate through the micro-valve can also be controlled by applying another DC electric field for pumping. We have numerically shown that the applied DC electric field has inverse effect on the switching time of the ICEK micro-valve.

Replacing the Janus particle (which is used in designing the micro-valve) with (i) a fully conducting (ii) a non-conducting particle demonstrates that both of these valves have leakage problem since they are unable to block the inlet of the desired microchannel. Thus, they cannot be considered as applicable options to design a practical and reliable micro-valve. The proposed ICEK micro-valve, using a spherical Janus particle can be easily fabricated and controlled; thus it has a great potential for developing integrated LOC devices.

In next chapter we will introduce an ICEK micro-mixer with high performance which can be considered as a practical device to be used in microfluidic devices or LOC systems. This ICEK micro-mixer contains a fully conducting particle inside a microchamber. By controling the magnetude and direction of the applied DC electric fields, this ICEK micro-mixer is able to provide 100% homogeneous mixture of different liduid streams at the downstram of the system (numerically).

## CHAPTER VII: Application (2)

# Induced-Charge Electrokinetic Micro-Mixer

The system of the equations used for numerically modeling the induced-charge electrokinetics was introduced in chapters 2 and 3. Using those equations we numerically studied the behaviour of a heterogeneous particle and the vortices induced near its conducting section in a microchannel (chapter 4). We experimentally visualized the induced vortices around a conducting sphere when a DC electric field was applied. Also, our experiments verified the results of our numerical modeling (chapter5). Using these numerical and experimental results we introduced an ICEK micro-valve in chapter 6. In this chapter a novel micro-mixer based on the induced-charge electrokinetic motion of an electrically conducting particle is proposed. For most microfluidic applications, it is desired to mix different streams of fluids rapidly in a continuous flow mode. To achieve this goal, we consider a mixing-chamber containing a fully electrically conducting particle. This mixing chamber is connected to four electrodes. Once the electric field is applied vortices are induced around the electrically conducting particle due to the interaction of the applied electric field and the induced surface charge on the particle. These vortices will significantly enhance the mixing of the different fluid streams which are entering the mixing-chamber. The effects of applied electric field, size of the micro-chamber and particle on the performance of this ICEK micro-mixer are numerically studied. A homogeneous mixture can be

obtained when two equal but perpendicular DC electric fields are applied. The proposed micro-mixer does not have the complication of other micro-mixers for fabrication and can be considered as an efficient micro-mixer for LOC applications and in hand-held devices.

### 7-1. Geometry and Computational Domain

The structure of the proposed micro-mixer is shown in Figure 7-1a. One micro-chamber is connected to two microchannels. The inlet channel is placed on the left hand side of the chamber and delivers two parallel streams of two different fluids into the micro-chamber from entrance A and B (see Figure 7-1a). One stream contains a sample species with a concentration $C_0$. The other stream is the same fluid without the sample molecules (i.e., the sample concentration is zero). On the right-hand side of the micro-chamber, there is a microchannel which is used as an outlet. A circular fully conducting particle is placed in the middle of the micro-chamber. The density of this particle is chosen to be exactly the same as the fluid which is filled the micro-mixer. Thus the particle, initially, is suspended in the center of the micro-chamber. Four electrodes are used to control this micro-mixer. Applying voltage between electrodes 1 and 2 produces a potential difference and generates DC electric field in the E1 direction. This electric field is responsible to generate the electro-osmotic flow to transport the fluid in and out of the mixing-chamber, in addition to induce the vortices. Electrodes 3 and 4 are used to produce electric field in the E2 direction. To achieve the mixing function, it is necessary to control the positions of the particle and the induced vortices by the resultant applied DC electric field. The main function of the electric field E2 is for controlling the position of the particle.

In our micro-mixer, $D_p$ is the particle's diameter, and also the lengths of the microchannels in the computation domain. The width and height of the microchannels are 40% of $D_p$. The

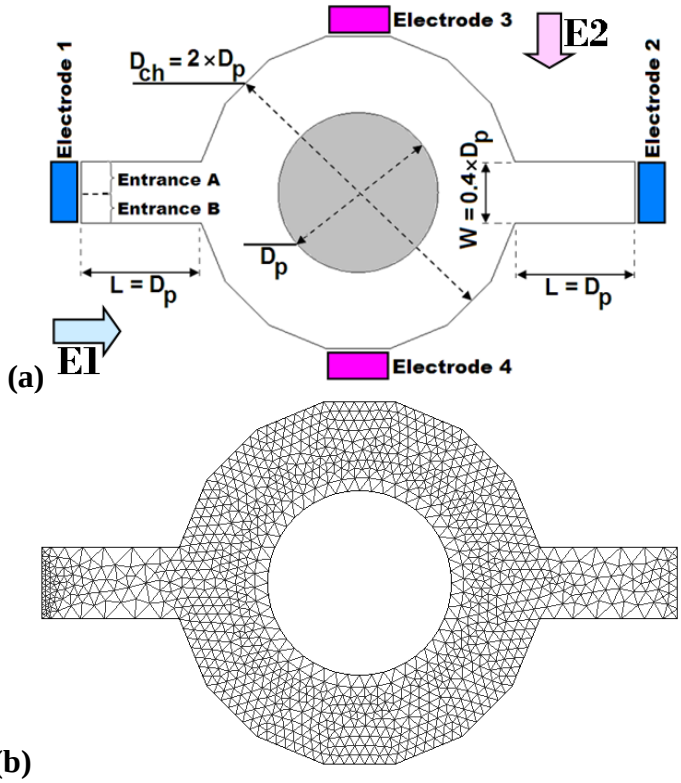


**Figure 7-1.** (a) Schematic diagram of the proposed micro-mixer with two micro-channels and one suspended fully conducting particle inside the micro-chamber, (b) computational domain and corresponding mesh distribution.

Cylindrical micro-chamber's diameter and depth are two times of the diameter of the particle. The zeta potential on the channel and the micro-chamber walls is -50mV. The fluid flow in this system is entirely driven by electro-osmosis; and the ends of the channel are connected to open reservoirs, so that no overall pressure gradient is present in the system.

The flow field and the coupled time-dependent concentration field in the micro-mixer were numerically studied using the governed equations and the boundary conditions (which were listed in chapter 2 and 3). The computational domain is fully covered by 2D tetra elements as presented in Figure 7-1b. The mathematical models in the computation domain were solved by the commercial software COMSOL Multiphysics3.5a. Grid independency study was conducted. The optimal number of grids used for the computational domain to obtain the grid-independent

results is 10753. Further increase in the number of grids leads to longer computational time without improving the results. ALE[5] moving grid technique was utilized to fulfill the numerical simulation of the particle–fluid coupled multi-physics system under various conditions.

Many micro-fabrication methods and alignment methods are available to fabricate a micro-structure as designed in this study [129]. Typically the microfluidic chip is made by bonding one layer having a microchannel structure (such as a PDMS plate) with another layer of flat substrate (such as a glass slide). The particle can be placed in the middle of the micro-chamber before bonding the two layers together. In this way the conducting particle is placed in the micro-chamber during the micro-fabrication of chip.

The Laplace equation (Eq. (3-2)) is solved to calculate the distribution the electric field in the computational domain. We used Eq. (3-3a, b, and c) to solve the Laplace equations as the boundary conditions subjected to this study. The continuity condition is valid all over the micro-mixer domain (Eq. (3-4). To solve the Navier-Stokes Equation (Eq. (3-5)) we used the following boundary conditions as mentioned in chapter 3: Eq. (3-6a to d). The concentration of the fluid in the micro-mixer is modeled by Eq. (3-17). The boundary conditions for the concentration equation are: (i) the concentration of the fluid stream at the inlet is constant and known (Eq.(3-18a); (ii) the micro-mixer walls are not permeable with respect to the species in the fluid; thus there is no concentration flux toward the walls and particle surface Eq. (3-18b). The initial condition for the presented system is set as Eq. (3-18c). This initial condition emphasis that the concentration of the electrolyte filled the microchamber at t=0s is zero.

[5] An Arbitrary Lagrangian Eulerian **(ALE)** moving grid method is used to couple Navier-Stokes and convection-diffusion equations with moving interface boundaries of particle-fluids. ALE technique is capable of modeling fluid-particle interactions in COMSOL Multiphysics by solving the coupled equations in a continuously deforming geometry since the position of the suspended particle in the micro-chamber changes as a result of EOF flow and EOP motion and vortices around the conducting particle.

Consider two types of fluids enter the inlet as two parallel streams as shown in Figure 7-1a. The concentrations in the two halves of the inlet channel are $C_A$ and $C_B$, respectively. To quantify the performance of the mixer, the mixing efficiency, $e$, is defined as:

$$e = (1 - \int_0^W (C - C_\infty) \Big/ \int_0^W (C_0 - C_\infty)) \times 100\% \qquad (7\text{-}1)$$

where $C_0$ is the concentration distribution at the entrance A and represents the concentration of species in the first fluid. C is the local concentration at the outlet of the micro-mixer. If $C_A=C_0$ and $C_B=0$ then the concentration of the resultant mixture will be defined by $C_\infty = (C_A+C_B)/2$. A fully mixed state therefore would have a 100% mixing efficiency while the unmixed state would have a 0% mixing efficiency. The properties that are used in this numerical modeling are listed in Table 7-1.

**Table 7-1** Constants used for our numerical simulations

| **Parameters** | **Values** |
|---|---|
| Dielectric constant $\varepsilon$ | 80 |
| Permittivity of vacuum, $\varepsilon_0$ (C $V^{-1}$ $m^{-1}$) | $8.854\times10^{-12}$ |
| Viscosity, $\mu$ (kg $m^{-1}$ $s^{-1}$) | $0.9\times10^{-3}$ |
| Density, $\rho$ (kg $m^{-3}$) | 998 |
| Zeta potential of channel walls, ζ (mV) | -50 |
| Particle Diameter, $D_p$ (μm) | 20 |
| Micro-channel width, $W$ | $0.4\times D_p$ |
| Microchannel length, L | $D_p$ |
| Micro-chamber diameter, $D_{ch}$ | $2 \times D_p$ |
| Diffusion coefficient, $D_i$ ($cm^2$ $S^{-1}$) | $1.52\times10^{-6}$ |
| Molar concentration at entrance A, $C_A$ ($mol/m^3$) | 10 |
| Molar concentration at entrance B, $C_B$ ($mol/m^3$) | 0 |
| Horizontal DC Electric Field, E1 (V/cm) | 40 |
| Vertical DC Electric Field, E2 (V/cm) | 40 |

## 7-2. Verifying the Accuracy of Our Numerical Simulation

To verify the proposed numerical technique, this method is applied to the electrokinetic mixing process of two different fluid streams in a straight microchannel. Two electrically conducting triangular hurdles are inserted into this microchannel walls as shown in Figure 7-2a. Once the electric field is applied vortices will be induced near these conducting hurdles. This system was studied by Wu and Li [36] to enhance the mixing in a straight microchannel. For comparison, Figure 7-2b shows the numerical result of our numerical method and the experimental and numerical results of Wu and Li. One can see the current numerical method is in good agreement with the experimental results.

## 7-3. Effects of the Conductivity of the Moving Particle

Consider a micro-chamber described in Figure 7-1 which has no particle inside. Two parallel streams of fluids enter the chamber, once the DC electric field E1 is applied. One stream is a buffer solution carrying a sample species with a sample concentration of $C_0$. The other stream is a pure buffer solution with zero sample concentration. The only mixing mechanism ( to mix these two parallel laminar flows) is the diffusion at the interface region along the micro-mixer. As demonstrated in Figure 7-3a, at the exit of the chamber, the two fluids are poorly mixed. The resultant mixture is not acceptable to be used in microfluidic devices. To improve this result we used a non-conducting particle. This non-conducting particle is initially released in the middle of the micro-chamber. Figure 7-3c demonstrates that, in case of using non-conducting particle, the mixing result is not improved. In addition to the heterogeneous mixture that obtained when using a non-conducting particle, this type of mixer has another critical drawbacks. This non-conducting particle tends to move forward while the electric field is applied; consequently this particle will blocks the flow exit, as shown in Figure 7-3c.

(a)

(b)

(c)

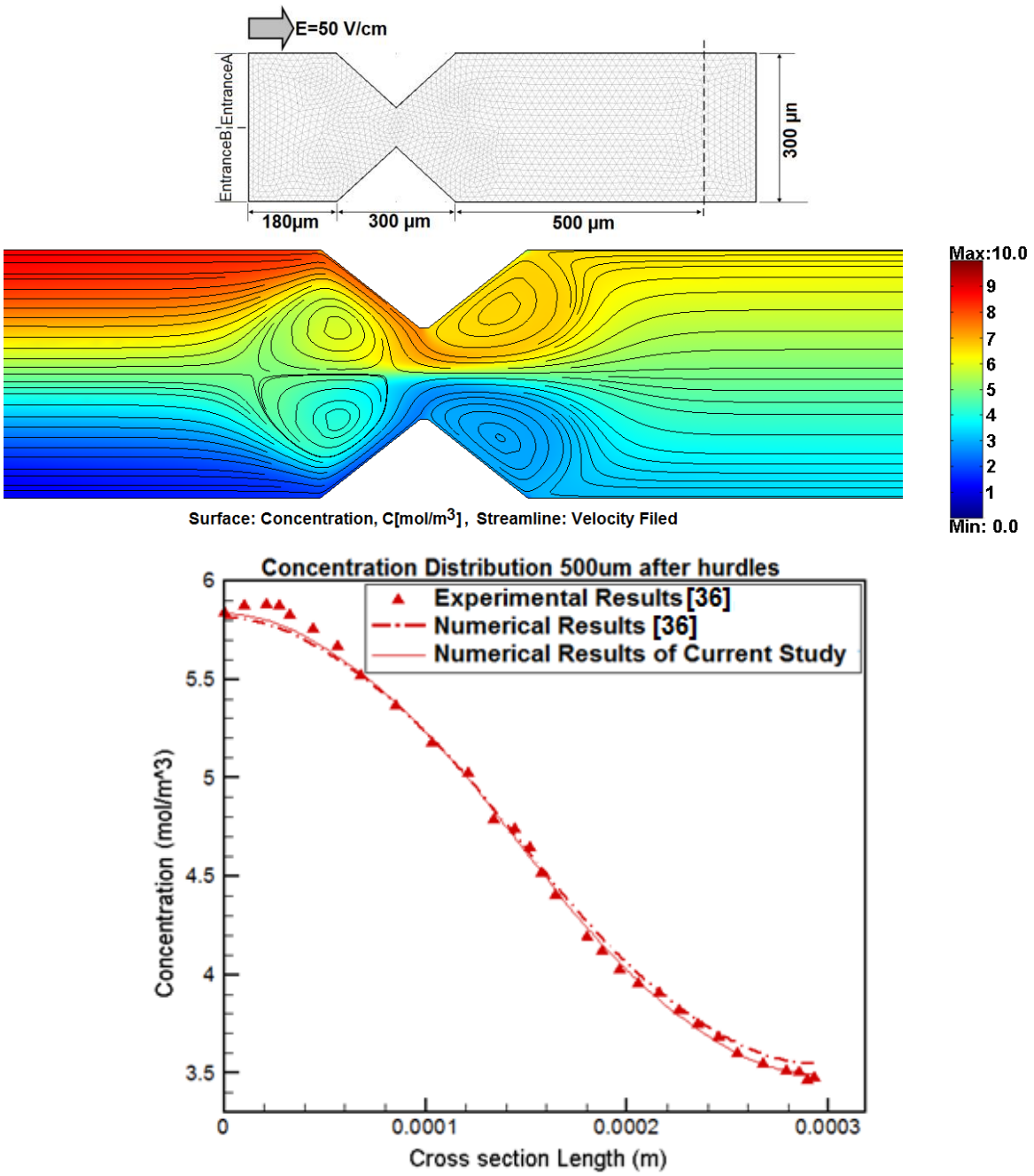


**Figure 7-2.** (a) Two fully conducting triangular hurdles are inserted into a straight microchannel (which has non-conducting walls) and two streams enter the microchannel inlet with different concentrations. The concentrations of the two parallel fluid streams are 10Mol/m$^3$ at entrance A and 0Mol/m$^3$at entrance B, (b) the concentration distribution and mixing result by using conducting hurdles in a microchannel. The corresponding flow pattern is shown by streamlines, (c) concentration distribution along the cross section of the microchannel. A DC electric field (50V/cm) is applied from left to right. The results are plotted at x=980µm at the downstream of the flow and is shown by the dash line in part (a).

Figure 3d and 3e show the effect of using a fully conducting particle in present micro-mixer. When a fully conducting particle is placed in the chamber, the induced-charge electrokinetic flow around the particle significantly changes the flow field in the chamber. Four vortices are induced around the fully conducting particle once the DC electric field is applied. These induced vortices circulate fluid across the streamlines of the two different fluid streams and boost the mixing process. The fully conducting particle moves toward the exit of the chamber driven by the applied electric field E1.

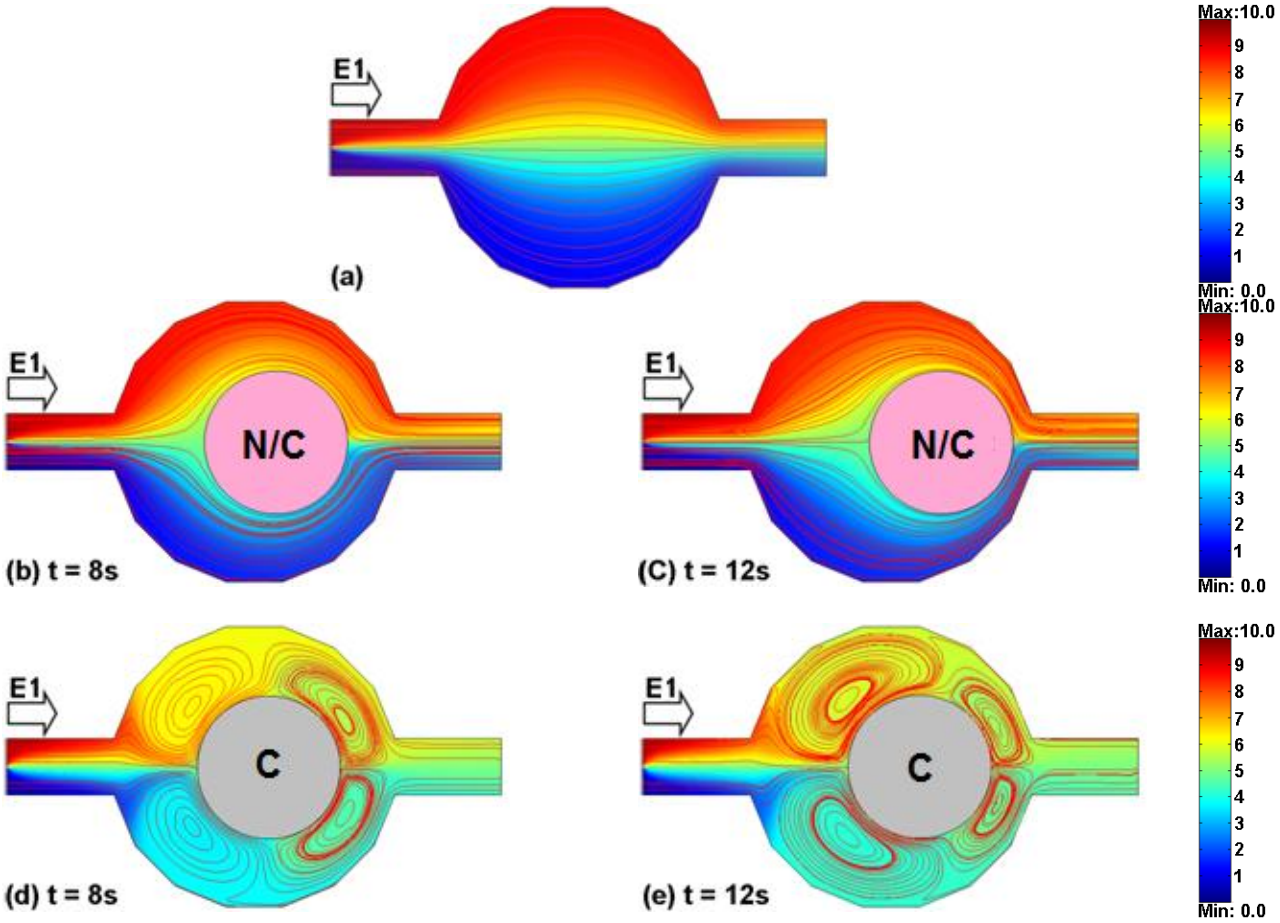


**Figure 7-3**. Flow pattern and concentration distribution in the micro-mixer. Red lines inside the micro-chamber represent the streamlines of the flow field. The color bar shows the concentration distribution. The figure shows a micro-mixing chamber (a) without a particle inside, (b and c) with a non-conducting particle and (d and e) with a fully conducting particle at different time steps. DC electric field (E1=40V/cm) is applied from left to right. "N/C" and "C" represent non-conductive and fully conductive materials respectively.

However, the particle stops moving when it gets close to the right hand side wall of the micro-chamber. The motion of the rotating fluid (caused by vortices) is restricted by the micro-chamber wall. Thus, the momentum of the fluid motion converts to pressure, which results in a repellent force between the wall and the particle. This repellent force pushes the fully conducting particle away from the right-side wall of the micro-chamber. At the same time, two vortices on the left hand side of the fully conducting particle push the particle to the right. When these forces are balanced, the particle stops at an equilibrium position. Consequently, the particle will not block the exit of the chamber. As shown in Figure 7-3e the induced vortices around the fully conducting particle significantly enhance the mixing process. The concentration profile at the exit of the micro-chamber is plotted in Figure 7-4 for three investigated cases of Figure 7-4.

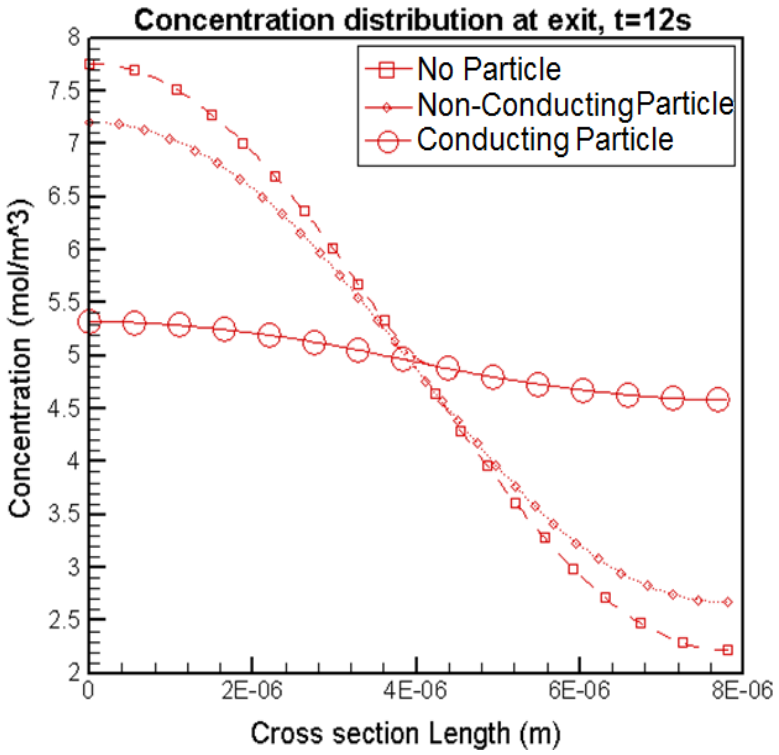


**Figure 7-4.** Comparison of the concentration distribution at the outlet of the micro-mixer at t=12s. E1 represents the horizontally applied electric field and is equal to 40V/cm.

### 7-4. Effect of the Position of the Conducting Particle on Mixing Result

Under the applied only one DC electric field, E1, from left to right, the induced vortices are symmetrical to the center line of the micro-chamber (as shown in Figure 7-3d and 7-3e). Each of these induces vortices covers only one quarter region of the micro-chamber and they are located in one stream only. In order to improve the mixing result, it is desirable to have each induced vortex positioned across the boundary of the two streams. Thus, such a vortex can circulate fluid from the high-concentration stream to the low-concentration stream and vice versa. To achieve this goal, a secondary electric field E2, perpendicular to E1, is added into the system with different strengths while the dominant electric field, E1, remains constant (see Figures 7-5a-d). In Figure 7-5a, the fully conducting particle has already reached its stable position and does not move any longer when the only applied electric field is E1.

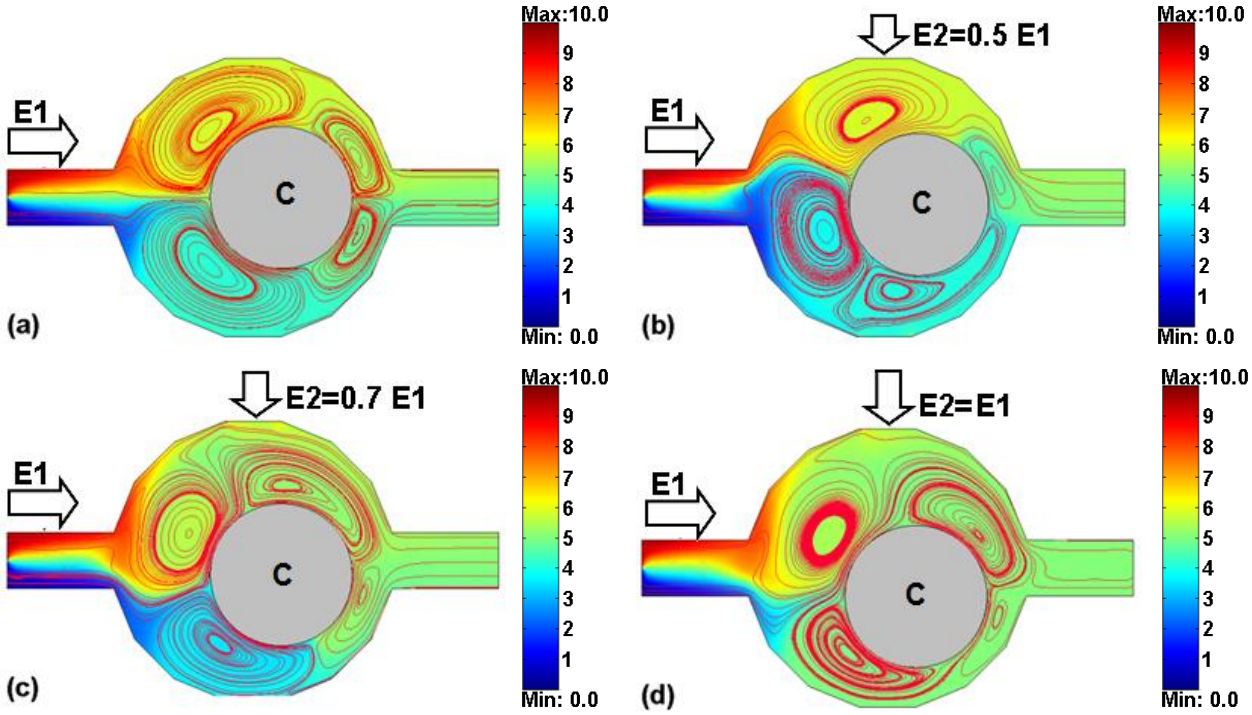


**Figure 7-5.** Control of the positions of the particle and corresponding induced vortices using different DC electric fields perpendicular to E1. The new configuration of electric fields boosts the mixing process. The red lines inside the micro-chamber represent the streamlines of the flow field. The color bar shows the concentration distribution. E1=40V/cm is applied from left to right; and E2 represent the horizontally and vertically applied electric fields. "C": conductive.

Figures 7-5b to 7-5d show that the secondary electric field, E2, changes the net electric field direction. Thus the positions of the vortices in the chamber are affected by net allied electric field. Consequently, some vortices cover both streams and boost the mixing process. Figure 7-6 compares the concentration field at the exit of the mixing chamber as a function of different values of E2. This figure demonstrates that the best mixing result is archived when the applied electric fields have the same magnitudes. At this case (E1=E2) the resultant mixture flow is completely homogeneous, and the efficiency of our proposed ICEK micro-mixer is e=100%.

When we only apply E1 to the ICEK micro-mixer (Figure 7.3e) the induced vortices around the conducting particle are generated in a symmetric form. Thus each pair of vortices is located in one half of the micro-chamber and cannot boost mixing process efficiently. Once the second electric field is applied perpendicular to the first electric field, the resultant electric field direction has -45 degree angle with the positive direction of the x-axis therefore the conducting particle is pushed to move in this new direction (Figure 7.4d).

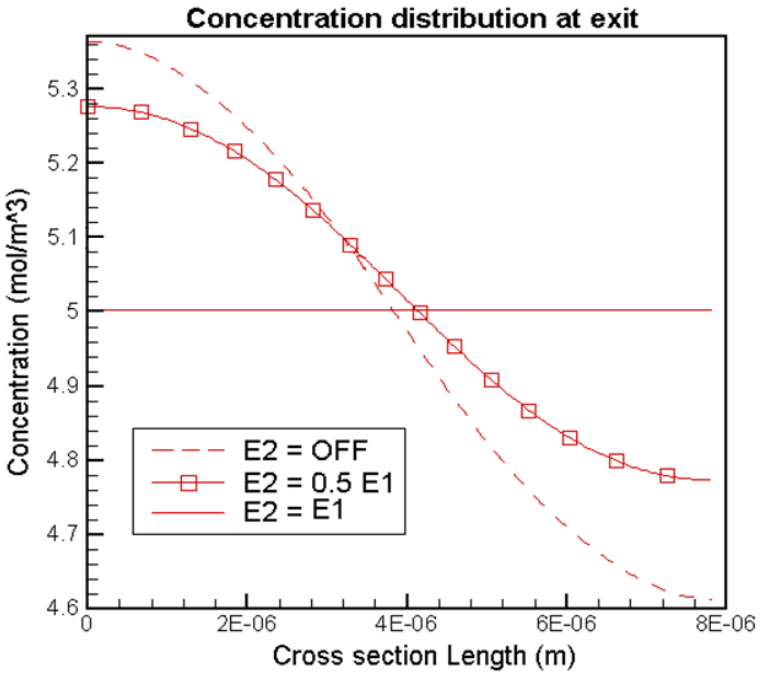


**Figure 7-6.** Comparison of the concentration distribution at the outlet of the micro-mixer at t=12s. E1 represents the horizontally applied electric field and is equal to 40V/cm.

Because of the displacement of conducting particle from the center of the micro-chamber to one side of the chamber, the vortices are not located in one region of fluid stream. The vortices now can enhance mixing process. However this is a numerical simulation and some facts have been ignored based on the assumptions we made to do this simulation (chapter 2- table 2-1). Predictably the efficiency equal to 100% is not reachable in real experimental cases. Our simulation shows we can improve mixing process by using a simple micro-chamber, a conducting particle when we apply an electric field in a direction that moves the particle from its symmetrical position (Figure 7-5). The comparison between other types of micro-mixer and the presented ICEK micro-mixer is summarized in Table 7-2. As one can see the presented ICEK requires small mixing length and can provide a homogeneous mixture at the exit of this mixer.

### 7-5. Effects of the Applied DC Electric Field

The motion of the fully conducting particle depends on the applied DC electric field. The size and the strength of the vortices around the particle also depend on the applied DC electric field. In section 7-4, it was shown that the best mixing effect is achieved when two equal and perpendicular electric fields are applied to the micro-mixer. According to this achievement, when

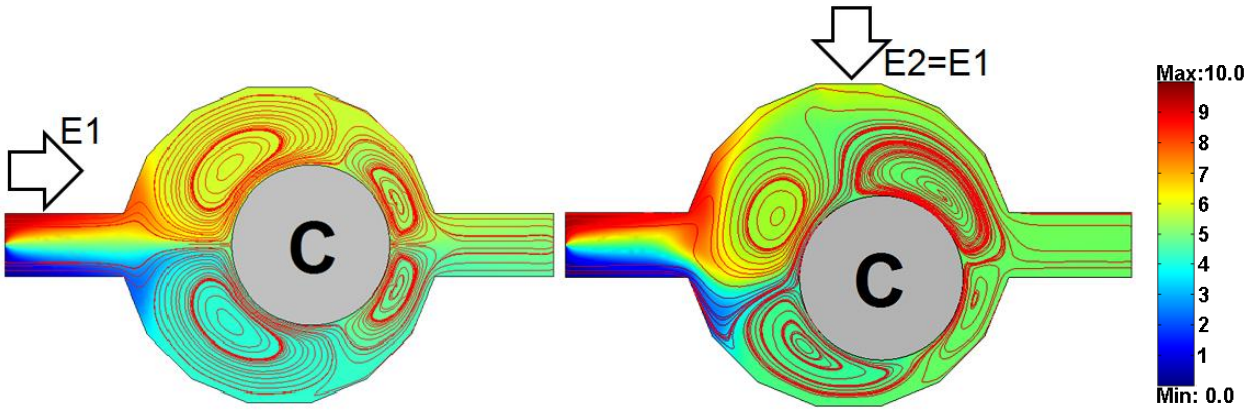


**Figure 7-7.** Comparison of the functionality of an ICEK micro-mixer (a) only horizontal electric field is applied, (b) horizontal and vertical electric fields are applied. E1= 40V/cm.

the resultant electric field has a -45$^{o}$ angle with the positive direction of the x-axis the best mixture result can be obtained. Consider a fully conducting particle of 20µm diameter is initially suspended in the middle of the micro-chamber (with a diameter of 40µm). Once the applied electric fields is increased in both vertical and horizontal directions (with the same magnitudes) the particle is pushed to move from its original position (x=0, y=0) to a different final and stationary position (Figure 7-8). Increasing the strength of the electric field will shorten this travel time as listed in Table 7-3. As long as the net electric field is applied in the -45$^{o}$, the mixing efficiency remains e=100% and homogeneous resultant mixture is independent from the strength of the applied electric fields. Changing the strength of the resultant applied electric field only changes the mixing time. It should be noted that the displacement distance and corresponding traveling time do not change linearly with the variation of the applied electric fields.

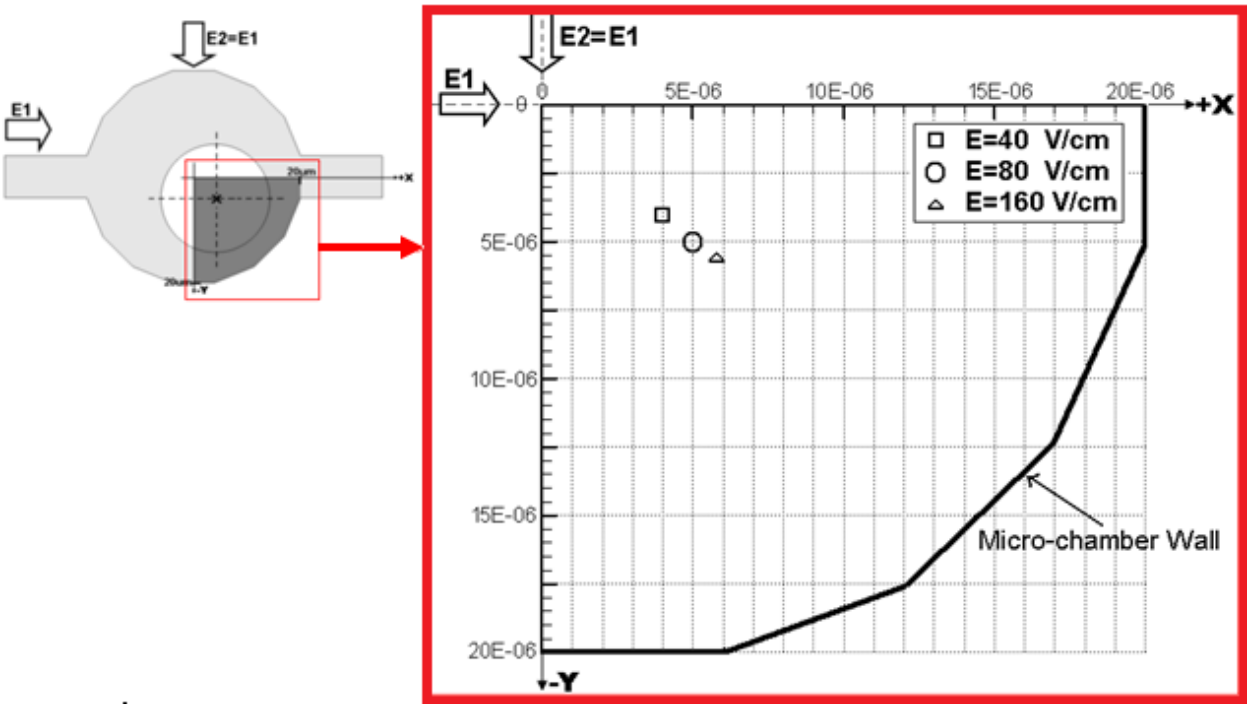


**Figure 7-8.** The final position of the fully conducting particle center under the different applied DC electric fields.

**Table 7-2.** The comparison between the performance of the presented ICEK micro-mixer and other types of active micro-mixers

| Reference | Mixing method | Mixing Technique | Mixing Length (µm) | Mixing time (ms) | Efficiency (%) |
|---|---|---|---|---|---|
| Lim, et al. [130] | Electrokinetic time-pulsed | Periodic electro-osmotic flow | 200 | N/R | 88 |
| Campisi, et al. [131] | Dielectrophoretic | Chaotic advection based on Linked Twisted Map | 1000 | N/R | 85 |
| Du, et al. [132] | Electrohydrodynamic force | Staggered herringbone structure | 825 | N/R | 20 |
| Wang, et al [69] | Magneto-hydrodynamic flow | High operating frequency | 1100 | 500 | 97.7 |
| Ahmed, et al. [133] | Acoustic / Ultrasonic | Acoustically driven sidewall-trapped micro-bubbles | 120 | 650 | 2.5 |
| Zhang et al. [134][85] | Electrohydrodynamic force | Staggered herringbone structure | 2300 | N/R | 50 |
| Presented Mixer | ICEK | Using the induced micro vortices to mix the fluid streams | 60 | 3s (can be reduced depending the applied electric fields) | 100 |

**N/R: Not reported**

**Table 7-3.** The final position of the fully conducting particle center under the different applied DC electric fields and the corresponding traveling time

| E (V/cm) | Center Position (µm) | | Δt (s) |
|---|---|---|---|
| | X | Y | |
| 40 | 4 | -4 | 4.6 |
| 80 | 5 | -5 | 2.8 |
| 160 | 5.6 | -5.6 | 1.2 |

## 7-6. Summary and Conclusions

A new and rapid ICEK micro-mixer using induced-charge electrokinetics is presented in this chapter. The proposed micro-mixer includes one cylindrical micro-chamber connecting to two microchannels. One spherical particle is located in the middle of this micro-chamber. Our numerical results illustrate that the only type of the particle which can provide a homogeneous mixture is fully conducting particle. This is as a result of micro-vortices which are induced around the conducting particle and boost the mixing process. The final position of the conducting particle and the strength of the induced vortices are controlled by two perpendicular DC electric fields. It is found that applying the electric field in a $-45^{o}$ angle (from the horizontal axis direction) will achieve the best mixing result. In this case the efficiency of our proposed ICEK micro-mixer is 100% and a homogeneous mixture will be obtained at downstream of the micro-mixer. Applying higher electric fields will shorten the required tome for mixing and provide a rapid ICEK micro-mixer. This proposed ICEK micro-mixer has not the complexity and drawbacks of existence micro-mixers. Thus it can be a good alternative for current micro-mixer to be used I LOC devices or microfluidic applications.

In the next chapter (chapter 8) we will conduct numerical and experimental studies on ICEK motion of a particular triangular heterogeneous particle (THP). Applying a DC electric field, this THP starts rotating around a point near its center and will not stop as long as the electric field is applied. Such a design can be used as an ICEK micro-motor to manipulate and control the motion of fluids or as a stirrer to achieve a homogeneous mixture, etc. Furthermore, our numerical findings will be validated by experimental results in this chapter. In chapter 9 we will summarize the theory, numerical simulations and experimental validation of induced-charge electrokinetic phenomena that was presented in this thesis.

## CHAPTER VIII: Application (3)

# Induced-Charge Electrokinetic Micro-Motor

In chapters 2 and 3 we classified the system of the equations used for numerically modeling the induced-charge electrokinetics in this thesis. The behavior of a heterogeneous particle and the induced vortices around its conducting section is numerically investigated in chapter 4. The induced vortices around a conducting sphere (when a DC electric field is applied) are experimentally visualized in chapter 5. Our experiments verified the numerical modeling that we presented in chapter 4. Employing these numerical and experimental results, we numerically developed an ICEK micro-valve in chapter 6 and ICEK micro-mixer in chapter 7. This chapter presents a numerical and experimental study of the rotation of a triangular heterogeneous particle suspended in an aqueous solution under applied DC electrical field.

This equilateral triangle particle is electrically non-conducting, however has three electrically conducting corners. The DC applied electric field will induce charges at the conducting corners and consequently the induced electro-osmotic flow will generate vortices near the corners. Because of the intentionally designed asymmetrical sizes of the conducting area around each corner, the size and the strength of the induced vortices on the two sides of each corner are different, resulting in a net force on each corner. By designing the conducting corners, the net force acting on each corner can rotate the triangular particle continuously as long as the DC

electric field is applied. The effects on the angular velocity of applied DC electric field, the size of the particle and the conducting area of the corners were investigated by numerical simulation. We also investigate the effect of shape on the rotation of such heterogeneous particles. Experiments have proved the theoretically predicated phenomena successfully.

**8-1. Geometry and Computational Domain**

Consider a triangular heterogeneous particle (THP) suspended in the middle of a square chamber filled with an aqueous solution under applied DC field, as illustrated in Figure 8-1. This triangular heterogeneous particle (THP) has a non-conducting material body and its three corners are covered by an electrically conducting (metal) material, as indicated by the red lines in Figure 8-1. The length of the equilateral triangle side is L. The sizes of the conducting sections on the two sides of each corner are C1= 0.2L and C2=0.05L, respectively. C1 and C2 are chosen to break the symmetry of the induced vortices so that the particle can rotate. The size of the chamber is large enough to ignore the wall effects on the electrical field and the flow field. As indicated in Figure 8-1, the direction of the applied electric field is from left to right. θ is the alignment angle of the conducting surface C1 at each corner with respect to the direction of the applied electric field (the horizontal line). The zeta potential on the non-conducting sections of THP is assumed to be $\zeta_p = -50mV$. No overall pressure difference is present in the system. The effect of gravity is neglected.

In order to study the transient flow field and the motion of the triangular heterogeneous particle (THP) under an applied DC field, we used the transient mathematical model which describes the electric field, the flow field, and the particle motion in this system. This system was introduced in chapter 3.

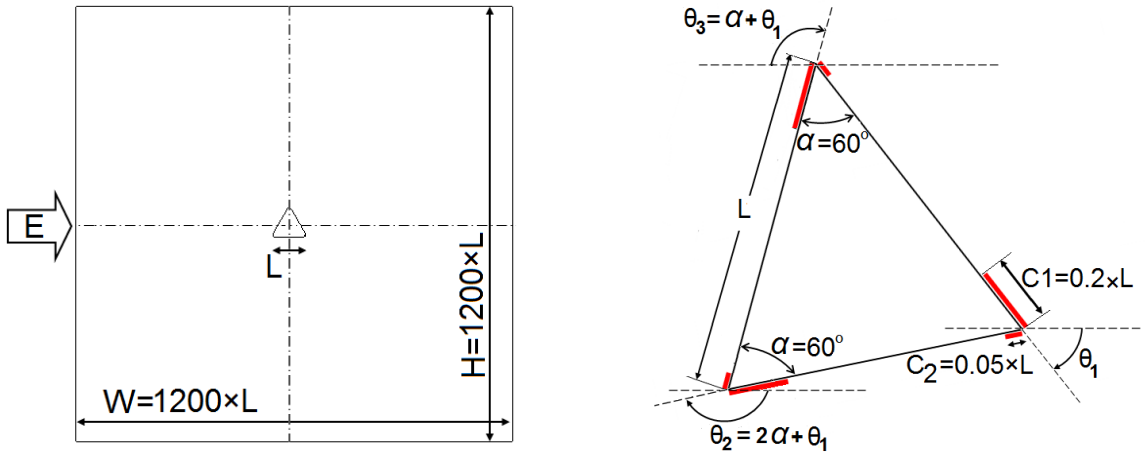


**Figure 8-1**. Schematic diagram of a triangular heterogeneous particle located at the center of a square chamber. E represents the external electric field direction. C1 and C2 are the conducting surfaces at each corner and the rest of the particle surface is non-conducting material. θ is the alignment angle of the conducting surface C1 at each corner with respect to the direction of the applied electric field (the horizontal line).

The motion of the THP is coupled with the applied electric field and the time-dependent flow field. The three-dimensional numerical simulation of the particle motion therefore requires solving the equations with the boundary conditions and initial conditions described above. In this chapter, the computational domain is fully covered by three-dimensional tetra meshes. The mathematical model is solved by the commercial software FLUENT13. A moving mesh technique was utilized in the numerical simulation of the particle–fluid coupled system under various conditions. According to conducted grid independency study, the optimal number of grids used for the computational domain to obtain the grid-independent results is 57271582 cells. To avoid dealing with damaged meshes and inaccurate results, it is necessary to re-mesh the computational domain after the particle rotates for a while since the cells become significantly deformed.

Using Laplace equation (Eq. (3-2)) we could calculate the distribution of the electric field in the square computational domain with the heterogeneous particle in the middle of it. The boundary condition on the left hand side boundary of the square well is addressed by Eq. (3-3b). The left hand side boundary of this well is set up as Eq. (3-3c), and c ). Considering the particle walls are insulating this boundary condition applies by Eq.(3-3a) to solve the Laplace equations. The continuity condition is valid all over the micro-mixer domain (Eq. (3-4). To solve the Navier-Stokes Equation (Eq. (3-5)) we used Eq. (3-6a to d) as the boundary conditions. There is no pressure gradient in the system when we set up all the boundaries of the square well as open boundary. There is no fluid flux toward the surface of the particle. The Helmholtz-Smoluchowski relation is valid on the non-conducting sections of the surface of the heterogeneous particle. The slipping velocity on the the conducting surfaces of the particle is calculated base on the numerical simulation of the induced-zeta potential on the surface.

**8-2. Motion of a Triangular Heterogeneous Particle**

Let's consider a non-conducting triangular particle with three conducting corners in the middle of an infinitely large fluid, as illustrated in Figure 8-1. Once a DC electric field is applied from the left to the right, charges are induced at conducting surfaces of the three corners. Because the local electrical field and the induced charges are different at different corners, and also the conducting surfaces have different sizes between the two sides of each corner, the interaction forces between the applied electric field and the these three corners are different. The net force acts to rotate the THP. However, because of the symmetry of the equilateral triangle, while the THP rotates, at least one of the alignment angles is always non-zero. Therefore, THP rotates continuously. Figure 8-2 illustrates rotation of a THP during for one cycle. The bright green spot on the top of one corner of the THP is used to trace the motion of the particle. For a THP with a

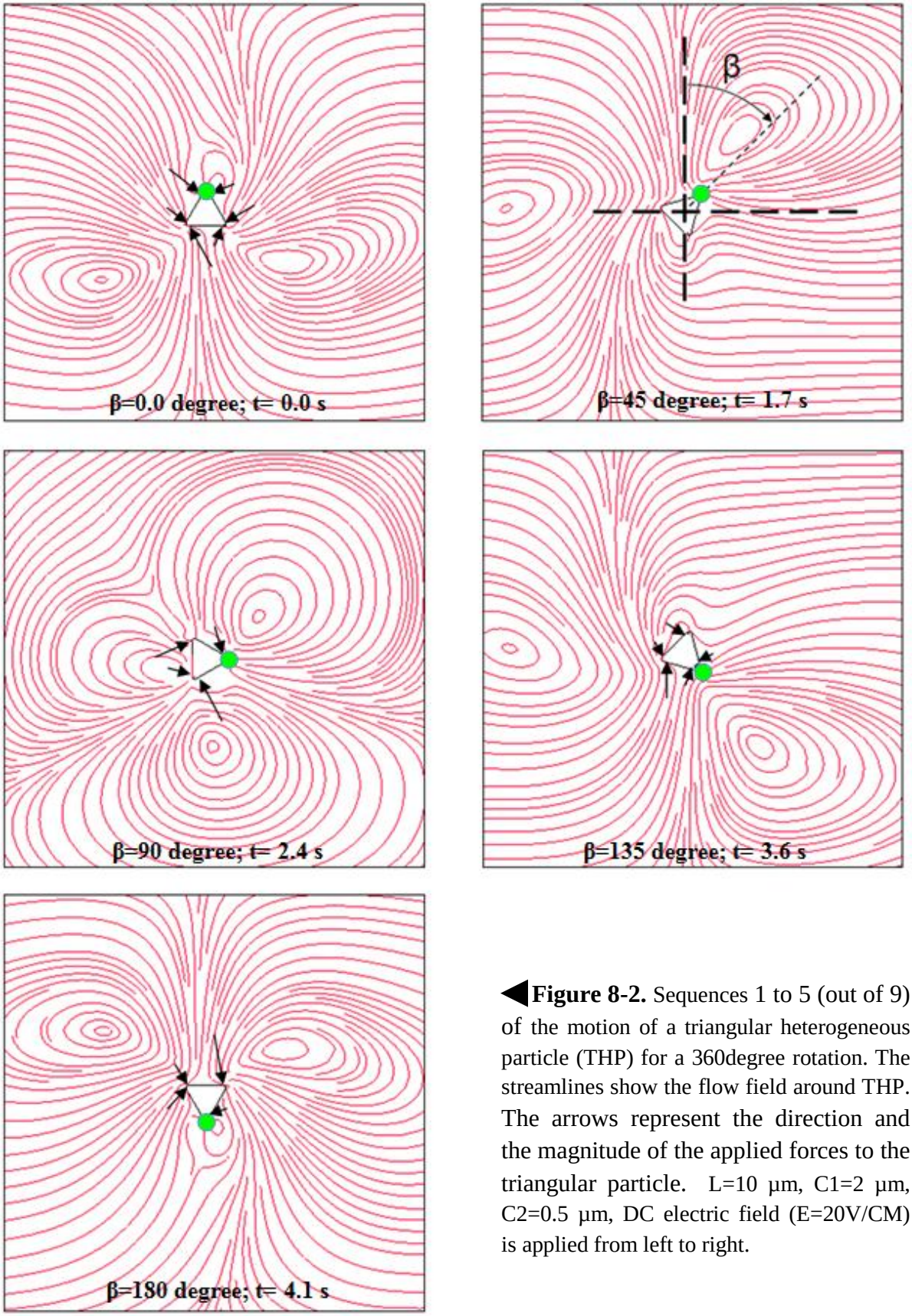


◀**Figure 8-2.** Sequences 1 to 5 (out of 9) of the motion of a triangular heterogeneous particle (THP) for a 360degree rotation. The streamlines show the flow field around THP. The arrows represent the direction and the magnitude of the applied forces to the triangular particle. L=10 μm, C1=2 μm, C2=0.5 μm, DC electric field (E=20V/CM) is applied from left to right.

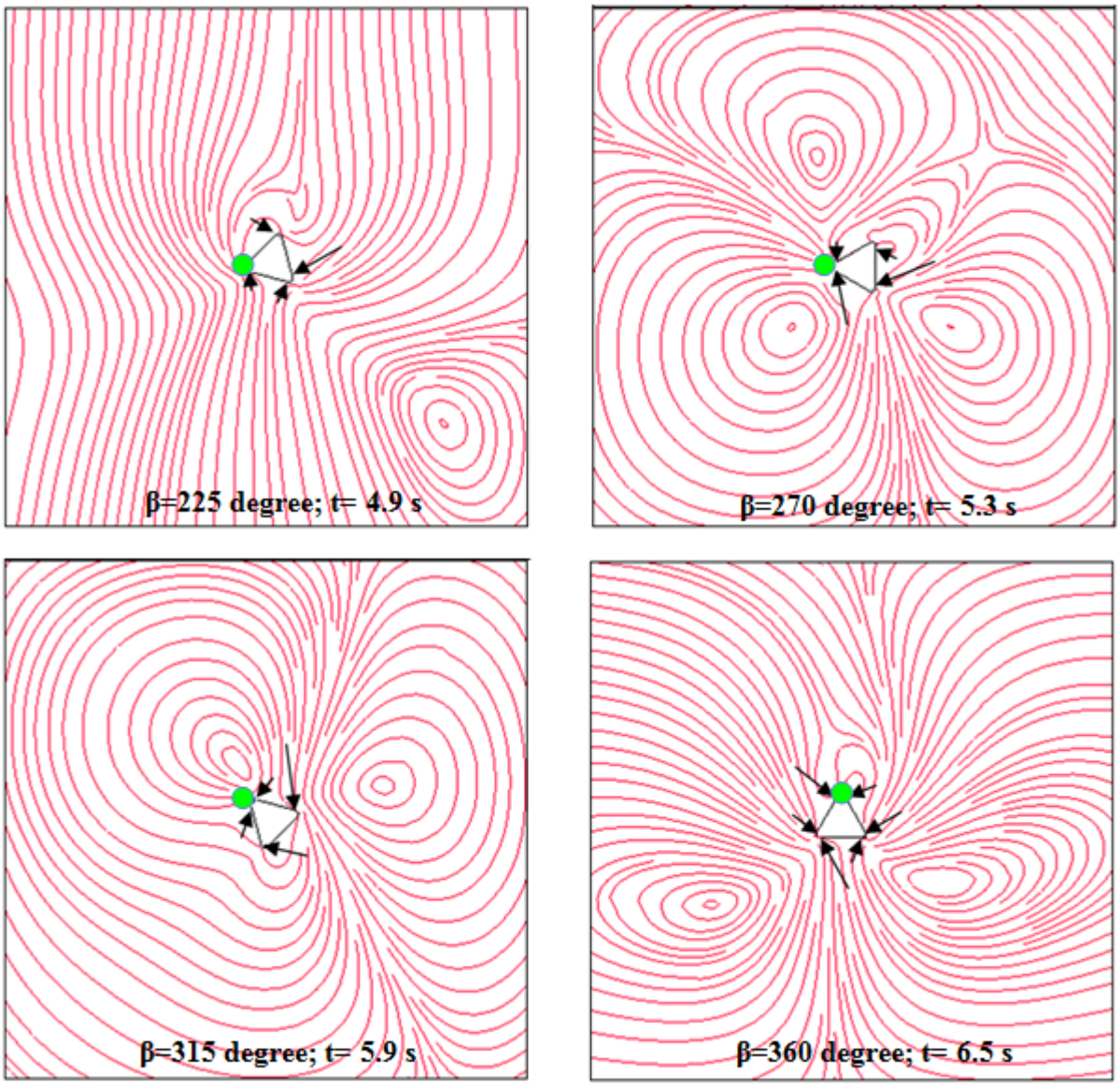


**Figure 8-3.** Sequences 6 to 9 (out of 9) of the motion of a triangular heterogeneous particle (THP) for a 360degree rotation. The streamlines show the flow field around THP. The arrows represent the direction and the magnitude of the applied forces to the triangular particle. L=10 μm , C1=2 μm, C2=0.5 μm, DC electric field (E=20V/CM) is applied from left to right.

size of L=10μm, C1=2μm, and C2=0.5μm, when the applied DC electric field E is 20V/cm, it takes 6.5 seconds for this particle to rotate 360 degrees. It means this particle will rotates 9.24 turns in one minute (ω=9.24rpm when E=20V/cm). Our numerical simulation reveals that this THP rotates continuously as long as the DC electric field is applied. The arrows in Figures 8-2

and 8-3 indicate the magnitude and the direction of the interaction forces at the corners of the triangle. Clearly the forces are not balanced and the net force keeps the particle rotating.

The numerical simulation shows that the instantaneous angular velocity of the THP varies during one rotation cycle. As an example, Figure 8-4 plots the instantaneous angular velocity for the case of E=20V/cm. This variation of the angular velocity is caused by variation of the net instantaneous interaction force due to the electric field and the vortices, and hence by the designed asymmetry of the conducting surfaces at each corner. As seen from this figure, the instantaneous angular velocity changes with time within one complete turn, however, the angular velocity variation repeats exactly in every single 360 degree rotation of the THP. The instantaneous angular velocity shown in Figure 8-4 is plotted after three full rotations of the triangular particle in order to ensure that a steady state condition is reached. In the following sections of this chapter, the term "the angular velocity" means the average angular velocity which is defined as the number of turns (360 degrees) a THP can rotates in one minute.

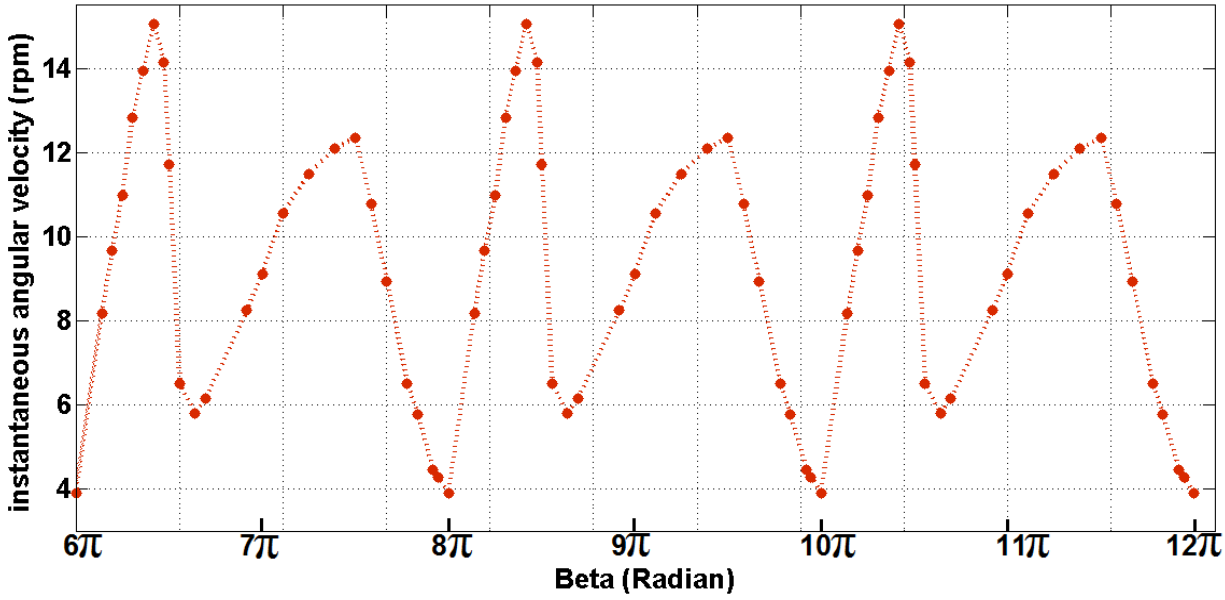


**Figure 8-4.** The Instantaneous angular velocity variation from 0 to 6π for three full continuous turns of a rotating THP. L=10 μm, C1=2 μm, C2=0.5 μm, DC electric field E = 20V/cm from left to right.

Apparently, the rotational speed of THP is proportional to the net interaction force on the particle, which directly depends on the applied electric field. Figure 8-5 presents the variation of the angular velocity of a THP particle as a function of applied DC electric field. The angular velocity of a THP increases linearly with the DC electric field. A THP of L=10μm, C1=2 μm, and C2=0.5 μm rotates 7.4 turns per minute when the applied DC electric field is 16V/cm. The same THP rotates only about a half turn per minute when E = 1V/cm. Overall, such a rotation of THP can take place in a large range of electric field.

To understand the effects of the size of the triangle and the size of the conducting section on the angular velocity, two sets of investigation have been done. First, the side of the equilateral triangle, L, is chosen as 10μm and 20μm, respectively; while the lengths for the conducting section at each corner are kept constant, C1=2μm and C2 =0.5μm. Figure 8-6a shows that the angular velocity of such a THP decreases with the size of the equilateral triangle for a constant electric field. This can be easily understood as the driving force for the rotation, i.e., the electrical interaction force becomes relatively smaller as the particle size increases.

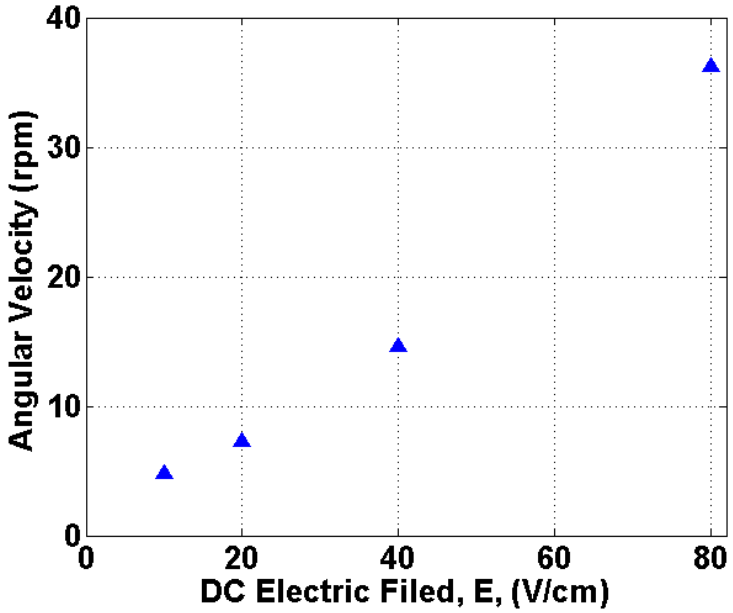


**Figure 8-5.** Relationship between the angular velocity of triangular heterogeneous particle and the applied DC eclectic fields (are applied from left to right). L=10μm , C1=2μm, C2=0.5μm.

In order to investigate the effect of the conducting section size on the rotation of the THP, the side of the equilateral triangle is kept constant, L=10μm, but C1 (and consequently C2 = 0.25C1) changes. Figure 8-6b shows that the angular velocity increases as the size of the conducting section increases. However, it should be noted that the size of the conducting section has a lower limit. As seen in Figure 8-6b, for a THP with L=10μm and under E=20V/cm, if C1 is smaller than 0.5μm the interaction force is so weak that it cannot rotate the THP.

Size of C1 is a critical parameter to achieve the non-stop rotational micro-motor. As figure 8-6b shows, a very small C1 is unable to generate the required vortices and thus effective forces to rotate the THP. On the other hand, a very large C1 (for example, larger than C1 = 4.5 μm) produces a very strong interaction force which rotates the particle fast; however, as soon as the position of the particle changes from its original orientation, the vortices on the other sides become strong and apply opposite forces to the THP. This results in the THP rotating backwards and returning to its original position after a very small period of time. At this time, once again the first vortex becomes strong and forces the particle to rotate forward.

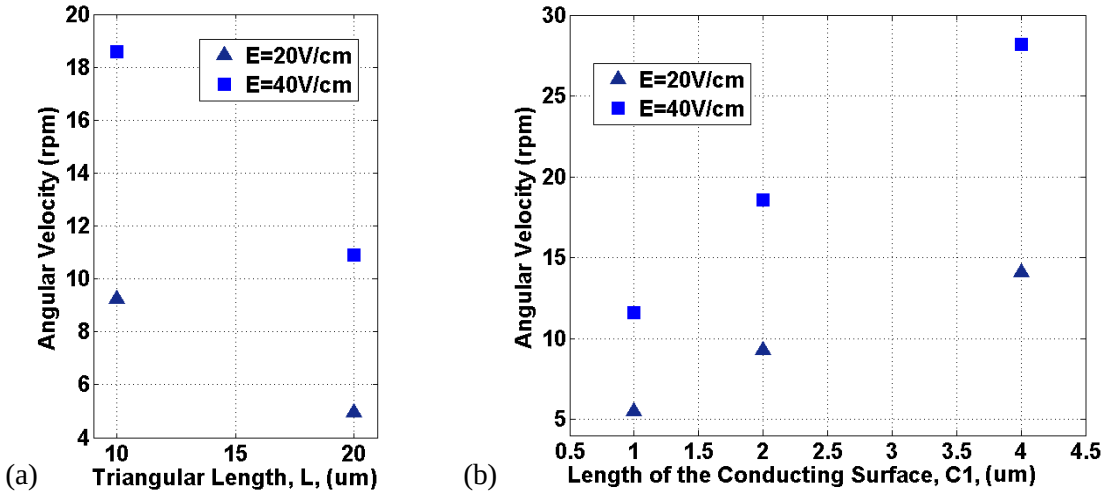


**Figure 8-6.** The dependence of the angular velocity on (a) the equilateral triangle length, L, with constant C1=2 μm, and C2=0.5 μm and (b) the conducting section size, C1 (C2=0.25C1), when L=10 μm. For both case two different DC electric fields are applied: E=20 V/cm and E=40V/cm.

Consequently these strong unbalanced forces cause an oscillating motion which results in the THP is shaking in its place without a rotational motion. This oscillation is qualitatively plotted in figure 8-7 by showing the flow field and the corresponding net forces. The THP starts its rotation at t=0s and at the direction of the resultant force which is clockwise (figure 8-7a). The opposite forces grow and reduce the effect of forces in the clockwise direction. This slows the particle motion until at some potion the forces in the opposite direction become stronger. Thus, the particle is pushed to rotate backwards in counterclockwise direction (figure 8-7c). This counterclockwise rotation does not last long as the balance of forces is altered as soon as the flow pattern changes (figure 8-7d) and the particle once again starts rotating in the clockwise direction. This alternating motion continues as long as the external DC electric field is applied.

Figure 8-8 demonstrates that when the sizes of C2 and C2 are chosen to be equal and symmetrical the THP will stop after rotating for a few degrees. In this case the forces balance at a specific position (β=42 degrees) and the particle will not move any longer. Thus using the symmetrical conducting surfaces at each corner of the THP will not results in an effective induced-charge micro-motor. The sizes of the conducting surfaces and their effective ratios are numerical investigated and the results are summarized in Table 8-1.

These results represent that for a constant length of triangular side, L, the conducting surface can be chosen in different sizes. However the THP will not rotates if C1 is too small which lead to induced forces that are not strong enough to move the particle. On the other hand, if C1 covers almost half of the triangular sides, the particle only rotates for a few degrees and then stop; which is not desired for the purpose of this study. Table 2, also, shows that for a constant triangle side size of L and C1, the size of C2 could be variable and we could still have an induced-charge micro-motor which rotates non-stop while the DC electric field is applied. Predictably, the

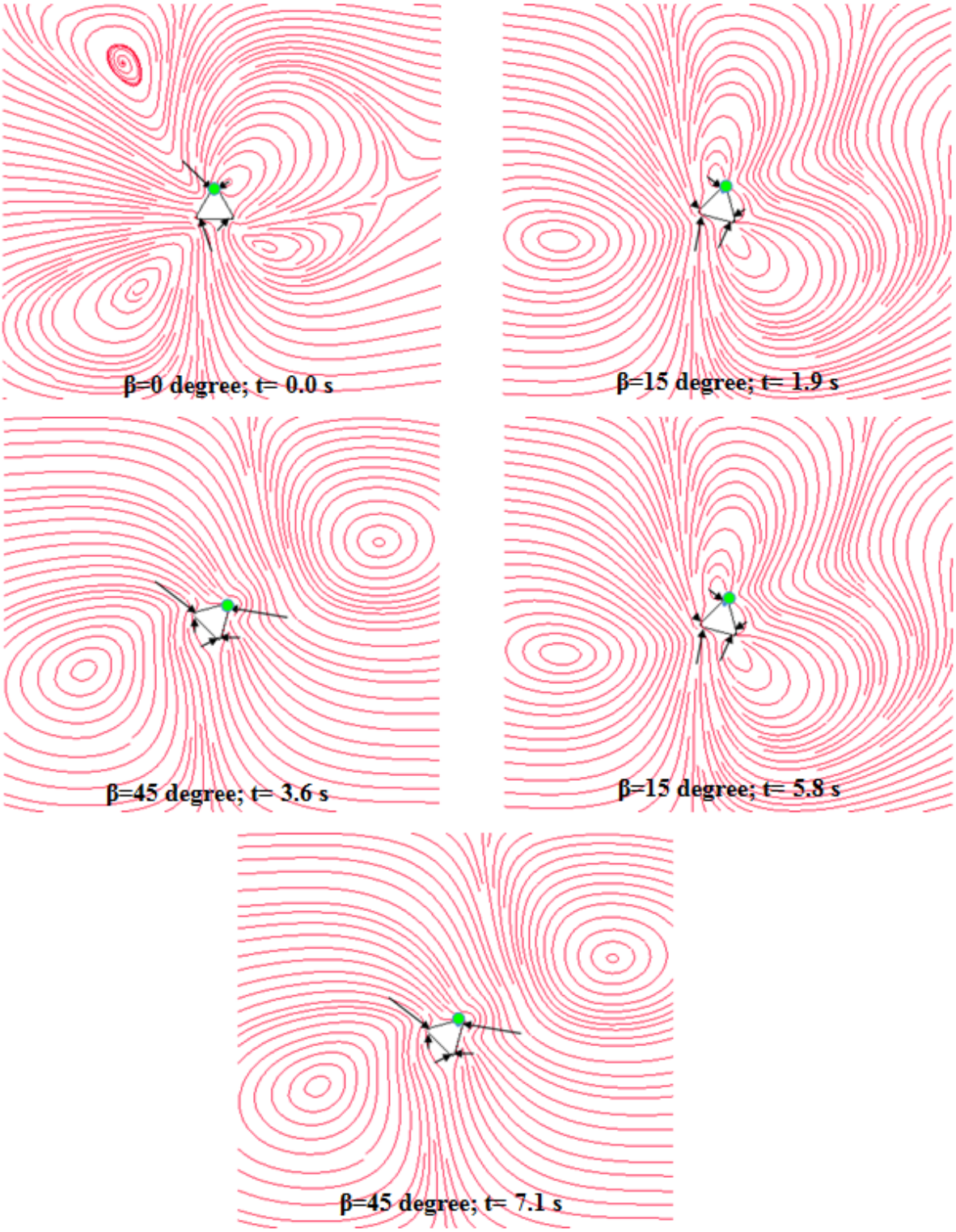


**Figure 8-7.** Oscillations of the THP when conducting sections size are comparable to the size of the non-conducting sections; thus the THP will not rotate. L=10μm, C1=5μm, and C2=1.25μm. The DC electric field (20V/cm) is applied from left to right. The streamlines show the flow pattern in different sequences. Arrows represent the applied forces to the THP sides. The length of the arrow shows higher strength.

angular velocity of two THP is less when for constant L and C1 the C2 is smaller. This is because the smaller size of C2 has limited space for being polarized; and thus, the induced vortices and applied induced forces to the particle will be smaller and the rotation speed will decrease.

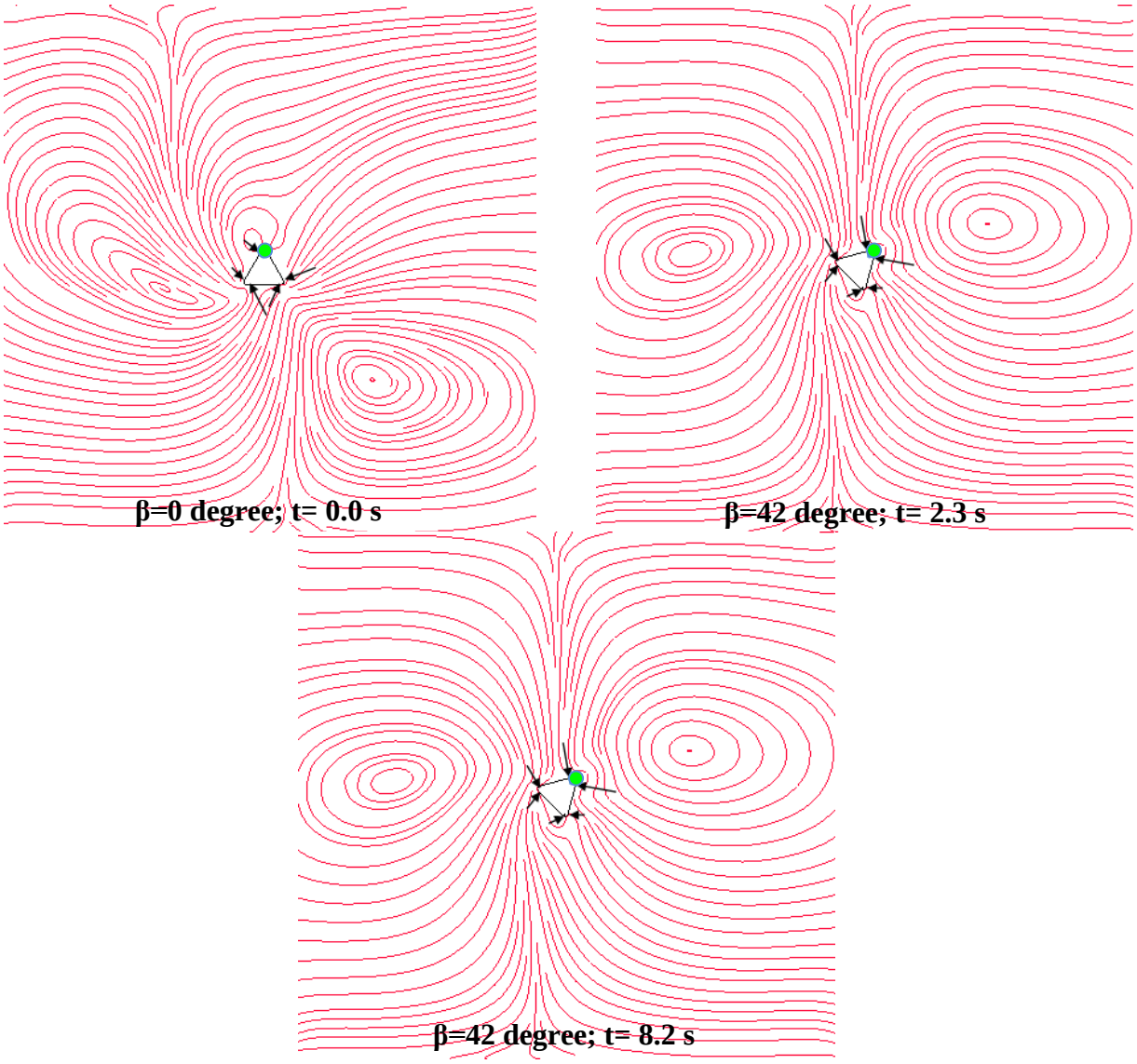


**Figure 8-8.** The THP stops moving and becomes stationary once the forces on the conducting sections are balanced for C1=C2. The DC electric field of 20V/cm is applied from left to right. L=10μm and C1=C2=2μm. The streamlines show the flow pattern in different time steps. Arrows represent the applied forces to the THP sides. The length of the arrows show is proportional to the strength of the applied forces.

**Table 8-1.** Selecting the size of the conducting section in compare to the size of the THP

| The THP characteristics | | | Dose THP rotates a full circle? |
|---|---|---|---|
| L(μm) | C1(μm) | C2(μm) | |
| 10 | 1 | 0.25 | NO |
| 10 | 2 | 0.5 | YES |
| 10 | 4 | 0.5 | NO |
| | | 1 | YES |
| | | 2 | YES |
| | | 3 | NO |
| | | 4 | NO |
| 10 | 5 | 1.25 | NO |

### 8-3. Motion of a Circular Heterogeneous Particle

A circular heterogeneous particle (CHP) as shown in Figure 8-9a is also studied. For comparison, the lengths of the conducting section and the non-conducting section are chosen to be the same as that of the triangle heterogeneous particle (THP). Applying a DC electric field from left to right, the circular heterogeneous particle also starts clockwise rotation, similar to the triangular heterogeneous particle. As shown in Figure 8-9b, the triangular particle rotates slightly faster than the circular particle under the same conditions. This might be an effect of their differences in shape and corresponding induced vortices.

### 8-4. Experimental Study

In this study, the chamber for holding the particle and water is made of a PDMS (polydimethylsiloxane) plate bonded on a glass substrate by using the soft lithography method (as described in chapter 5). The chamber has a length 5cm, a width 3cm, and a depth 3mm. To

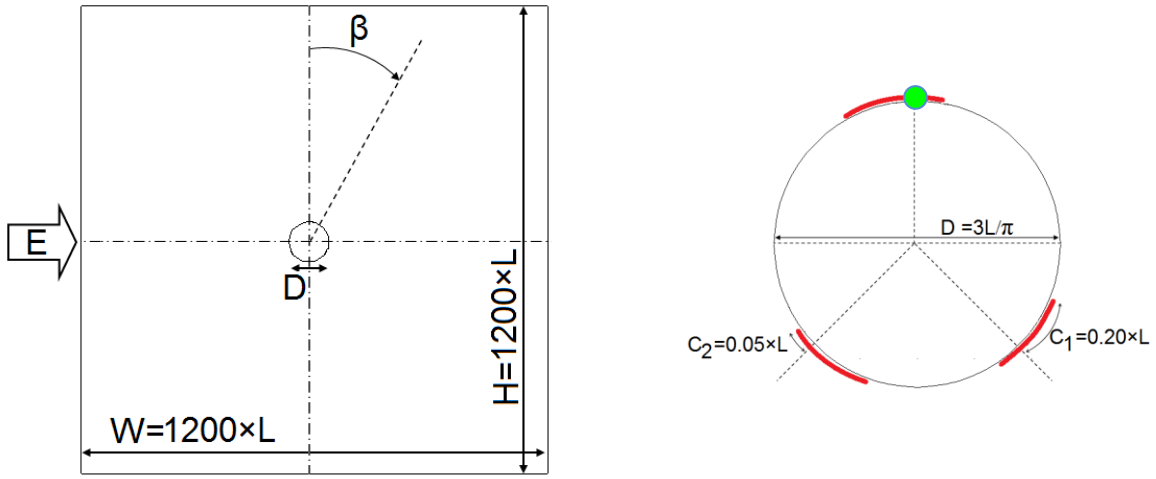


(a)

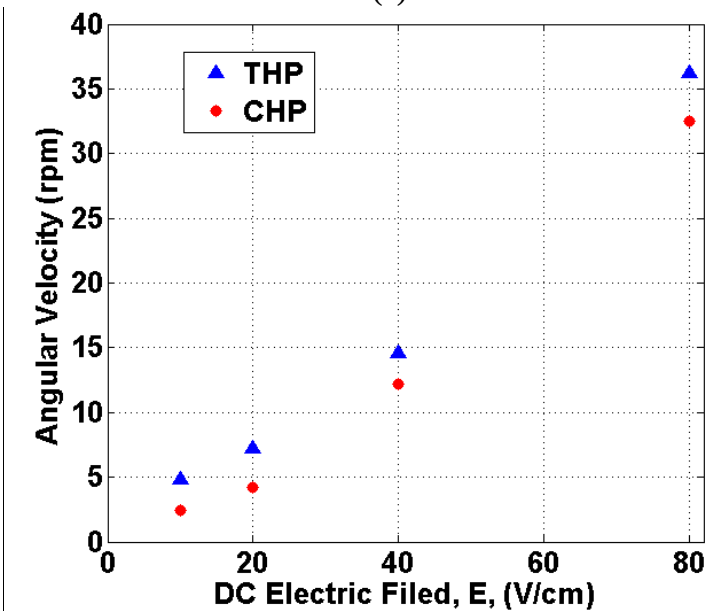


(b)

**Figure 8-9.** (a) Schematic diagram of the micro-motor with one circular heterogeneous particle at the center of a square micro-chamber. (b) Comparison between the angular velocity of the circular and the triangular heterogeneous particles under different applied DC electric fields. C1 and C2 are the conducting surfaces while the rest of the particle surfaces are non-conducting. L=10 μm, C1=2 μm, C2=0.5 μm. DC electric field is applied from left to right.

prepare the triangular heterogeneous particles, both sides of an aluminum triangle (thickness 0.142μm) were coated with a thin layer of a nail polish (major component is nitrocellulose dissolved in a solvent); after drying, an electrically non-conducting film was formed on the triangle. Two equilateral triangles were made in this study, one with a side length L=3mm,

another with a side length L=1.7mm. To make the corners electrically conducting, a specially designed mask was used to cover the most part of the triangle coated with the nail polish film, except the corners. Each exposed corner has a longer side (C1) and a shorter side (C2). Acetone was used to remove the nail polish film from the exposed corners. In this way, a non-conducting triangle with three conducting corners was made. A black spot was left on the particle for tracing the particle's rotation. Although the size of the triangles made in this study is relatively large, these triangles can be used to demonstrate the rotation as predicted by the model and numerical simulation (Figure 8-10).

### 8-4-1. Experimental Setup and Operation

The experimental system consists of the following major components: a chip with the chamber (5cm×3cm×3mm), a fluorescence microscope and image system (TE2000-E, Nikon), a DC power supply (CSI12001X, Circuit Specialists Inc., USA), and a data acquisition system, as shown in Figure 8-10a. The chip was fixed on the observation platform of the microscope. The DC power supply was used to control the voltages applied to the electrodes. The images were captured by the digital camera and digitized by computer software (NIS-Elements BR 3.0). In the experiments, a triangular heterogeneous particle was released in the middle of the chamber on the surface of de-ionized water. Two platinum wires were placed at the two ends (5 cm distances) of the chamber as the electrodes, and connected to the power supply to produce the desired electric field. Once the electrical field was applied, the images of the particles were taken continuously. The angular velocity of the particle’s rotation was determined by analyzing these sequential images. The dimensions of the triangular heterogeneous particle are shown in Figure 8-10c. Also Figure 8-10d determines the definition of rotational angle, β, according to the dark trace point.

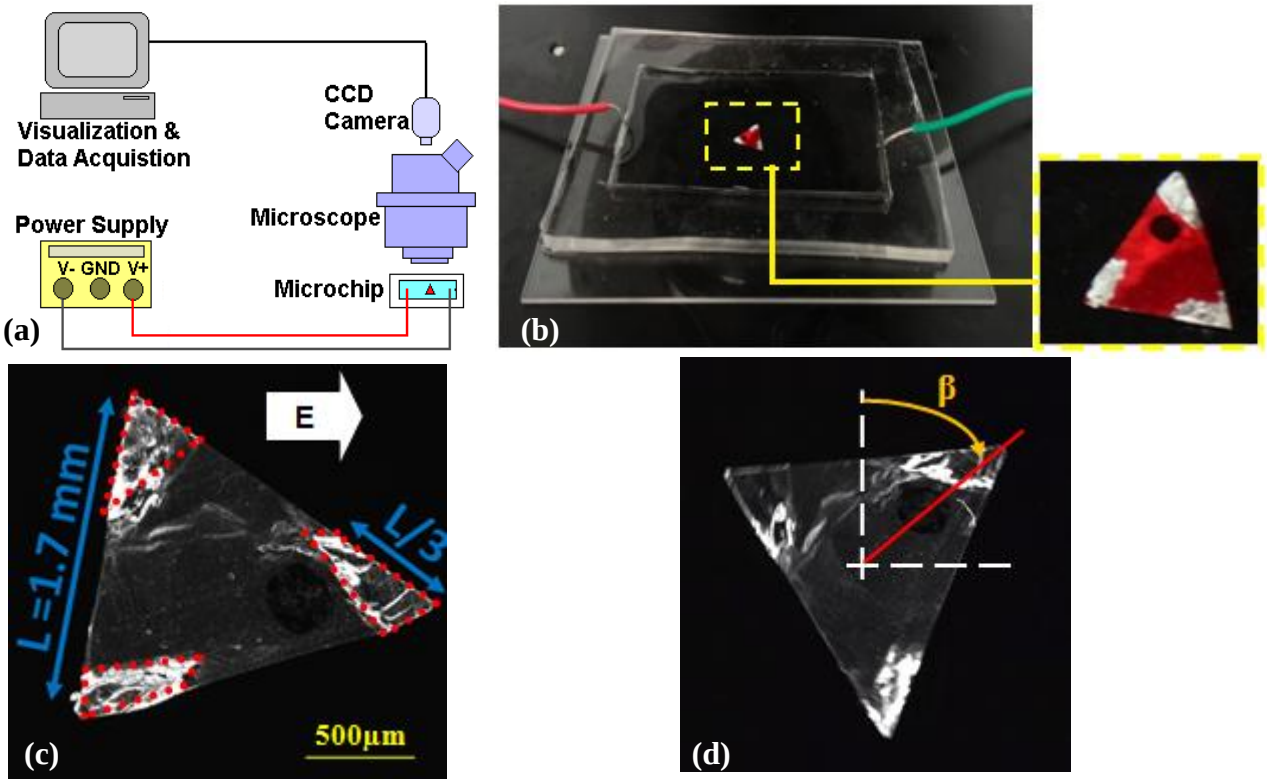


**Figure 8-10.** (a) Schematic of the experimental system. (b) A triangular heterogeneous particle is suspended in DI water in the chamber with two electrodes. (c) The dimensions of the triangular heterogeneous particle. (d) The definition of rotational angle, β according to the dark trace point. L=1.7mm, C1=0.57mm.

### 8-4-2. Experimental Observation

As an example, a sequence of images is shown in Figure 8 to display the observed rotation of a THP. This particle has a side length L=1.7mm, C1=0.57mm, C2 = 0.32mm (Figure 8-10). The DC electric field (E=80V/cm) is applied from left to right. Under these conditions, the particle took 117.6s to complete a full turn (360$^{o}$). As observed in the experiments, the particle rotated continuously as long as the electric field was applied (Figure 8-11).

Figure 8-12 reports the measured angular velocity of two THP of different sizes. One particle has a side length L=1.7mm, C1=0.57mm, C2=0.32mm, and the second one has a side length L=3mm, C1=1.1mm, C2=0.57mm. As predicted by the numerical simulations, the bigger particle moves slower in comparison with the smaller one.

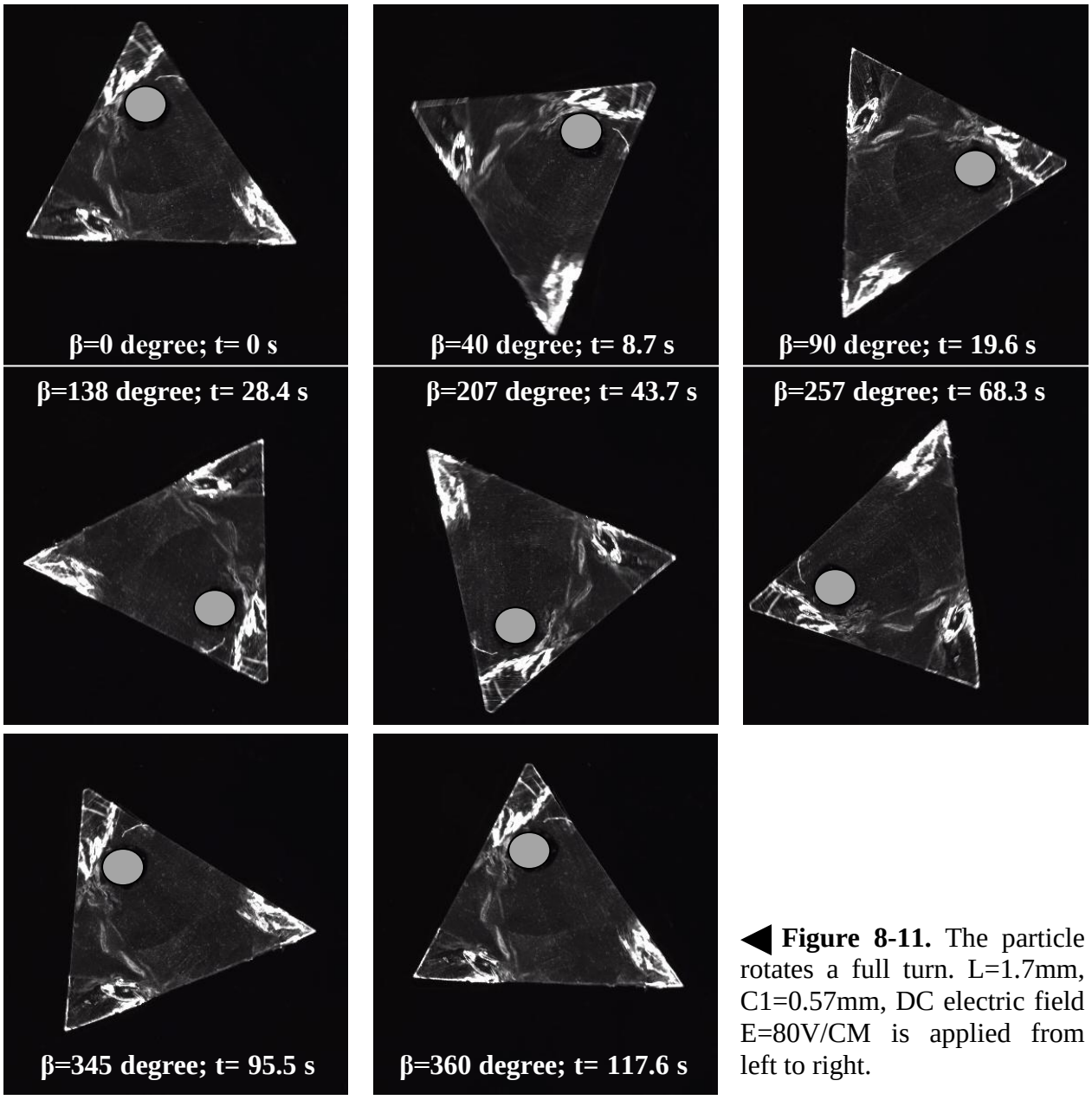


◀ **Figure 8-11.** The particle rotates a full turn. L=1.7mm, C1=0.57mm, DC electric field E=80V/CM is applied from left to right.

**8-5. Summary and Conclusions:**

The induced-charge electrokinetic motion of an equilateral triangular heterogeneous particle was studied numerically and experimentally. If the three corners of the triangle are electrically conducting and the conducting surface areas are asymmetrical between the two sides of each corner, such an equilateral triangular heterogeneous particle can rotate continuously around a

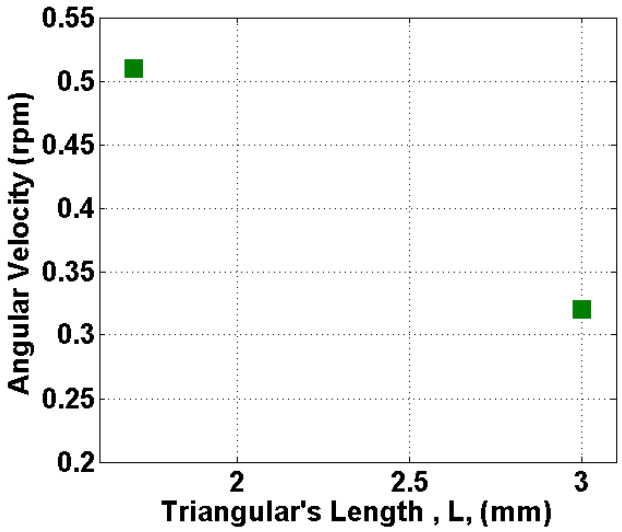


**Figure 8-12.** The measured angular velocity of two triangular heterogeneous particles (THP) of different sizes, under constant DC electric field, E=80V/cm. THP1: L=1.7mm, C1=0.57mm, C2=0.32mm, and the THP2: L=3mm, C1=1.1mm, C2=0.57mm.

fixed point in an aqueous solution under a constant applied DC field. The angular velocity of the rotation increases with the applied electrical field, and the size of the conducting area (C1), but decreases with the particle size. As mentioned in this chapter, one of the most important characteristics of presented ICEK micro-motor is that has a steady rotational motion as long as the DC electric field is applied. This motor can be stopped easily by Turing off the applied voltages to the electrodes to cut off the applied electric field.

# CHAPTER IX: Conclusions

## Summary of Induced-Charge Electrokinetics

In this thesis we introduced the basics of induced-charge electrokinetics (ICEK) and highlighted ICEK differences with classical electrokinetics (EK). Using our proposed numerical method we studied the behavior of a heterogeneous particle located in a microchannel under an applied DC electric field. This method was capable of calculating the induced-zeta potential on the conducting section of a heterogeneous particle and combined the mathematical methods utilized for classic EK and ICEK. Modeling the electric field, fluid flow and particle motion in a microchannel in 3D, we numerically showed that micro-vortices induce around the conducting section of a heterogeneous particle.

The numerical modeling presented in this thesis showed that the induced vortices act like an engine. These micro-vortices push the Janus particles faster compared to non-conducting particles and fully conducting particles. Moreover, a Janus particle with bigger size moves faster if its conducting section is facing the positive voltage. The orientation of the Janus particle defines the direction and speed of its motion.

By our experimental investigation we could visualize the induced vortices around a conducting particle under DC electric field for the first time. These experiments also verified our numerical finding that Janus particle moves faster than other types of particles and, the Janus

particles with opposite orientations move in different directions. Using our numerical and experimental results we developed three applications of ICEK that could be integrated with microfluidic devices: ICEK micro-valve, micro-mixer, and micro-motor.

The existing micro-valves have many drawbacks, such as: long response time, large dead volume, instability, leakage, complicated fabrication process, etc. Our proposed ICEK micro-valve has a short response time and could control the flow rate and flow direction using different configurations of the applied DC electric fields. This ICEK micro-valve is numerically tested for different types of particles: Janus particle, non-conducting and fully conducting particles. According to our results this micro-valve is stable, fast, easy to fabricate and has no leakage when a Janus particle is used in its design. But this micro-valve shows instability and leakage problems if any other type of particles is used.

Most of present micro-mixers are unable to provide a homogeneous mixture of different fluid streams; while a well mixed mixture is a key in improving accuracy and reliability of the biological and medical experiments. Employing the induced vortices around a conducting particle (released in a micro-chamber), we developed an ICEK micro-mixer capable of mixing different streams of fluids with high efficiency. This proposed ICEK micro-mixer could be operated in low-voltage ranges and provided 100% heterogeneous mixture at its downstream. The effects of the strength and direction of the applied electric field are also examined for this ICEK micro-mixer.

Fabricating micro-motors with moving parts, gears, coils and rotors is complicated and not easy. Also, micro-motors with no moving parts (e.g. electrostatic micro-motor) are unable to provide enough torque to run the fluids in micro-scales. We introduced a non-stop ICEK micro-motor using a triangular shaped heterogeneous particle. The rotation of this triangular

heterogeneous particle under a DC field is numerically investigated and experimentally developed. The effects of applied electric field, the geometry of the heterogeneous particle and its size on the performance of the micro-motor are numerically and experimentally reported in this thesis. These ICEK devices can be used in microfluidics devices or LOC equipments in various fields and applications such as medicine, biochemistry, outer space and industrial fields.

## References


[1] C. J. Easley, J. M. Karlinsey, J. M. Bienvenue, L. A. Legendre, M. G. Roper, S. H. Feldman, M. A. Hughes, E. L. Hewlett, T. J. Merkel, J. P. Ferrance and J. P. Landers, "A fully integrated microfluidic genetic analysis system with sample-in-answer-out capability," *Proc. Natl. Acad. Sci. U. S. A.*, vol. 103, pp. 19272-19277, 2006.

[2] A. Ould El Moctar, N. Aubry and J. Batton, "Electro-hydrodynamic micro-fluidic mixer," *Lab on a Chip - Miniaturisation for Chemistry and Biology*, vol. 3, pp. 273-280, 2003.

[3] L. -. Lu, K. S. Ryu and C. Liu, "A magnetic microstirrer and array for microfluidic mixing," *J Microelectromech Syst*, vol. 11, pp. 462-469, 2002.

[4] M. L. Chabinyc, D. T. Chiu, J. C. McDonald, A. D. Stroock, J. F. Christian, A. M. Karger and G. M. Whitesides, "An integrated fluorescence detection system in poly(dimethylsiloxane) for microfluidic applications," *Anal. Chem.*, vol. 73, pp. 4491-4498, 2001.

[5] E. A. S. Doherty, R. J. Meagher, M. N. Albarghouthi and A. E. Barron, "Microchannel wall coatings for protein separations by capillary and chip electrophoresis," *Electrophoresis*, vol. 24, pp. 34-54, 2003.

[6] H. Jiang, Y. Daghighi, C. H. Chon and D. Li, "Concentrating molecules in a simple microchannel," *J. Colloid Interface Sci.*, vol. 347, pp. 324-331, 2010.

[7] Y. Daghighi and D. Li, "Numerical studies of electrokinetic control of DNA concentration in a closed-end microchannel," *Electrophoresis*, vol. 31, pp. 868-878, 2010.

[8] F. F. Reuss, "Sur un nouvel effet de 1'electricite galvanique," in *Imperial Russian Naturalist Society*, Moscow, 1809, pp. 327-337.

[9] G. Wiedemann, "Movement of fluids in a closed galvanic column ciinders," vol. 163, pp. 321-352, 16 MAR 2006, 1862.

[10] G. Quincke, "About the continuation of the property of materials under the electric filed," vol. 189, pp. 513-598, 1861.

[11] H. Helmholtz, "Studies on Eletrical boundary layers," vol. 243, pp. 337-398, 1879.

[12] E. Dorn, "About the continuation of electricity by flowing water in tubes and Related Phenomena," vol. 246, pp. 46-77, 1880.

[13] V. G. Levich, *Physicochemical Hydrodynamics.* Englewood Cliffs, N.J., Prentice-Hall, 1962.

[14] A. S. Dukhin, "PAIR INTERACTION OF DISPERSE PARTICLES IN ELECTRIC FIELD. 3. HYDRODYNAMIC INTERACTION OF IDEALLY POLARIZABLE METAL PARTICLES AND DEAD BIOLOGICAL CELLS." *Colloid Journal of the USSR,* vol. 48, pp. 376-381, 1986.

[15] A. S. Dukhin, "Biospecific mechanism of double layer formation and peculiarities of cell electrophoresis," *Colloids Surf. Physicochem. Eng. Aspects,* vol. 73, pp. 29-48, 1993.

[16] N. I. Gamayunov, V. A. Murtsovkin and A. S. Dukhin, "PAIR INTERACTION OF PARTICLES IN ELECTRIC FIELD. 1. FEATURES OF HYDRODYNAMIC INTERACTION OF POLARIZED PARTICLES." *Colloid Journal of the USSR,* vol. 48, pp. 197-203, 1986.

[17] N. I. Gamayunov, G. I. Mantrov and V. A. Murtsovkin, "Investigation of the flows induced by an external electric field in the vicinity of conducting particles," *Kolloidn. Zh.,* vol. 54, pp. 26-30, 1992.

[18] I. N. Simonov and S. S. Dukhin, "Theory of electrophoresis of solid conducting particles in case of ideal polarization of a thin diffuse double-layer," vol. 35, pp. 191-193, 1973.

[19] S. S. Dukhin and B. V. Derjaguin, Eds., *Electrokinetic Phenomena.* NY: J. Willey and Sons, 1974.

[20] V. A. Murtsovkin and G. I. Mantrov, "The transient regime of streamlining of metal particles in the electric field," *Kolloidnyj Zhurnal,* vol. 54, pp. 136-140, 1992.

[21] V. A. Murtsovkin and G. I. Mantrov, "Investigation of the flows induced by an alternating electric field close to ionite particles," *Kolloidn. Zh.,* vol. 54, pp. 105-109, 1992.

[22] A. Ramos, H. Morgan, N. G. Green and A. Castellanos, "AC electric-field-induced fluid flow in microelectrodes," *J. Colloid Interface Sci.,* vol. 217, pp. 420-422, 1999.

[23] A. Ajdari, "Pumping liquids using asymmetric electrode arrays," *Physical Review E - Statistical Physics, Plasmas, Fluids, and Related Interdisciplinary Topics,* vol. 61, pp. R45-R48, 2000.

[24] N. G. Green, A. Ramos, A. Gonzalez, H. Morgan and A. Castellanos, "Fluid flow induced by nonuniform ac electric fields in electrolytes on microelectrodes. III. Observation of streamlines and numerical simulation," *Physical Review E - Statistical, Nonlinear, and Soft Matter Physics,* vol. 66, pp. 026305/1-026305/11, 2002.

[25] N. G. Green, A. Ramos, A. González, H. Morgan and A. Castellanos, "Fluid flow induced by nonuniform ac electric fields in electrolytes on microelectrodes. I. Experimental measurements," *Physical Review E - Statistical Physics, Plasmas, Fluids, and Related Interdisciplinary Topics,* vol. 61, pp. 4011-4018, 2000.

[26] A. González, A. Ramos, N. G. Green, A. Castellanos and H. Morgan, "Fluid flow induced by nonuniform ac electric fields in electrolytes on microelectrodes. II. A linear double-layer

analysis," *Physical Review E - Statistical Physics, Plasmas, Fluids, and Related Interdisciplinary Topics,* vol. 61, pp. 4019-4028, 2000.

[27] A. B. D. Brown, C. G. Smith and A. R. Rennie, "Pumping of water with ac electric fields applied to asymmetric pairs of microelectrodes," *Physical Review E - Statistical, Nonlinear, and Soft Matter Physics,* vol. 63, pp. 1-8, 2001.

[28] V. Studer, A. Pépin, Y. Chen and A. Ajdari, "An integrated AC electrokinetic pump in a microfluidic loop for fast and tunable flow control," *Analyst,* vol. 129, pp. 944-949, 2004.

[29] J. A. Levitan, S. Devasenathipathy, V. Studer, Y. Ben, T. Thorsen, T. M. Squires and M. Z. Bazant, "Experimental observation of induced-charge electro-osmosis around a metal wire in a microchannel," *Colloids Surf. Physicochem. Eng. Aspects,* vol. 267, pp. 122-132, 2005.

[30] E. Yariv, "Induced-charge electrophoresis of nonspherical particles," *Phys. Fluids,* vol. 17, pp. 1-4, 2005.

[31] D. Saintillan, E. Darve and E. S. G. Shaqfeh, "Hydrodynamic interactions in the induced-charge electrophoresis of colloidal rod dispersions," *J. Fluid Mech.,* vol. 563, pp. 223-259, 2006.

[32] D. Saintillan, E. S. G. Shaqfeh and E. Darve, "Stabilization of a suspension of sedimenting rods by induced-charge electrophoresis," *Phys. Fluids,* vol. 18, 2006.

[33] K. A. Rose, J. A. Meier, G. M. Dougherty and J. G. Santiago, "Rotational electrophoresis of striped metallic microrods," *Physical Review E - Statistical, Nonlinear, and Soft Matter Physics,* vol. 75, 2007.

[34] Z. Wu, Y. Gao and D. Li, "Electrophoretic motion of ideally polarizable particles in a microchannel," *Electrophoresis,* vol. 30, pp. 773-781, 2009.

[35] Z. Wu and D. Li, "Induced-charge electrophoretic motion of ideally polarizable particles," *Electrochim. Acta,* vol. 54, pp. 3960-3967, 2009.

[36] Z. Wu and D. Li, "Micromixing using induced-charge electrokinetic flow," *Electrochim. Acta,* vol. 53, pp. 5827-5835, 2008.

[37] Z. Wu and D. Li, "Mixing and flow regulating by induced-charge electrokinetic flow in a microchannel with a pair of conducting triangle hurdles," *Microfluidics and Nanofluidics,* vol. 5, pp. 65-76, 2008.

[38] W. Kim, J. Chun Ryu, Y. Kweon Suh and K. Hyoung Kang, "Pumping of dielectric liquids using non-uniform-field induced electrohydrodynamic flow," *Appl. Phys. Lett.,* vol. 99, 2011.

[39] S. Gangwal, O. J. Cayre, M. Z. Bazant and O. D. Velev, "Induced-charge electrophoresis of metallodielectric particles," *Phys. Rev. Lett.,* vol. 100, 2008.

[40] S. C. Terry, J. H. Jerman and J. B. Angell, "A gas chromatographic air analyzer fabricated on a silicon wafer," *IEEE Trans. Electron Devices,* vol. 26, pp. 1880-1886, 1979.

[41] A. Meckes, J. Behrens, O. Kayser, W. Benecke, T. Becker and G. Müller, "Microfluidic system for the integration and cyclic operation of gas sensors," *Sens Actuators A Phys,* vol. 76, pp. 478-483, 1999.

[42] H. J. Cho, K. W. Oh, C. H. Ahn, P. Boolchand and T. -. Nam, "Stress analysis of silicon membranes with electroplated permalloy films using Raman scattering," *IEEE Trans. Magn.,* vol. 37, pp. 2749-2751, 2001.

[43] B. Bae, N. Kim, H. Kee, S. -. Kim, Y. Lee, S. Lee and K. Park, "Feasibility test of an electromagnetically driven valve actuator for glaucoma treatment," *J Microelectromech Syst,* vol. 11, pp. 344-354, 2002.

[44] C. Fu, Z. Rummler and W. Schomburg, "Magnetically driven micro ball valves fabricated by multilayer adhesive film bonding," *J Micromech Microengineering,* vol. 13, pp. S96-S102, 2003.

[45] K. W. Oh, R. Rong and C. H. Ahn, "Miniaturization of pinch-type valves and pumps for practical micro total analysis system integration," *J Micromech Microengineering,* vol. 15, pp. 2449-2455, 2005.

[46] M. J. Zdeblick and J. B. Angell, "A microminiature electric-to-fluidic valve," in *the 4th International Conference on Solid-State Sensors and Actuators,* Tokyo, Japan, 1987, pp. 827-829.

[47] M. J. Zdeblick, R. Anderson, J. Jankowski, B. Kline-Schoder, L. Christel and R. Miles, "Thermopneumatically actuated microvalves and integrated electro-fluidic circuits," in *Technical Digest of the Solid-State Sensor and Actuator Workshop, ,* Hilton Head, South Carolina, USA, 1994, pp. 251-255.

[48] D. Baechi, R. Buser and J. Dual, "A high density microchannel network with integrated valves and photodiodes," *Sens Actuators A Phys,* vol. 95, pp. 77-83, 2002.

[49] H. Jerman, "Electrically-activated, normally-closed diaphragm valves," *J Micromech Microengineering,* vol. 4, pp. 210-216, 1994.

[50] C. A. Rich and K. D. Wise, "A high-flow thermopneumatic microvalve with improved efficiency and integrated state sensing," *J Microelectromech Syst,* vol. 12, pp. 201-208, 2003.

[51] H. Takao, K. Miyamura, H. Ebi, M. Ashiki, K. Sawada and M. Ishida, "A MEMS microvalve with PDMS diaphragm and two-chamber configuration of thermo-pneumatic actuator for integrated blood test system on silicon," *Sens Actuators A Phys,* vol. 119, pp. 468-475, 2005.

[52] X. Yang, C. Grosjean and Y. -. Tai, "Design, fabrication, and testing of micromachined silicone rubber membrane valves," *J Microelectromech Syst,* vol. 8, pp. 393-402, 1999.

[53] X. Yang, C. Grosjean, Y. -. Tai and C. -. Ho, "A MEMS thermopneumatic silicone rubber membrane valve," *Sens Actuators A Phys,* vol. 64, pp. 101-108, 1998.

[54] J. -. Kim, K. -. Na, C. J. Kang, D. Jeon and Y. -. Kim, "A disposable thermopneumatic-actuated microvalve stacked with PDMS layers and ITO-coated glass," *Microelectronic Engineering,* vol. 73-74, pp. 864-869, 2004.

[55] C. M. Pemble and B. C. Towe, "Miniature shape memory alloy pinch valve," *Sens Actuators A Phys,* vol. 77, pp. 145-148, 1999.

[56] M. Kohl, D. Dittmann, E. Quandt, B. Winzek, S. Miyazaki and D. M. Allen, "Shape memory microvalves based on thin films or rolled sheets," *Materials Science and Engineering A,* vol. 273-275, pp. 784-788, 1999.

[57] C. R. Tamanaha, L. J. Whitman and R. J. Colton, "Hybrid macro-micro fluidics system for a chip-based biosensor," *J Micromech Microengineering,* vol. 12, pp. N7-N17, 2002.

[58] P. W. Barth, "Silicon microvalves for gas flow control," in *International Conference on Solid-State Sensors and Actuators, and Eurosensors IX, Proceedings,* 1995, pp. 276-279.

[59] R. H. Wolf and A. H. Heuer, "TiNi (shape memory) films on silicon for MEMS applications," *J Microelectromech Syst,* vol. 4, pp. 206-212, 1995.

[60] D. Reynaerts, J. Peirs and H. Van Brussel, "An implantable drug-delivery system based on shape memory alloy micro-actuation," *Sens Actuators A Phys,* vol. 61, pp. 455-462, 1997.

[61] M. Kohl, D. Dittmann, E. Quandt and B. Winzek, "Thin film shape memory microvalves with adjustable operation temperature," *Sens Actuators A Phys,* vol. 83, pp. 214-219, 2000.

[62] Y. Liu, M. Kohl, K. Okutsu and S. Miyazaki, "A TiNiPd thin film microvalve for high temperature applications," *Materials Science and Engineering A,* vol. 378, pp. 205-209, 2004.

[63] K. Sato and M. Shikida, "An electrostatically actuated gas valve with an S-shaped film element," *J Micromech Microengineering,* vol. 4, pp. 205-209, 1994.

[64] A. H. Epstein, S. D. Senturia, G. Anathasuresh, A. Ayon, K. Breuer, K. -. Chen, F. E. Ehrich, G. Gauba, R. Ghodssi, C. Groshenry, S. Jacobson, J. H. Lang, C. -. Lin, A. Mehra, J. M. Miranda and et. al., "Power MEMS and microengines," in *International Conference on Solid-State Sensors and Actuators, Proceedings,* 1997, pp. 753-756.

[65] J. K. Robertson and K. D. Wise, "A low pressure micromachined flow modulator," *Sens Actuators A Phys,* vol. 71, pp. 98-106, 1998.

[66] L. Yobas, M. A. Huff, F. J. Lisy and D. M. Durand, "A novel bulk-micromachined electrostatic microvalve with a curved-compliant structure applicable for a pneumatic tactile display," *J Microelectromech Syst,* vol. 10, pp. 187-196, 2001.

[67] W. Van Der Wijngaart, H. Ask, P. Enoksson and G. Stemme, "A high-stroke, high-pressure electrostatic actuator for valve applications," *Sens Actuators A Phys,* vol. 100, pp. 264-271, 2002.

[68] M. M. Teymoori and E. Abbaspour-Sani, "Design and simulation of a novel electrostatic peristaltic micromachined pump for drug delivery applications," *Sens Actuators A Phys,* vol. 117, pp. 222-229, 2005.

[69] Y. Wang, J. Zhe, B. T. F. Chung and P. Dutta, "A rapid magnetic particle driven micromixer," *Microfluidics and Nanofluidics,* vol. 4, pp. 375-389, 2008.

[70] Y. -. Wang, M. H. Choi and J. Han, "Two-dimensional protein separation with advanced sample and buffer isolation using microfluidic valves," *Anal. Chem.,* vol. 76, pp. 4426-4431, 2004.

[71] A. Wego, S. Richter and L. Pagel, "Fluidic microsystems based on printed circuit board technology," *J Micromech Microengineering,* vol. 11, pp. 528-531, 2001.

[72] S. Santra, P. Holloway and C. D. Batich, "Fabrication and testing of a magnetically actuated micropump," *Sensors and Actuators, B: Chemical,* vol. 87, pp. 358-364, 2002.

[73] S. Chung, J. K. Kim, K. C. Wang, D. -. Han and J. -. Chang, "Development of MEMS-based cerebrospinal fluid shunt system," *Biomed. Microdevices,* vol. 5, pp. 311-321, 2003.

[74] G. -. Feng and E. S. Kim, "Micropump based on PZT unimorph and one-way parylene valves," *J Micromech Microengineering,* vol. 14, pp. 429-435, 2004.

[75] D. J. Beebe, J. S. Moore, J. M. Bauer, Q. Yu, R. H. Liu, C. Devadoss and B. -. Jo, "Functional hydrogel structures for autonomous flow control inside microfluidic channels," *Nature,* vol. 404, pp. 588-590, 2000.

[76] Y. Liu, C. B. Rauch, R. L. Stevens, R. Lenigk, J. Yang, D. B. Rhine and P. Grodzinski, "DNA amplification and hybridization assays in integrated plastic monolithic devices," *Anal. Chem.,* vol. 74, pp. 3063-3070, 2002.

[77] L. Klintberg, M. Karlsson, L. Stenmark, J. -. Schweitz and G. Thornell, "A large stroke, high force paraffin phase transition actuator," *Sens Actuators A Phys,* vol. 96, pp. 189-195, 2002.

[78] E. T. Carlen and C. H. Mastrangelo, "Surface micromachined paraffin-actuated microvalve," *J Microelectromech Syst,* vol. 11, pp. 408-420, 2002.

[79] A. D. Stroock, S. K. Dertinger, G. M. Whitesides and A. Ajdari, "Patterning flows using grooved surfaces," *Anal. Chem.,* vol. 74, pp. 5306-5312, 2002.

[80] H. Chen and J. -. Meiners, "Topologic mixing on a microfluidic chip," *Appl. Phys. Lett.,* vol. 84, pp. 2193-2195, 2004.

[81] A. D. Stroock, S. K. W. Dertinger, A. Ajdari, I. Mezić, H. A. Stone and G. M. Whitesides, "Chaotic mixer for microchannels," *Science,* vol. 295, pp. 647-651, 2002.

[82] J. T. Coleman and D. Sinton, "A sequential injection microfluidic mixing strategy," *Microfluidics and Nanofluidics,* vol. 1, pp. 319-327, 2005.

[83] C. -. Chen and C. -. Cho, "Electrokinetically-driven flow mixing in microchannels with wavy surface," *J. Colloid Interface Sci.,* vol. 312, pp. 470-480, 2007.

[84] E. Biddiss, D. Erickson and D. Li, "Heterogeneous surface charge enhanced micromixing for electrokinetic flows," *Anal. Chem.,* vol. 76, pp. 3208-3213, 2004.

[85] J. -. Zhang, G. -. He and F. Liu, "Electro-osmotic flow and mixing in heterogeneous microchannels," *Physical Review E - Statistical, Nonlinear, and Soft Matter Physics,* vol. 73, 2006.

[86] H. J. Kim and A. Beskok, "Quantification of chaotic strength and mixing in a micro fluidic system," *J Micromech Microengineering,* vol. 17, pp. 2197-2210, 2007.

[87] D. A. Boy and B. D. Storey, "Electrohydrodynamic instabilities in microchannels with time periodic forcing," *Physical Review E - Statistical, Nonlinear, and Soft Matter Physics,* vol. 76, 2007.

[88] B. Stoeber, C. -. J. Hu, D. Liepmann and S. J. Muller, "Passive flow control in microdevices using thermally responsive polymer solutions," *Phys. Fluids,* vol. 18, 2006.

[89] M. H. Oddy, J. G. Santiago and J. C. Mikkelsen, "Electrokinetic instability micromixing," *Anal. Chem.,* vol. 73, pp. 5822-5832, 2001.

[90] C. K. Harnett, J. Templeton, K. A. Dunphy-Guzman, Y. M. Senousy and M. P. Kanouff, "Model based design of a microfluidic mixer driven by induced charge electroosmosis," *Lab on a Chip - Miniaturisation for Chemistry and Biology,* vol. 8, pp. 565-572, 2008.

[91] A. Ramos, A. González, A. Castellanos, N. G. Green and H. Morgan, "Pumping of liquids with ac voltages applied to asymmetric pairs of microelectrodes," *Physical Review E - Statistical, Nonlinear, and Soft Matter Physics,* vol. 67, pp. 056302/1-056302/11, 2003.

[92] F. Zhang, Y. Daghighi and D. Li, "Control of flow rate and concentration in microchannel branches by induced-charge electrokinetic flow," *J. Colloid Interface Sci.,* vol. 364, pp. 588-593, 2011.

[93] L. H. Olesen, H. Bruus and A. Ajdari, "Ac electrokinetic micropumps: The effect of geometrical confinement, Faradaic current injection, and nonlinear surface capacitance," *Physical Review E - Statistical, Nonlinear, and Soft Matter Physics,* vol. 73, 2006.

[94] H. Sugioka, "Suppression of reverse flows in pumping by induced-charge electro-osmosis using asymmetrically stacked elliptical metal posts," *Physical Review E - Statistical, Nonlinear, and Soft Matter Physics,* vol. 78, 2008.

[95] H. Zhao and H. H. Bau, "Microfluidic chaotic stirrer utilizing induced-charge electro-osmosis," *Physical Review E - Statistical, Nonlinear, and Soft Matter Physics,* vol. 75, 2007.

[96] M. Jain, A. Yeung and K. Nandakumar, "Induced charge electro osmotic mixer: Obstacle shape optimization," *Biomicrofluidics,* vol. 3, 2009.

[97] M. Jain, A. Yeung and K. Nandakumar, "Efficient micromixing using induced-charge electroosmosis," *J Microelectromech Syst,* vol. 18, pp. 376-384, 2009.

[98] P. Benjamin, *History of Electricity.* NY: John Wiley, 1898.

[99] M. Gad-el-Hak, "Fluid mechanics of microdevices-the freeman scholar lecture," *J Fluids Eng Trans ASME,* vol. 121, pp. 5-33, 1999.

[100] L. Fan, Y. Tai and R. S. Muller, "INTEGRATED MOVABLE MICROMECHANICAL STRUCTURES FOR SENSORS AND ACTUATORS." *IEEE Trans. Electron Devices,* vol. 35, pp. 724-730, 1988.

[101] W. S. N. Trimmer and K. J. Gabriel, "MICRO MECHANICAL DOMAIN." in *American Society of Mechanical Engineers, Dynamic Systems and Control Division (Publication) DSC,* 1987, pp. 393-396.

[102] O. D. Jefimenko, *Electrostatic Motors: Their History, Types, and Principles of Operation.* Star City, LCCN 73180890: Electret Scientific Co., 1973.

[103] B. Franklin and J. Sparks, *The Works of Benjamin Franklin.* Boston: Whittemore, News, and Hall, 1856.

[104] S. F. Bart, T. A. Lober, R. T. Howe, J. H. Lang and M. F. Schlecht, "Design considerations for micromachined electric actuators," *Sensors and Actuators,* vol. 14, pp. 269-292, 1988.

[105] Y. Tai, L. Fan and R. S. Muller, "IC-processed micro-motors: Design, technology, and testing." in 1989, pp. 1-6.

[106] L. Fan, Y. Tai and R. S. Muller, "IC-processed electrostatic micro-motors," in *Technical Digest - International Electron Devices Meeting,* 1988, pp. 666-669.

[107] T. Morita, "Miniature piezoelectric motors," *Sens Actuators A Phys,* vol. 103, pp. 291-300, 2003.

[108] Y. Daghighi and D. Li, "Micro-valve using induced-charge electrokinetic motion of Janus particle," *Lab on a Chip - Miniaturisation for Chemistry and Biology,* vol. 11, pp. 2929-2940, 2011.

[109] M. Darbandi, S. O. Torabi, M. Saadat, Y. Daghighi and D. Jarrahbashi, "A moving-mesh finite-volume method to solve free-surface seepage problem in arbitrary geometries," *Int. J. Numer. Anal. Methods Geomech.,* vol. 31, pp. 1609-1629, 2007.

[110] M. Moghiman, T. Hashemi, I. Zahmatkesh and Y. Daghighi, "Effects of particle size and equivalence ratio on cyclone gasification of wood powder," *Journal of the Energy Institute,* vol. 80, pp. 29-34, 2007.

[111] D. Li, *Electrokinetics in Microfluidics.* Academic Press, 2004.

[112] R. J. Hunter, *Zeta Potential in Colloid Science. Principles and Applications.* NY: Academic Press, 1981.

[113] C. Ye and D. Li, "3-D transient electrophoretic motion of a spherical particle in a T-shaped rectangular microchannel," *J. Colloid Interface Sci.,* vol. 272, pp. 480-488, 2004.

[114] C. Ye and D. Li, "Electrophoretic motion of two spherical particles in a rectangular microchannel," *Microfluidics and Nanofluidics,* vol. 1, pp. 52-61, 2004.

[115] V. L. Streeter, E. B. Wylie and K. W. Bedford, *Fluid Mechanics.* WCB/McGraw Hill, 1998.

[116] Y. Daghighi, Y. Gao and D. Li, "3D numerical study of induced-charge electrokinetic motion of heterogeneous particle in a microchannel," *Electrochim. Acta,* vol. 56, pp. 4254-4262, 2011.

[117] C. J. Behrend, J. N. Anker, B. H. McNaughton, M. Brasuel, M. A. Philbert and R. Kopelman, "Metal-capped brownian and magnetically modulated optical nanoprobes (MOONs): Micromechanics in chemical and biological microenvironments," *J Phys Chem B,* vol. 108, pp. 10408-10414, 2004.

[118] S. -. Kang and D. Huang, "Fabrication of star grooves and rhombus grooves micro heat pipe," *J Micromech Microengineering,* vol. 12, pp. 525-531, 2002.

[119] L. -. Yang, Y. -. Chen, S. -. Kang and Y. -. Wang, "Fabrication of SU-8 embedded microchannels with circular cross-section," *Int. J. Mach. Tools Manuf.,* vol. 44, pp. 1109-1114, 2004.

[120] V. Maselli, R. Osellame, G. Cerullo, R. Ramponi, P. Laporta, L. Magagnin and P. L. Cavallotti, "Fabrication of long microchannels with circular cross section using astigmatically shaped femtosecond laser pulses and chemical etching," *Appl. Phys. Lett.*, vol. 88, 2006.

[121] S. -. Song, C. -. Lee, T. -. Kim, I. -. Shin, S. -. Jun and H. -. Jung, "A rapid and simple fabrication method for 3-dimensional circular microfluidic channel using metal wire removal process," *Microfluidics and Nanofluidics*, vol. 9, pp. 533-540, 2010.

[122] M. Shikida, K. Sato, S. Tanaka, Y. Kawamura and Y. Fujisaki, "Electrostatically driven gas valve with high conductance," *J Microelectromech Syst*, vol. 3, pp. 76-80, 1994.

[123] C. Goll, W. Bacher, B. Büstgens, D. Maas, R. Ruprecht and W. K. Schomburg, "An electrostatically actuated polymer microvalve equipped with a movable membrane electrode," *J Micromech Microengineering*, vol. 7, pp. 224-226, 1997.

[124] H. Takao, M. Ishida and K. Sawada, "A pneumatically actuated full in-channel microvalve with MOSFET-like function in fluid channel networks," *J Microelectromech Syst*, vol. 11, pp. 421-426, 2002.

[125] J. -. Choi, K. W. Oh, A. Han, N. Okulan, C. Ajith Wijayawardhana, C. Lannes, S. Bhansali, K. T. Schlueter, W. R. Heineman, H. B. Halsall, J. H. Nevin, A. J. Helmicki, H. Thurman Henderson and C. H. Ahn, "Development and characterization of microfluidic devices and systems for magnetic bead-based biochemical detection," *Biomed. Microdevices*, vol. 3, pp. 191-200, 2001.

[126] T. Rogge, Z. Rummler and W. K. Schomburg, "Polymer micro valve with a hydraulic piezo-drive fabricated by the AMANDA process," *Sens Actuators A Phys*, vol. 110, pp. 206-212, 2004.

[127] J. Peirs, D. Reynaerts and H. Van Brussel, "Design of miniature parallel manipulators for integration in a self-propelling endoscope," *Sens Actuators A Phys*, vol. 85, pp. 409-417, 2000.

[128] D. Baechi, R. Buser and J. Dual, "High-density microvalve arrays for sample processing in PCR chips," *Biomed. Microdevices*, vol. 3, pp. 183-190, 2001.

[129] S. -. Wang, Y. -. Lai, Y. Ben and H. -. Chang, "Microfluidic mixing by dc and ac nonlinear electrokinetic vortex flows," *Industrial and Engineering Chemistry Research*, vol. 43, pp. 2902-2911, 2004.

[130] C. Y. Lim, Y. C. Lam and C. Yang, "Mixing enhancement in microfluidic channel with a constriction under periodic electro-osmotic flow," *Biomicrofluidics*, vol. 4, 2010.

[131] M. Campisi, D. Accoto, F. Damiani and P. Dario, "A soft-lithographed chaotic electrokinetic micromixer for efficient chemical reactions in lab-on-chips," *Journal of Micro-Nano Mechatronics*, vol. 5, pp. 69-76, 2009.

[132] Y. Du, Z. Zhang, C. Yim, M. Lin and X. Cao, "A simplified design of the staggered herringbone micromixer for practical applications," *Biomicrofluidics,* vol. 4, 2010.

[133] D. Ahmed, X. Mao, B. K. Juluri and T. J. Huang, "A fast microfluidic mixer based on acoustically driven sidewall-trapped microbubbles," *Microfluidics and Nanofluidics,* vol. 7, pp. 727-731, 2009.

[134] Z. Zhang, C. H. Yim, M. Lin and X. Cao, "Quantitative characterization of micromixing simulation," *Biomicrofluidics,* vol. 2, 2008.